POLITECNICO DI MILANO
SCUOLA DI DOTTORATO
DOTTORATO DI RICERCA IN BIOINGEGNERIA

Advanced MRI techniques in multiple sclerosis: multimodal assessment of WM and GM damage mechanisms

Doctoral dissertation of:
Niels Peter Bergsland

Advisors:
Prof. Giuseppe Baselli
Dr. Marco Rovaris
Prof. Robert Zivadinov
Dr. Francesca Baglio
Dr. Maria Marcella Laganà

Tutor:
Prof. Gabriele Candiani

Chair of the PhD program:
Prof. Andrea Aliverti

XXVIII cycle
2013-2015

Acknowledgements

First, my thanks go to Professor Giuseppe Baselli for guiding me through the maze of the PhD at Politecnico di Milano. His guidance was invaluable for helping me arrive here today.

I would like also to thank Dr. Francesca Baglio, Dr. Marcella Laganà and the rest of my colleagues in the MR Research Lab at Fondazione Don Gnocchi for making the workplace a nice and friendly environment. I've enjoyed the many coffees, desserts and lively discussions that we have had over these years.

My deepest gratitude goes to Professor Robert Zivadinov for being my mentor and friend since the beginning of my journey in the field of research. I would especially like to acknowledge and thank you for believing in me as well as the possibility of keeping an active and fruitful scientific collaboration over these years, despite the ocean between us.

Thanks to Mike for not only being a close friend but someone with whom I have the immense pleasure of exchanging ideas and sharing a path of professional growth.

I would like to thank Professor Ralph Benedict for his support and guidance in our collaborative efforts.

I would like to thank Dr. Marco Rovaris who has always had very useful suggestions for improving the overall quality of my work.

The support from my colleagues and friends at the Buffalo Neuroimaging Analysis Center, especially Jackie, Mariya and Deepa, needs to be acknowledged. It has been nice seeing familiar faces during my yearly visits!

My warmest thanks go to my birth family (my mother, my father, Annette and Christian) and my Italian family (Gigi, Marina, Guido and Paola) as well as my grandparents. All of my family has been incredibly supportive and interested in my work since the very beginning. I have enjoyed being able to share with you the passion I have for my work!

Very special thanks go to Jordan for always sharing his house and great times together when visiting Buffalo as part of my research. It has been great being able to see you on a yearly basis since having moved to Italy.

Finally, none of this work would have been possible without the unconditional love from my wife Ele and daughter Cecilia. The need to spend long hours was never questioned nor criticized. Their unwavering support and encouragement allowed me to focus on my work at times when it seemed never ending. I hope that I have been able to show you just how much your love means to me!

Table of Contents

Acknowledgements 2
Abstract 5
Abstract (Italiano) 8
Extended Summary 12
Aims and background 12
Methods 17
Results 23
Discussion 35
Conclusion 38
Chapter 1: Aims and background 39
Aims of the study 39
Advanced MR imaging techniques for the study of multiple sclerosis 40
Structural segmentation 41
Diffusion-weighted imaging 50
Susceptibility-weighted imaging 56
Multimodal imaging 60
Thesis structure and author's personal contribution 61
Scientific publications 64
Full papers based on this study 64
Conference Proceedings 65
Scientific publications not part of the thesis 66
Full papers 66
Conference Proceedings 66
Chapter 2: Corticospinal tract integrity is related to primary motor cortex thinning in relapsing-remitting multiple sclerosis. 69
Abstract 70
Introduction 71
Materials and Methods 72
Results 84
Discussion 92
Acknowledgements 97
Chapter 3: Improving the quality of automated deep gray matter structural segmentations in multiple sclerosis 98
Abstract 99

Introduction 101
Materials and Methods 104
Reproducibility analysis 107
Results: 109
Discussion 115
Chapter 4: Localized atrophy of the thalamus and slowed cognitive processing speed in MS patients. 119
Abstract 119
Introduction 121
Methods 122
Results 129
Discussion 140
Chapter 5: White matter tract injury is associated with deep gray matter iron deposition in multiple sclerosis patients 147
Abstract 148
Introduction 149
Materials and Methods 150
Results 155
Discussion 167
Acknowledgements 173
Chapter 6: Discussion and conclusions 174
Addressing the aspect of focal WM pathology 174
The role of tractography in characterizing WM damage 175
The relationship between WM pathology and GM injury 177
The advantage of surface-based approaches in characterizing GM damage 179
Conclusion 181
References 183
Appendix A: Abbreviations 196
Appendix B: Processing pipelines and software used 199

Abstract

Aim: The aim of this study was to implement and test objective methods for quantifying the relationships between gray matter (GM) and white matter (WM) damage, applicable in regards to neurodegenerative diseases, with a particular focus on multiple sclerosis (MS).

Background: Conventional imaging techniques are insufficient to fully characterize the underlying pathological substrates involved in MS. Moreover, it is now widely recognized that MS damage is much more widespread than just focal WM lesions. A number of advanced acquisition and post-processing techniques have been developed for both a more precise description and a better localization of the effects of the disease. However, the effects of MS-related focal damage often require careful evaluation and tuning of the algorithms commonly in use within the neuroimaging community. Nonetheless, advanced techniques offer the possibility to interrogate the various pathological processes involved in MS. Examples include morphological reconstruction of the cortex and subcortical GM structures for a better characterization of tissue atrophy, diffusion imaging and tractographic reconstruction for quantitative assessment of WM characteristics (including the so-called normal appearing WM (NAWM)) and susceptibility-weighted imaging for assessing iron deposition. Furthermore, the integration of the aforementioned techniques can provide information on the associations and interactions between tissue damage in the WM and GM compartments.

Protocol and Results: *(i) Methodological Developments*: The impact of WM lesions on cortical reconstructions was qualitatively assessed in a sample of relapsing remitting MS patients. As WM lesions were found to negatively affect automated cortical reconstructions, we developed

and implemented an optimized process for lesion filling as pre-processing step. We combined cortical reconstruction and tractography techniques to assess the relationship between WM injury and cortical thinning in a functionally and anatomically connected region. As WM pathology was found to interfere with tractography of the WM fiber tracts (both for deterministic and probabilistic approaches), we implemented a method for generating probabilistic atlases based on successful reconstructions in healthy controls (HC). The effect of lesions on automated deep GM (DGM) segmentations was also quantified. Finally, we implemented a novel, optimized and unbiased processing pipeline for assessing the relationship between putative iron deposition in the DGM and injury within the connected WM tracts.

(ii) Applications: The optimized lesion filling process was used in all four studies that make up the current work. In a sample of 51 MS patients, we found that NAWM injury within the corticospinal tract (CST) was the best predictor of cortical thinning in the primary motor cortex. This appears to be specific to MS as no such relation was found in the HC group. In a group of 152 MS patients, we demonstrated a clear effect of WM lesions on automated thalamic and caudate segmentations. This motivated the use of lesion filled images in our third study which investigated the relationships between DGM atrophy and cognitive status in a sample of 64 MS patients. We highlighted the advantage of surface-based methods for a more precise localization of the effects of atrophy. Specifically, anterior thalamic atrophy was found to correlate with decreased processing speed over the course of three years of follow-up. Notably, such an effect was not detectable when using other commonly used imaging assessments. Lastly, we applied our processing pipeline for combining iron-sensitive imaging and tractography techniques in a sample of 66 MS patients. Our results demonstrated for the first time in the literature an

association between putative iron deposition in the DGM and increased WM damage in the associated tracts.

Conclusion: The aim of this study was to implement and test objective methods for quantifying the relationships between GM and WM damage in multiple sclerosis. We consistently demonstrated the importance of paying close attention, in the preprocessing phase, to the confounding effects of WM lesions in terms of obtaining reliable results. In two separate studies, we found clear evidence of an association between WM injury and GM pathology. For the former, we used WM tractographic methodologies while for the latter we utilized both cortical morphological reconstruction and iron-sensitive acquisition/post-processing techniques. We found that both cortical thinning and a putative marker of increased iron deposition were related to increased NAWM injury in the connected tracts. We also showed for the first time that focal atrophy of the thalamus is associated with a decline in cognitive processing speed over three years of follow-up.

Taken together, the results obtained from the investigations performed as part of this thesis appear to be promising in leading to a better characterization of the association between structure-specific GM, both deep and cortical, and WM injury in multiple sclerosis. These results, moreover, foster new insights yielded by multimodal imaging approaches for studying the multifaceted aspects of the disease.

Abstract (Italiano)

Aim: Lo scopo di questo studio è di implementare e validare metodi di quantificazione oggettiva della relazione tra danno della sostanza grigia (SG) e sostanza bianca (SB) applicabili a malattie neurodegenerative, con particolare interesse per la sclerosi multipla (SM).

Background: le tecniche di imaging convenzionale non sono in grado di caratterizzare adeguatamente il substrato patologico sottostante la SM. Per di più, è stato dimostrato che i danni provocati dalla SM non si limitano alle lesioni della SB ma appaiono molto più diffusi. Per ovviare a questo problema, sono state sviluppate diverse tecniche avanzate di acquisizione e post-processing per caratterizzare meglio qualitativamente l'entità e la localizzazione del danno correlato alla patologia. Spesso però, gli effetti della patologia focale tipica della SM richiedono una valutazione attenta e un adeguamento degli algoritmi normalmente utilizzati nella comunità di neuroimaging. Le tecniche avanzate di neuroimaging consentono la possibilità di valutare i diversi processi patologici coinvolti nella SM. Alcuni esempi includono la ricostruzione morfologica della SG corticale e sottocorticale allo scopo di caratterizzare l'atrofia tissutale, le tecniche di diffusione per definire quantitativamente le caratteristiche della SB (inclusa la cosiddetta sostanza bianca apparentemente normale), la ricostruzione trattografica dei fasci di fibre di interesse e il *susceptibility-weighted imaging* per lo studio dei depositi di ferro. Inoltre, l'uso integrato delle tecniche sopramenzionate può fornire informazioni preziose sulle associazioni, ed eventuali interazioni tra il danno della SB e della SG.

Protocolllo e risultati- *(i) sviluppo delle metodologie*: è stata quantificata l'influenza delle lesioni focali della SB sulla ricostruzione della corteccia di pazienti affetti da SM recidivante remittente. Siccome è stato verificato un impatto negativo delle lesioni sulla ricostruzione

automatica del distretto corticale, abbiamo sviluppato e implementato un processo ottimizzato per il *filling* delle lesioni in fase di pre-processing. Abbiamo quindi combinato la ricostruzione della corteccia e le tecniche di trattografia per studiare la relazione tra la riduzione dello spessore corticale e il danno della SB in aree funzionalmente ed anatomicamente correlate. Il danno tissutale a carico della SB interferisce con la ricostruzione trattografica dei fasci di fibre di SB (sia utilizzando un approccio deterministico che probabilistico); abbiamo quindi implementato un metodo di generazione di atlanti probabilistici basati sulla ricostruzione degli stessi fasci di fibre in un campione di soggetti sani. È stato inoltre quantificato l'effetto delle lesioni focali sulla segmentazione automatica delle strutture di SG profonda. Da ultimo, abbiamo implementato una nuova procedura, ottimizzata e libera da *bias* per la definizione della relazione tra depositi di ferro nella SG profonda e danno all'interno dei fasci di fibre di SB ad essa connessi.

(ii): applicazioni: il processo ottimizzato di *filling* delle lesioni è stato utilizzato in tutti e 4 gli studi descritti nel presente lavoro. Abbiamo analizzato un campione di 51 pazienti affetti da SM, in cui il danno della SB apparentemente normale appartenente al tratto cortico-spinale (CST) è risultato essere il maggiore fattore predittivo di riduzione dello spessore corticale nella corteccia motoria primaria. Questo dato, non essendo presente nella popolazione di soggetti sani, pare essere specificamente correlato alla patologia in esame. Abbiamo anche dimostrato un evidente effetto delle lesioni della SM sulla segmentazione automatica di talamo e nucleo caudato in un campione di 152 pazienti affetti da SM. Questo riscontro ha motivato l'utilizzato di immagini *lesion filled* nel terzo lavoro qui descritto, in cui abbiamo studiato la relazione tra atrofia della SG profonda e stato delle funzioni cognitive in una popolazione di 64 pazienti affetti da SM. Abbiamo sottolineato il vantaggio di metodi *surface-based* per una localizzazione più precisa degli effetti dell'atrofia tissutale. Più nel dettaglio, l'atrofia delle regioni anteriori del talamo

correla con una riduzione della velocità di processazione delle informazioni, nell'ambito di un follow-up di tre anni. È interessante sottolineare che non è stato possibile riscontrare lo stesso dato utilizzando altri metodi di imaging comunemente utilizzanti. Infine, abbiamo applicato la nostra procedura ottimizzata al fine di combinare tecniche di trattografia a imaging sensibile al ferro in un campione di 66 pazienti affetti da SM. I nostri risultati hanno dimostrato per la prima volta in letteratura una associazione tra la probabile presenza di depositi di ferro nella SG profonda e un aumento del danno della SB nei tratti associati.

Conclusioni: lo scopo del presente studio era identificare e validare l'efficacia di metodi di imaging oggettivi per la quantificazione della relazione tra danno della SB e nella SG nella SM. Abbiamo ripetutamente dimostrato l'importanza di tenere in considerazione nel *preprocessing* gli effetti delle lesioni in SB, per ottenere risultati attendibili. In due diversi studi abbiamo riscontrato una chiara evidenza di associazione tra danno della SB e della SG. Per indagare e quantificare il danno della SB abbiamo utilizzato metodiche trattografiche, mentre per quanto riguarda la SG abbiamo utilizzato sia tecniche di ricostruzione morfologica della corteccia che tecniche di imaging sensibili al ferro per l'acquisizione e il post-processing. A questo proposito abbiamo rilevato che il danno della SG in termini sia di assottigliamento corticale che di indici di possibile presenza di depositi di ferro erano correlati ad un aumento del danno della SB nei tratti anatomicamente connessi. Abbiamo anche dimostrato per la prima volta che l'atrofia focale del talamo è associata ad un declino delle funzioni cognitive, in particolare della velocità di processazione delle immagini nel corso di un follow-up della durata di tre anni.

Considerati globalmente, i risultati ottenuti dagli studi presentati sembrano aprire uno scenario promettente nell'ambito della ricerca di imaging sulla SM, avendo ottenuto una migliore caratterizzazione dell'associazione tra danno, struttura-specifico, della SG, sia profonda che

corticale, e della SB nella sclerosi multipla. Questi risultati, in aggiunta, promuovono una migliore comprensione fornita da un approccio multimodale per lo studio delle varie caratteristiche della patologia in esame.

Extended Summary

Aims and background

Aims of the study

The aim of this study was to implement and test objective methods for quantifying the relationships between gray matter (GM), both deep and cortical, and white matter (WM) damage, applicable in regards to neurodegenerative diseases, with a particular focus on multiple sclerosis (MS).

In this context, four main studies were performed which are outlined as part of the specific objectives of this doctoral thesis:

- To study the relationship between damage within the WM and an area of anatomically/functionally connected GM area via the use of tractography and morphological reconstruction of the cortex
- To assess potential improvements in the processing pipeline for the automated segmentation of deep GM (DGM) structures. This objective was done by 1) evaluating the impact of using white matter lesion filling as a pre-processing step and 2) implementing and evaluating a proposed modification for improved precision of segmentations for longitudinal analyses.
- To evaluate the utility of surface-based analysis of DGM structures to more precisely localize the effects of atrophy than is possible using other commonly used imaging techniques such as region of interest and voxel-based morphometry
- To develop a method for more precisely characterizing the relationship between iron deposition within the DGM and associated white matter tracts

Background

Multiple sclerosis (MS) is an auto-immune mediated inflammatory disorder causing widespread damage throughout the central nervous system (CNS). Although MRI has allowed for the monitoring of the effects of the disease within the CNS in vivo, conventional imaging techniques and measures are generally lacking in their specificity. For example, the classic WM lesions, easily identified on a T2-weighted scan, correspond to a wide range of pathological substrates. Moreover, conventional measures may not be sensitive enough to detect changes within the so-called normal appearing WM (NAWM)[1, 2].

From both an acquisition as well as a post-processing point of view, a number of advanced MRI-based methods have been developed in recent years. Such techniques have the possibility to quantitatively characterize tissue properties in a way that is not possible using conventional imaging.

MS is characterized by an increased rate of tissue atrophy with respect to healthy controls (HC). Indeed, disability progression[3] and cognitive impairment[4, 5] appear to be heavily dependent on irreversible GM loss. Thus, in recent years, there has been considerable interest in the development and validation of automated (or at least semi-automated) methods for structural segmentation as a means to quantitatively measure tissue characteristics such as its volume, shape or thickness (as regards the cortical ribbon). In this context, two of the most widely used methods in the neuroimaging community are FreeSurfer[6] and FMRIB's Integrated Registration and Segmentation Tool (FIRST)[7]. Both algorithms require a high resolution, 3D T1-weighted scan as their input. One of the key advances utilized in both of these methods is the surface-based representation that they use for modeling the underlying brain tissue. Surfaces are

represented as a mesh of vertexes. With FreeSurfer, this allows for one to obtain cortical parcellations that respect the inherent sheet-like nature of the cortex as well as allowing for the sharper identification of cortical anatomy. For FIRST, the surface-based representation is used in the construction of trained models that allow for a more accurate segmentation as well as for the possibility to assess local shape difference in group-based analyses. For example, one can examine the effects of atrophy with respect to HCs or relationships with cognitive measures.

In the case of FreeSurfer, the outer WM surface is first identified based on a voxel-wise tissue class segmentation. The result is then refined in such a way to respect topological constraints and prevent surface reconstructions that would be anatomically impossible (e.g. holes within the WM or "islands" of isolated WM tissue). The pial surface (corresponding to the boundary between cortical GM and sulcal cerebrospinal fluid (CF)) is then found by expanding the final WM surface. In both cases, intensity gradients are followed such that the surfaces are optimally placed at the tissue borders. Once the cortical surface has been reconstructed, high dimension nonlinear spherical registration allows for the mapping of probabilistic cortical atlases to individual subjects.

For FIRST, a surface-based representation is used in the construction of trained models which represent the mean shape and modes of variation derived from a large sample of manually segmented data. The trained models are provided as part of the software and integrated as the *a-priori* of a Bayesian framework. The incorporation of shape data into the models allows for a more accurate segmentation, particularly in the case where GM/WM contrast is generally poor (e.g. the thalamus). FIRST uses a fixed number of vertexes for each subcortical structure and vertex correspondence is maintained throughout the segmentation procedure. This opens the door to the possibility of performing group-based, vertexwise analyses to reveal localized shape

changes. As no smoothing is required, this approach potentially provides a more selective method to characterize the localization of atrophy, which allows improved sensitivity to focal changes.

Diffusion-weighted imaging (DWI) exploits the physical process governing the Brownian motion of water molecules within tissue. Diffusion tensor imaging (DTI) is a widely used model for describing the random motion of water molecules in brain tissue. The key concept is that that tissue characteristics such as its type (i.e. GM or WM), architecture, inter-/intra-cellular barriers and overall integrity will ultimately influence the diffusion of water molecules. In general, diffusion within WM tends to be the most restrictive due to the axonal membrane and surrounding myelin. As a natural consequence, WM diffusion is largely anisotropic, as water molecules will preferentially diffuse along the direction of the axon. However, tissue injury may be reflected by altered diffusivity characteristics. Indeed, diffusion imaging and the DTI model have enjoyed widespread use in imaging studies of MS patients as a means to measure damage, particularly within the NAWM, that cannot be resolved using conventional imaging methods[1, 2, 8-10].

Diagonalization of the diffusion tensor yields the eigenvalues and eigenvectors. The former can be used for quantitatively characterizing the underlying tissue microstructure via parameters such as fractional anisotropy and mean diffusivity. On the other hand, under the assumption that the primary eigenvector reflects the orientation of the underlying fiber bundle, tractographic reconstruction of the WM tracts can be performed. The approach is conceptually simple but is hindered in the case of multiple fiber populations with different orientations within a given voxel. In this case, the DTI model breaks down since there is no longer a single coherent direction that can be described by the primary eigenvector. This limitation has motivated the

development of more advanced methods such as probabilistic tractography which can more elegantly handle the uncertainty inherent in DTI. Nonetheless, tractographic reconstructions can be severely affected by the presence of WM lesions[11]. As the latter is one of the hallmark features of MS, alternative approaches are often required, particularly in the case of patients with long standing disease and/or more severe pathology where increased tissue destruction will be even more of a problem. One such solution is the use of probabilistic atlases generated from tractography in healthy controls, where tractographic results should be more reliable[11-13]. Such atlases can then be nonlinearly registered to patient data such that imaging parameters can be extracted from tracts of interest, without the interference of focal pathology.

An increased degree of iron deposition, particularly within the DGM, is also a commonly reported feature of MS[14-17]. It is still a matter of debate as to whether iron deposition plays a role in the neurodegenerative aspects of the disease or is merely an epiphenomenon. Nevertheless, a number of iron-sensitive imaging markers have been developed and validated in the last several years. One such technique is susceptibility-weighted imaging (SWI), which exploits the effect of paramagnetic materials on the phase component of the complex MRI signal. Historically discarded due to contamination by the background field, the SWI approach uses a homodyne filter in k-space to obtain a high-pass filtered phase image. In this case, the background field has been effectively eliminated for the most part. This allows for the characterization of the local field, which is of particular interest in terms of assessing the effects of local iron deposition. Indeed, a strong relationship has been found between iron content and SWI high pass filtered-phase values within the DGM. This has been shown using both synchrotron X-ray fluorescence[18] and comparisons with published reports of putative iron concentrations acquired from post-mortem data[19].

The use of multiple MR imaging modalities for a given study has seen a dramatic rise in popularity in recent years. There are several advantages that stem from combining the often complementary information provided by different sequences or image weightings. Perhaps the biggest impact that multimodal imaging has had is on shedding further light on the underlying pathological substrates involved in MS. The integration of multiple techniques can be used to provide insight into the association between pathogenic mechanisms or how damage in one tissue compartment might be related to that in another. For example, DTI-derived measures of WM microstructure can be combined with structural segmentations/reconstructions of the GM to quantify associations between damage the two tissue compartments[20, 21]. Integrated post-processing pipelines can also aid in automated analyses whereby segmentations from high resolution structural data is used to extract quantitative measures from another acquisition type.

Methods

Assessing the relationship between WM tract injury and cortical damage (Study 1)

Diffusion weighted, high resolution 3D T1-weighted structural and dual echo spin echo PD/T2-weighted images were acquired in a group of 51 relapsing-remitting MS (RRMS) patients and 30 HCs. The diffusion weighted sequences were used for DTI modeling, the 3D T1-weighted image for morphological reconstruction of the cortex and the PD/T2-weighted images for WM lesion identification and segmentation. Prior to performing the primary analyses, standard pre-processing steps were utilized. In the case of the diffusion weighted acquisitions, these steps included correction for eddy currents and diagonalization of the diffusion tensor. 3D T1-weighted images were pre-processed using an optimized lesion filling pipeline based on co-registered PD/T2 lesion masks. Manual edits of the co-registered lesion masks were made as necessary. A qualitative comparison of lesion filled T1-weighted images versus the original

images was made to assess the impact of WM hypointensities on cortical reconstruction. Ultimately, FreeSurfer was used with the lesion filled images as inputs in order to obtain measures of cortical thickness and surface area within the primary motor (PMC) and auditory cortices.

Figure 1

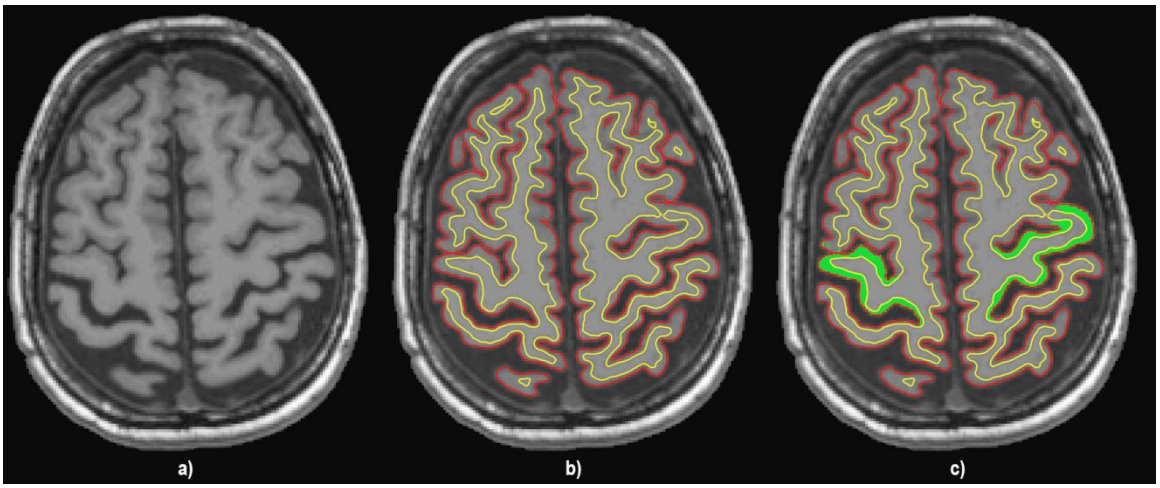

a) Representative T1-3D image of an RRMS patient
b) White matter and pial surfaces shown in yellow and red, respectively.
c) Parcellated primary motor cortex shown in green.

Based on the results obtained from deterministic tractographic reconstruction of the corticospinal tract (CST), a probabilistic atlas was generated. In all subjects, the atlas was used to extract DTI-derived parameters within focal WM pathology as well within the NAWM. Although focal WM lesions were seen on the DTI-images themselves, we opted to co-register PD/T2 lesion masks into the space of the subject's fractional anisotropy (FA) image.

Figure 2

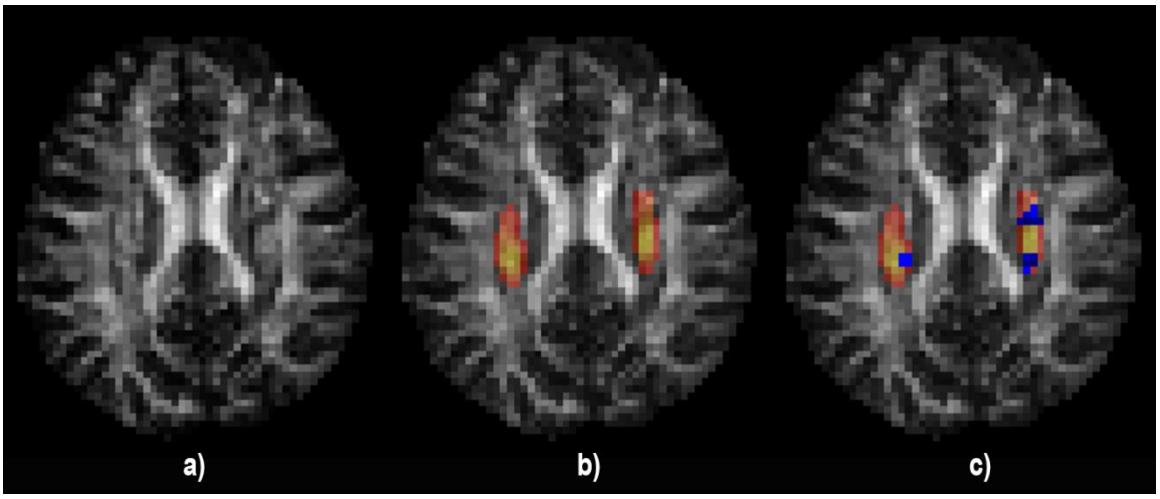

a) Representative fractional anisotropy (FA) image of an RRMS patient
b) The same FA image with the probabilistic CST atlas overlaid. Warmer colors represent an increased probability of corresponding to the CST in the atlas.
c) Segmented lesions within the CST atlas are shown in blue. PD/T2 lesion masks were co-registered into the space of the FA image.

Associations between the aforementioned values and cortical measures were assessed using partial correlations and multiple linear regression models. Lesion probability maps (LPM) were also generated for assessing the relationship between lesion location within the CST and cortical thinning within the PMC. All analyses were adjusted for age and sex.

Assessing potential improvements in the processing pipeline for the automated segmentation of deep gray matter structures (Study 2)

Two groups of subjects were analyzed. The first group consisted of 152 MS patients imaged on the same 1.5T scanner whereas 64 MS patients and 22 HCs were examined on a 3T scanner as part of the second group. FMRIB's Integrated Registration and Segmentation Tool (FIRST) was used for automated segmentation from 3D T1-weighted images of the thalamus, caudate nucleus,

globus pallidus and putamen. The effect of WM lesions was assessed using the former group by comparing segmented structural volumes and surface-based analysis, before and after lesion filling. The effect of WM lesions on the two key steps in the FIRST pipeline were assessed (i.e. registration and fitting of the trained models.) This resulted in the investigation of four different methods: 1) original 3D T1 (i.e. no modifications) ; 2) lesion filled 3D T1 ; 3) original 3D T1 using registration matrix derived in 2) ; 4) lesion filled 3D T1 using registration matrix derived in 1) In the second group, the use of common registration to standard space was investigated as a potential means for reducing intra-subject variability. In both groups of subjects, fluid attenuated inversion recovery (FLAIR), dual echo spin echo PD/T2-weighted and high resolution 3D T1-weighted structural images were acquired. PD/T2-weighted and FLAIR images were used for WM lesion identification and segmentation. Lesion filling was performed using the optimized method developed in the "Assessing the relationship between WM tract injury and cortical damage" section of the thesis. For analysis assessing the impact of lesions, differences in segmented volumes were tested using a one-way repeated measures ANOVA with Bonferroni correction for pairwise comparisons. LPM and vertex-wise analyses were also used to assess the effect of focal WM pathology on structural segmentations. For the modified longitudinal method, we first assessed its reproducibility with respect to the standard approach of comparing cross-sectional measures in a post-hoc manner. Reproducibility of the two methods was first assessed in the scan-rescan dataset using intra-class correlation (ICC). Next, for each method, the MS patient and HC groups were compared using Student's *t*-tests and then Cohen's d was calculated as a measure of the effect size.

Surface-based analysis of deep gray matter structures (Study 3)

64 MS patients and 22 HC were examined on a 3T scanner for the acquisition of FLAIR, dual echo spin echo PD/T2-weighted and high resolution 3D T1-weighted structural images. PD/T2-weighted and FLAIR images were used for WM lesion identification and segmentation. Lesion filling was performed using the optimized method developed in the "Assessing the relationship between WM tract injury and cortical damage" section of the thesis. All subjects underwent a neuropsychological (NP) examination that emphasized consensus standard tests of processing speed and memory. Specifically, the Symbol Digit Modalities Test (SDMT) was used for the former while the Brief Visuospatial Memory Test - Revised (BVMT-R) and California Verbal Language Test – 2nd edition (CVLT-2) were used for the latter. FIRST was used for both volumetric and shape analysis of DGM structures and differences between MS patients and HCs were assessed. In MS patients, we also evaluated their relationships with cognition both at baseline and over three years of follow-up. General linear models, adusting for age and sex, were used for statistical modeling. For comparison purposes, we also implemented an optimized longitudinal voxel-based morphometry pipeline.

Characterizing the relationship between iron deposition within the DGM and WM injury (Study 4)

Diffusion weighted, high resolution 3D T1-weighted structural, dual echo spin echo PD/T2-weighted and susceptibility-weighted (SWI) images were acquired in a group of 66 MS (RRMS) patients and 29 HCs on a 1.5T scanner. SWI and DTI were used for assessing high-pass filtered phase values, indicative of iron content, in the DGM and normal appearing WM (NAWM) integrity, respectively. An optimized group-wise analysis was implemented for assessing areas of increased iron deposition in MS patients. Briefly, an unbiased group template was first created from the high resolution 3D T1-weighted images. Next, all 3D T1-weighted images were

nonlinearly registered to the template. SWI high-pass filtered phase images were then brought into the space of the template using the corresponding warp field derived from the 3D T1-weighted normalization. Permutation-based testing was used to identify clusters of voxels where SWI-filtered phase values were significantly higher (as images were obtained from a left-handed system) in the MS patient group. The analysis was also repeated with the inclusion of a voxelwise covariate of GM volume as SWI high-pass filtered phase changes may potentially be influenced by atrophy (due to possible change in structural shape), even in the absence of any true change in underlying tissue susceptibility. The clusters obtained from the voxelwise analysis of the high-pass filtered phase data were subsequently used as seeds for probabilistic tractography in HCs with the final aim of generating tract atlases for atlas-based tractography. Partial correlations were then used to assess the relationships between focal iron deposition and tract-specific WM injury as assessed using DTI-derived parameters and focal lesion volumes. All analyses controlled for the effects of age and sex.

Summary of datasets

Table 1 presents a summary of the datasets used in the four studies that were performed as part of the thesis.

Table 1

	Subjects scanned	Key MRI sequences	Primary aims
Study 1	51 RRMS / 30 HC	3D T1-w PD/T2-w 12 direction DWI	Assess relationships between WM damage and cortical atrophy
Study 2	Group 1: 152 RRMS Group 2: 64 MS / 22 HC	3D T1-w FLAIR	Assess potential improvements for automated deep GM segmentation
Study 3	64 MS / 22 HC	3D T1-w	Investigate the use of

		FLAIR	surface-based measures for more preicesly characterizing GM atrophy
Study 4	66 RRMS / 29 HC	3D T1-w PD/T2-w 12 direction DWI SWI	Invesitigate the potential relationship between deep GM iron deposition and damage in connected WM tracts

Results

Assessing the relationship between WM tract injury and cortical damage

The qualitative comparison of results using lesion filled images with respect to the original ones demonstrated that cortical reconstructions were biased by the presence of focal WM pathology, particularly juxtacortical lesions. With respect to HC subjects, MS patients presented with significantly decreased PMC thickness ($p = .017$) and increased CST NAWM diffusivity parameters ($p < .0001$ for all measures investigated). In patients only, however, decreased cortical thickness was related to increased CST NAWM mean, axial and radial diffusivities in addition to CST lesion volume. LPM analysis revealed that lesions throughout much of the CST were associated with decreased PMC thickness (Figure 3).

Figure 3

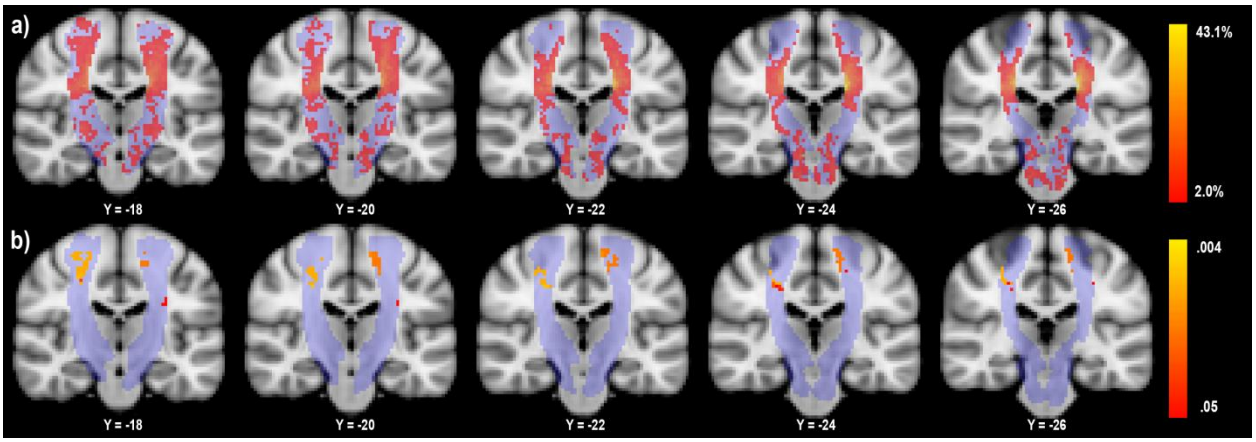

a) The T2-lesion probability map (LPM) shows the percentage of patients with a lesion in a given voxel. The probabilistic CST atlas is shown in light blue.
b) Lesional voxels that significantly correlate with primary motor cortex thickness are shown in red-yellow. The probabilistic CST atlas is shown in light blue.

The final multiple linear regression model for PMC thickness retained only NAWM axial diffusivity as a significant predictor (adjusted R^2=.270, p=.001). These results have been published in Multiple Sclerosis Journal (Bergsland N, Laganà MM, et al., 2015).

Assessing potential improvements in the processing pipeline for the automated segmentation of DGM structures

A representative case showing the original and lesion filled segmentation is shown in Figure 4.

Figure 4

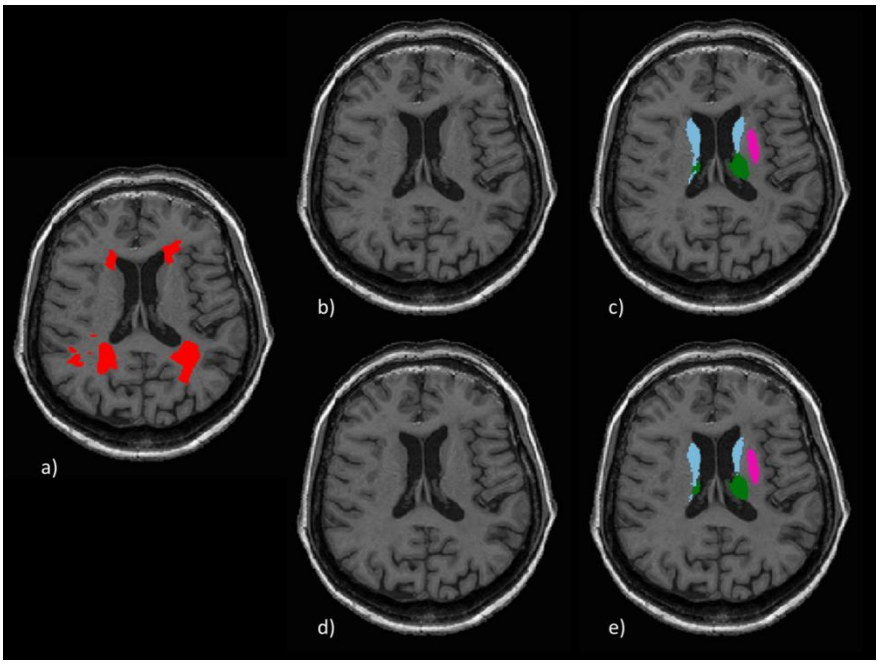

a) Representative 3D T1image with co-registered lesions shown in red. b) Original 3D T1 image
c) FIRST segmentation of original 3D T1 image d) Lesion filled 3D T1 image
e) FIRST segmentation of lesion filled 3D T1 image

Caudates are shown in light blue, thalami are shown in green and putamens are shown in magenta.

With respect to the original segmentations, lesion filled structural volumes were significantly smaller for both left and right thalami ($p < .015$) and caudates ($p < .0001$). Globus pallidus and putamen volumes were not significantly different between the four methods. Thalamic volumes were dependent on the registration while they were independent of the image used for

segmentation ($p = .999$ and $p < .01$, for the same image and same registration comparisons, respectively). Caudate volumes were dependent on the image used for segmentation while they were independent of the registration while they were independent of the registration used for segmentation ($p < .0001$ and $p = .999$ for same image and same registration, respectively).

Vertex-wise analysis of the subcortical surfaces yielded similar results as the volumetric analysis but showed that large portions of the surface were affected beyond just areas of focal WM lesions (Figure 5). These findings were presented as an abstract at the annual ECTRIMS congress (Bergsland N, Dwyer MG, et al., 2015).

Figure 5

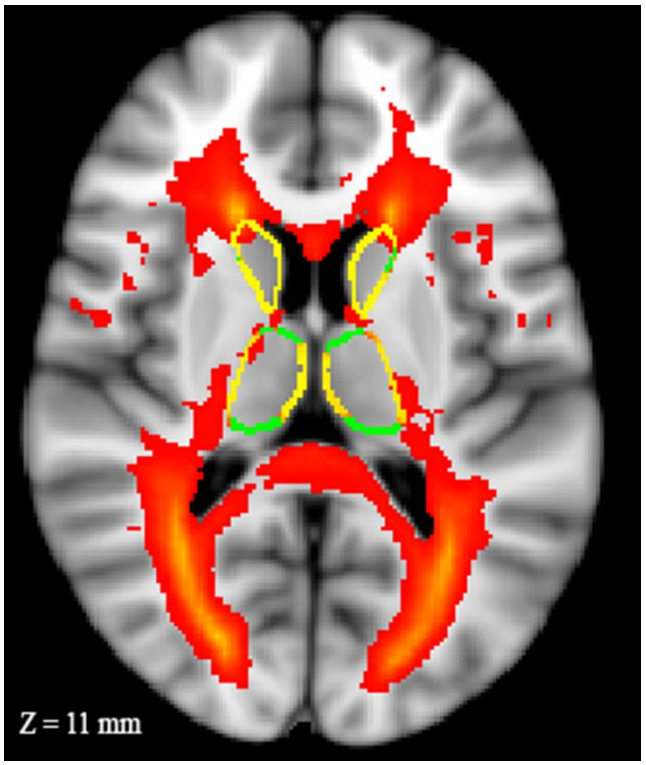

Vertex-wise analysis of the thalami and caudates. Surfaces are shown in green and significant differences where lesion filled segmentations are smaller are shown in yellow ($p < .01$). Vertex-wise analysis of the putamens and globus pallidi did not yield any significant differences along the surface. The lesion probability map is shown in red-yellow, with yellow indicating higher lesion probability. The peak probability is 51%.

With respect to the results obtained when running FIRST independently, the midspace registration technique for longitudinal analysis yielded slightly worse reproducibility and significantly reduced effect sizes.

Assessing potential improvements in the processing pipeline for the automated segmentation of DGM structures

At baseline, MS patients performed worse on all neuropsychological tests; tissue volumes were also smaller while lateral ventricle volume was increased. For both left and right thalami, significant differences between HCs and MS patients were seen with regards to the mean thalamic shape of the cohort (left and right separately). In both cases, shape differences, corresponding to localized atrophy in MS patients, spanned more than half of the surface, including the anterior, medial, and posterior portions of the thalamus. For the left putamen MS patients showed more atrophy along the inferior and lateral surface, whereas no shape differences were found for the right structure. A single cluster showing shape differences along the medial caudate surface was found bilaterally. An additional cluster in the anterior head of the caudate was found on the left side.

Figure 6

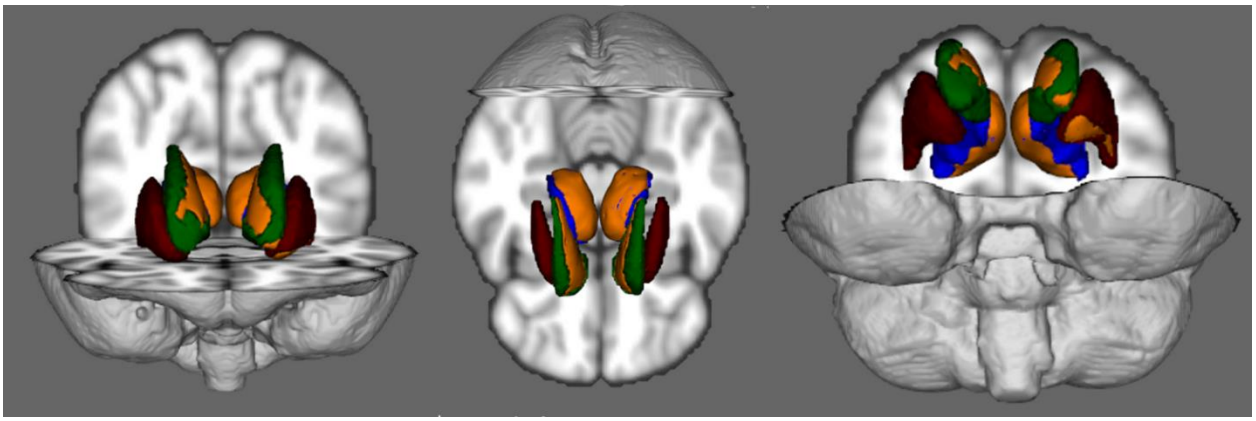

Shape differences between multiple sclerosis patients and healthy controls at baseline. The figure shows the mean shape of the thalamus (blue), caudate (green) and putamen (red). Significant clusters of shape difference, representing local atrophy, between the two groups are shown in orange.

Differences in the rates of change were in the expected direction over the course of the study, with MS patients exhibiting larger degrees of atrophy. However, most of the comparisons did not reach statistical significance. The only significant interaction effect seen was for the putamen ($p = .034$) and with the caudate showing a trend ($p = .074$). In terms of the VBM analyses, no significant differences were found regardless of the smoothing kernel used. With respect to shape changes over time, a significant group by time interaction effect was not seen for any of the examined structures.

At baseline, cross-sectional correlations between neuropsychological tests and shape tended to yield consistent results in terms of both localization and extent across tests (i.e. percentage of surface showing significant relationships). Areas on the surface correlating with SDMT and BVMT-R performance overlapped to a large degree while associations with CVLT-2 performance yielded somewhat smaller clusters (Figure 7).

Figure 7

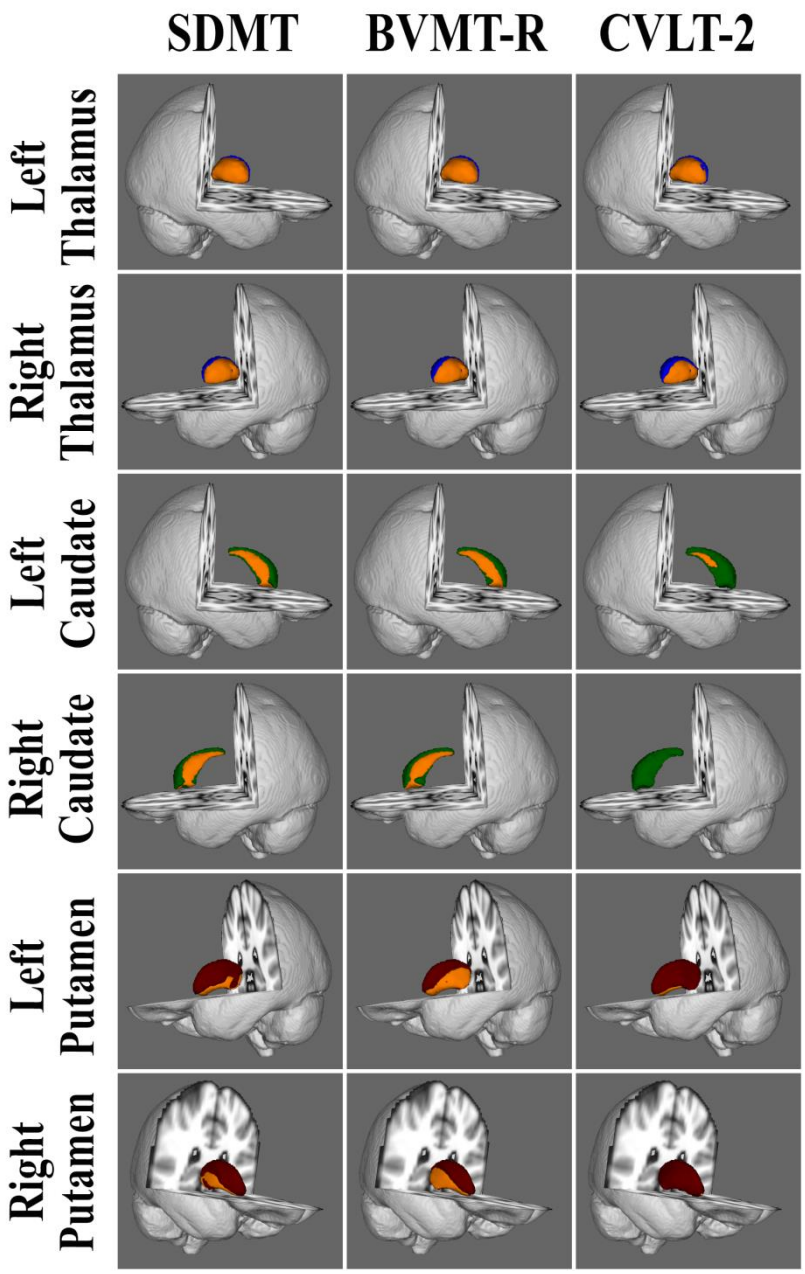

Correlation between localized atrophy and neuropsychological outcomes in multiple sclerosis patients. Significant clusters are shown in orange.
Columns from left to right: SDMT = Symbol Digit Modalities Test; BVMT-R = Brief Visuospatial Memory Test - Revised; CVLT-2 = California Verbal Learning Test - Second Edition

Over the course of the three years of follow-up, focal atrophy of the anterior region of the left thalamus was related to a decrease in cognitive processing speed in MS patients. This effect was only demonstrated when using the surface-based analysis (Figure 8).

Figure 8

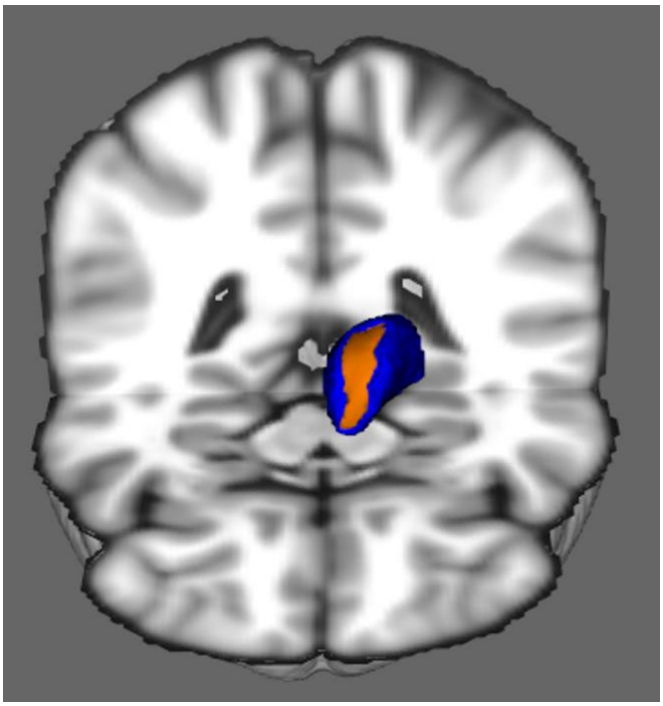

Correlation between localized atrophy over three years of follow-up and decreased performance on the Symbol Digit Modalities Test in multiple sclerosis patients. The figure shows the mean shape of the left thalamus in blue and the significant cluster, spanning 18% of the surface, in orange.

These results were published in Multiple Sclerosis Journal (Bergsland N, Zivadinov R et al., 2015).

Characterizing the relationship between iron deposition within the DGM and WM injury

The voxelwise comparison of high-pass filtered phase images yielded three significant clusters within the DGM where MS patients presented with significantly increased SWI-filtered phase values with respect to HCs (Figure 9). There were no areas of increased phase values in the HC group with respect to MS patients.

Figure 9

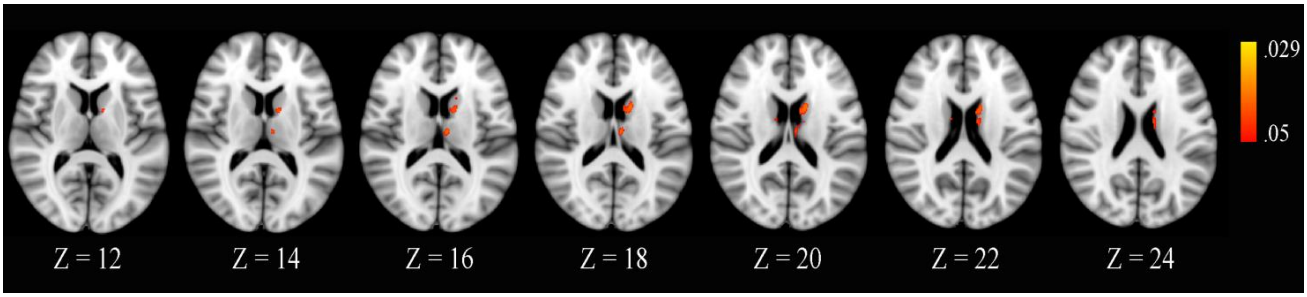

Voxelwise analysis of SWI high-pass filtered phase images within the deep gray matter. Red-yellow clusters are indicative of increased iron concentrations in MS patients with respect to healthy controls, with warmer colors representing smaller p-values. Slices are shown in MNI space for visualization purposes.

The probabilistic atlases generated from seeds within the caudates (left and right separately) consisted of the anterior thalamic radiations and the prefronto-caudate pathway. For the left thalamic seed region, there was considerable overlap for the generated atlas with respect to the one from the left caudate. However, the thalamic seed resulted in an atlas extending through a larger portion of the white matter throughout the brain, as might be expected (Figure 10).

Figure

10

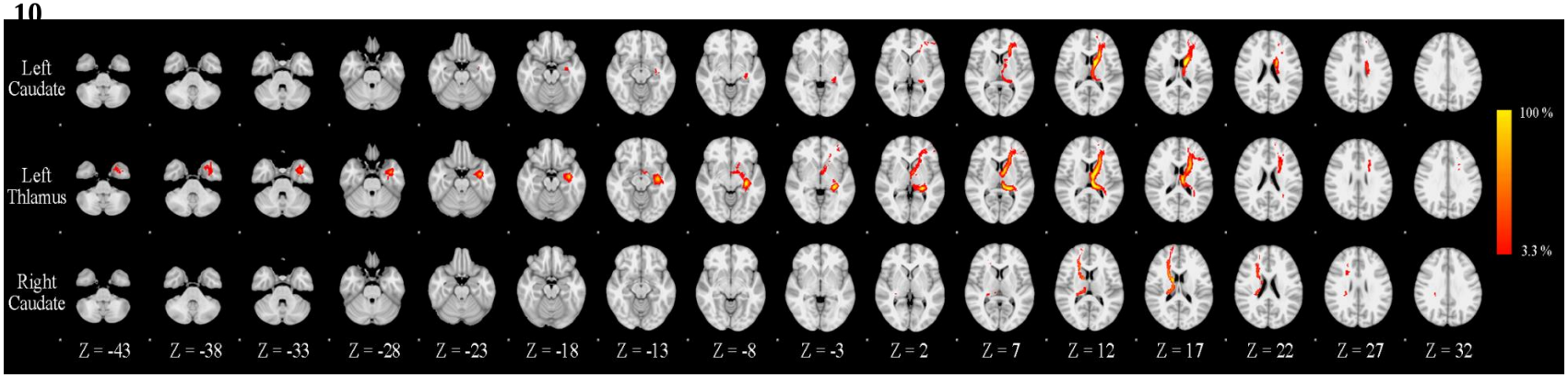

Probabilistic atlases constructed from the healthy control subjects. Probabilistic tractography was performed using seed points derived from the voxelwise SWI high-pass filtered phase analysis. Warmer colors represent an increased probability of a given voxel corresponding to the tract in the sample of healthy controls. Atlases are shown in MNI space for visualization purposes.

As regards the correlations between the cluster-derived SWI-filtered phase values and the associated WM tracts, we consistently found relationships of similar magnitudes with all three measures of diffusivity (i.e. MD, AD and RD) in MS patients as shown in Table 2.

Table 2

	Tract-specific measure								
Phase cluster	Fractional anisotropy		Mean diffusivity		Axial diffusivity		Radial diffusivity		Lesion volume
	HC	MS	HC	MS	HC	MS	HC	MS	MS
L. caudate	**-.467 (.036)**	-.034 (.822)	.193 (.467)	**.452 (<.0001)**	.118 (.639)	**.514 (< .0001)**	.234 (.357)	**.424 (.003)**	**.516 (< .0001)**
L. thalamus	-.008 (.970)	-.207 (.187)	.117 (.639)	**.408 (.003)**	.121 (.639)	**.439 (<.0001)**	.100 (.678)	**.393 (.003)**	**.345 (.012)**
R. caudate	-.363 (.131)	.163 (.321)	.243 (.348)	**.421 (.003)**	.138 (.639)	**.442 (< .0001)**	.293 (.248)	**.400 (.003)**	.230 (.131)

Legend: HC = healthy control; MS = multiple sclerosis; L. = left; R. =right

Partial correlations controlled for age, sex and respective mean diffusivity parameter within the entire normal appearing white matter. Data are shown as r (p). Benjamini-Hochberg correction was used to control the false discovery rate and p-values <0.05 were considered significant (bold). The associated tracts were constructed by seeding the tractography algorithm in HCs in areas where MS patients presented with significantly increased SWI high-pass filtered phase values.

The results from this study are currently under review in AJNR (Bergsland N, Tavazzi E, et al., 2015).

Discussion

In this work, we utilized a broad variety of multimodal, advanced MRI acquisition and processing techniques in an attempt to better characterize and quantitatively measure the multifaceted and still obscure aspects of a complex disease such as MS. In this regard, the core aspects of this thesis related to: the association between WM tract injury and cortical thinning; the association between putative iron deposition within the DGM and damage in the connected WM tracts; the relationship between DGM atrophy and cognitive impairment. Moreover, the effect of WM lesions on performance of some of the key algorithms utilized for this thesis was also assessed. Investigating the aforementioned aspects of the disease was made possible only by exploiting state of the art MRI techniques.

In the first study, which investigated a cohort of patients with RRMS, we showed that MRI measures of WM integrity are related to cortical thickness of an anatomically and functionally connected cortical area. While the investigation of the association between WM injury and cortical damage has been a matter of intense investigation in recent years, very few studies have used such a targeted approach to more precisely characterize these aspects of the pathology. Moreover, we demonstrated that the association between decreased WM tissue integrity and cortical thinning appears to be specific to MS as we did not find this relationship in the HC group. Also of potential interest is the fact that only imaging marker retained in the multiple linear regression model used to predict cortical thickness was a marker of NAWM injury, not focal WM lesions. This finding highlights the role played by advanced imaging methods in leading to a better understanding of MS-related pathology, considering that NAWM injury, by definition, cannot be quantified using conventional MRI measures. The proposed method for studying the way in which WM relates to GM injury is only the first step in leading

to a better understanding of the interplay between these pathogenic mechanisms. To characterize the temporal relation between the two, longitudinal studies are needed. It would also clearly be of interest to assess whether similar patterns are seen when investigating other WM fiber bundles and associated cortical regions. Finally, the qualitative analysis demonstrated that lesion filling should be as a pre-processing technique prior to cortical reconstruction. This is likely to be especially needed when investing samples of MS patients with longer disease durations and larger degrees of focal WM pathology where a greater frequency of juxtacortical lesions is expected, as it was in our study.

In the second study, we assessed two methods with the aim of improving the precision and reliability of DGM segmentation via FIRST. We demonstrated a clear effect of WM lesions for thalamic and caudate segmentations. We found that thalamic segmentation differences were dependent on effects of lesions in registration step used to bring the trained models into the native space of the image. On the other hand, caudate segmentations depended on whether or not the fitting was performed when using either a lesion filled image or one where lesions were still present. Moreover, the surface-based analysis of the thalamus and caudate revealed lesions exerted an influence on the segmentation beyond areas of focal WM injury. This is of particular importance for studies investigating shape changes of the DGM in MS as it suggests that WM lesions, if not corrected for, may explain the findings to some degree. The same argument can be made for longitudinal studies where new or enlarging lesions occurring at follow up may confound the interpretation of shape changes over time if not corrected for in preprocessing. Our proposed approach for improving the sensitivity of longitudinal analyses, however, was not successful as demonstrated by slightly worse ICC values but more importantly, by significantly reduced effect sizes when comparing MS patients to HCs over the course of three years of

follow-up. While these results are somewhat disappointing, they have motivated us to pursue alternative methods for improving the reliability and sensitivity of automated segmentations of the DGM structures in the context of longitudinal studies.

Our third study utilized the FIRST segmentation technique to study the relationship between DGM atrophy and cognitive deficits in a sample of MS patients. Cross-sectionally, a more precise localization of the associations between atrophy of the thalamus, putamen and caudate versus cognitive deficits were revealed than has been previously reported in the literature. The most novel finding though from this study was the demonstration that only via surface-based were we able to relate focal atrophy of the anterior region of the thalamus to decreased cognitive processing speed over the course of three years of follow-up. Nearly all other studies in the literature have relied on using either region of interest based measures of voxel-based morphometry techniques. Our results show, however, that such methods may not be sensitive enough to characterize subtler aspects of atrophy.

In our final study conducted as part of this thesis, we developed and implemented a novel voxelwise-based technique for analyzing SWI-filtered high-pass filtered phase as means to localize areas of putative increased iron deposition within the DGM of MS patients. Using the results from this analysis as means to seed probabilistic tractography allowed us the opportunity to quantitatively assess the potential relationship between WM tract damage and focal iron deposition in the DGM. To the best of our knowledge, the results represent the first time that these two aspects of the disease have been associated by means of such a targeted approach. The exact interpretation of our findings remains to be clarified in future work, particularly in a longitudinal setting. Nonetheless, the results may help shed further light on the pathogenic mechanisms involved and the interplay between these two facets of the disease. Moreover, the

processing pipeline has been implemented in such a way that other iron-sensitive imaging measures can easily be integrated. Thus, the use of techniques such as quantitative susceptibility mapping and R2* mapping may provide additional confirmation of our results.

Conclusion

The aim of this study was to implement and test objective methods for quantifying the relationships between GM and WM damage in multiple sclerosis. We consistently demonstrated the importance of paying close attention, in the preprocessing phase, to the confounding effects of WM lesions in terms of obtaining reliable results. In two separate studies, we found clear evidence of an association between WM injury and GM pathology. For the former, we used WM tractographic methodologies while for the latter we utilized both cortical morphological reconstruction and iron-sensitive acquisition/post-processing techniques. We found that both cortical thinning and a putative marker of increased iron deposition were related to increased NAWM injury in the connected tracts. We also showed for the first time that focal atrophy of the thalamus is associated with a decline in cognitive processing speed over three years of follow-up.

Taken together, the results obtained from the investigations performed as part of this thesis appear to be promising in leading to a better characterization of the association between structure-specific GM, both deep and cortical, and WM injury in multiple sclerosis. These results, moreover, foster new insights yielded by multimodal imaging approaches for studying the multifaceted aspects of the disease.

Chapter 1: Aims and background

In this chapter, the scientific and clinical background of MRI-based methods for quantifying tissue parameters within the gray and white matter will be discussed. The general and specific aims of integrating multiple imaging modalities for the study of multiple sclerosis will be described.

Aims of the study

The aim of this study was to implement and test objective methods for quantifying the relationships between gray matter (GM) and white matter (WM) damage, applicable to the context of neurodegenerative diseases, with a particular focus on multiple sclerosis (MS).

In this context, four main studies were performed which are outlined as part of the specific objectives of this doctoral thesis:

- To study the relationship between damage within the white matter and an area of anatomically/functionally connected gray matter area via the use of tractography and morphological reconstruction of the cortex (Chapter 2)
- To assess potential improvements in the processing pipeline for the automated segmentation of deep gray matter structures using FIRST This objective was done by 1) evaluating the impact of using white matter lesion filling as a pre-processing step and 2) implementing and evaluating a proposed modification for improved precision of segmentations for longitudinal analyses. (Chapter 3)
- To evaluate the utility of surface-based analysis of the deep gray matter structures to more precisely localize the effects of atrophy than is possible using other commonly used techniques such as region of interest and voxel-based morphometry (Chapter 4)

- To develop a method for more precisely characterizing the relationship between iron deposition within the deep gray matter and associated white matter tracts (Chapter 5)

In summary, a broad variety of multimodal, advanced MRI acquisition and processing techniques was used to address the multifaceted and still obscure aspects of a complex disease such as MS. In doing this, the core aspects which were the target of this thesis related to: the association between WM tract injury and cortical thinning; the association between putative iron deposition within the deep GM (DGM) and damage in the connected WM tracts; the relationship between DGM atrophy and cognitive impairment. Moreover, the effect of focal WM pathology on performance of some of the key algorithms utilized for this thesis was also assessed. Investigating the aforementioned aspects of the disease was made possible only by exploiting state of the art MRI techniques, as introduced below.

Advanced MR imaging techniques for the study of multiple sclerosis

MS is an auto-immune mediated inflammatory disorder causing widespread damage throughout the central nervous system (CNS). The exact etiology of the disease is still not fully understood, but it is likely due to the interaction of genetic, viral and environmental factors[22]. The diagnosis and follow-up of MS patients has been revolutionized with the aid of magnetic resonance imaging (MRI). MRI has allowed for the monitoring of the effects of the disease within the CNS in vivo.

Although conventional imaging methods (e.g. PD/T2-weighted) are very sensitive to inflammation within the white matter (WM), they are severely lacking in their specificity. A T2 hyperintensity may correspond to a number of different pathological substrates, including inflammation, demyelination, oligodendrocyte injury, gliosis or axonal loss[23]. Moreover, while

lesion counts and localization are highly important in making a diagnosis of MS[24], they remain relatively modest predictors of clinical disability. This discrepancy, often referred to as the clinico-radiologcal paradox[25], has motivated the investigation and development of other imaging measures in an aim to better characterize the disease.

Conventional MRI techniques have also proven to be relatively insensitive to pathology within the gray matter (GM). Unlike within the WM, normal GM and lesional GM relaxation times are relatively similar due to mid blood-brain barrier disruption and much less inflammation due to minimal T-cell infiltration[26]. However, due in large part to the development of more advanced MRI measures with greater specificity[27, 28], as well as data from histopathological studies[26, 29, 30], MS has increasingly been recognized as having a neurodegenerative component as well[31]. The role of the GM in this regard has drawn a significant amount of attention in the past decade as GM measures have been often shown to serve as better prognostic indicators of the disease than those of the WM[32-34].

From both an acquisition as well as a post-processing point of view, a number of advanced MRI-based methods have been developed in recent years. Such techniques have the possibility to quantitatively characterize tissue properties in a way that is not possible using conventional imaging. The following sections discuss several of the advances in the field which have been utilized in this thesis. The motivation for having used these specific techniques is also given.

Structural segmentation

MS is characterized by an increased rate of tissue atrophy with respect to healthy controls (HC). Indeed, disability progression[3] and cognitive impairment[4, 5] appear to be heavily dependent on

irreversible GM loss. Initial reports that focused on quantifying structural atrophy in MS generally relied on manual, region of interest measures. Several different methods have been proposed in the literature, including the measure of third ventricular width[33], corpus callosum midline area[35], bicaudate ratio[36]. However, manual tracing/measuring techniques are labor intensive and potentially more user dependent. These drawbacks are particularly true for methods that require a high level of expertise. For example, due to its highly convoluted nature, with a remarkable individual diversity, in addition to the immense number of anatomically/functionally distinct regions, the task of cortical parcellation presents a considerable challenge. Moreover, some structures have ill-defined borders when imaged using conventional imaging techniques. To help overcome such issues, protocols have been developed to establish clear guidelines to reduce intra-subject variability and increase the precision/accuracy of the obtained measures[37-40]. However, the shear amount of time and work required to process even a single case often puts fully manual methods beyond the reach of most researchers. The use of surrogate measures, such as measuring third ventricular width as an indirect measure of thalamic atrophy, provides a potential solution but such methods are unlikely to be perfectly related to the target of interest. As a consequence, there has been considerable interest in the development and validation of automated (or at least semi-automated) methods for structural segmentation.

Cortical reconstruction and labeling

FreeSurfer is one of the most widely used tools for the morphological reconstruction of the cortex. FreeSurfer requires a high resolution, 3D T1-weighted image with sufficient GM/WM contrast, at least. One of the key advances in the processing methodology used by FreeSurfer is

that it works with a surface-based representation of brain tissue classes. After initial preprocessing (including registration to Talairach space, skull stripping, and B1 bias field correction), the processing pipeline identifies the WM on a voxelwise basis. The resulting WM mask is converted into a 2D surface which is subsequently refined such that it more accurately follows the intensity gradient between WM and cortical GM. Geometrical constraints are imposed along with automated topology correction to prevent surface reconstructions that would be anatomically impossible (e.g. holes within the WM or "islands" of isolated WM tissue). The pial surface, which corresponds to the boundary between cortical GM and sulcal CSF, is then identified by expanding the WM surface, again following the intensity gradient. The use of the intensity gradients rather than individual voxel intensity values directly allows for optimal placement of the surface boundaries at subvoxel resolution. Specifically, surfaces are parametrized as mesh of vertexes. Once the WM/GM and pial surfaces have been identified, morphological measures such as cortical thickness and curvature can be calculated. In the case of cortical thickness, this corresponds to the distance between the two surfaces as shown in Figure 1. On the other hand, cortical curvature reflects the gyral/sulcal folding patterns within the brain, which is a key aspect in the algorithm for automated parcellation as further described below.

Figure 1

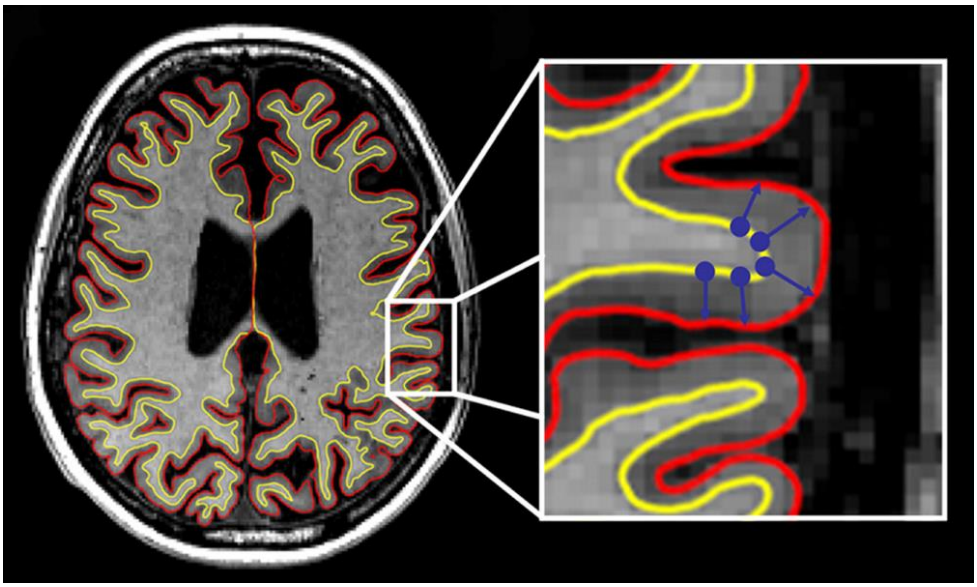

TheWM/WM surface is shown in yellow whereas the pial surface is shown in red.
In the insert, the blue arrows demonstrate how cortical thickness is calculated.
Figure adapted from Steenwijk et al., 2014 [20].

Based on manually labeled images created by expert readers, FreeSurfer also provides a set of probabilistic atlases for automated labeling of the cortical surface. The details of the atlas construction have been previously described and as the specifics are not the focus of the current study, only a summary will be given. Briefly, the manually labeled parcellations were mapped onto a sphere based on the individual cortical folding patterns of the training subjects. Once new subjects have been morphologically reconstructed, their surfaces can be aligned with this atlas using nonlinear registrations. As with the construction of the template itself, the registration is based on aligning the cortical folding patterns. This has the effect of aligning the anatomy itself rather than mapping image intensities. An example of a representative parcellation is shown in Figure 2.

Figure 2

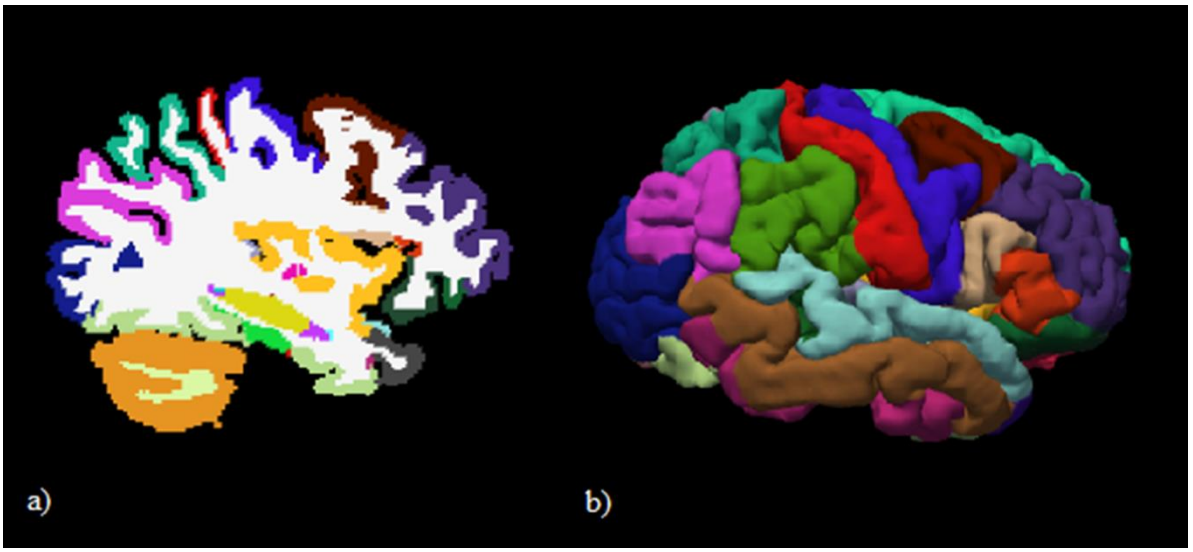

Labeling of a representative subject analyzed as part of the current study. The representation shown in a) shows the parcellation in a voxelwise manner such that each voxel is assigned as belonging to a discrete tissue class or structure. The labeling itself is done via nonlinear surface-based registration to a template. A 3D representation of the same cortex is shown in figure b). Note that the cortical reconstruction stream removes the cerebellum and is thus not shown despite being present in figure a).

Subcortical segmentation

Several algorithms have also been proposed for performing automatic segmentation of the subcortical GM structures. As previously mentioned, one of the inherent challenges is that conventional imaging techniques are often insufficient to depict the precise anatomical borders. For example, although the thalamus consists of primarily GM, several WM tracts pass through it resulting in an overall reduction in GM/WM contrast. As a result, it is much more difficult to outline it accurately without considerable training and thus motivates the use of automated methods (Figure 3).

Figure 3

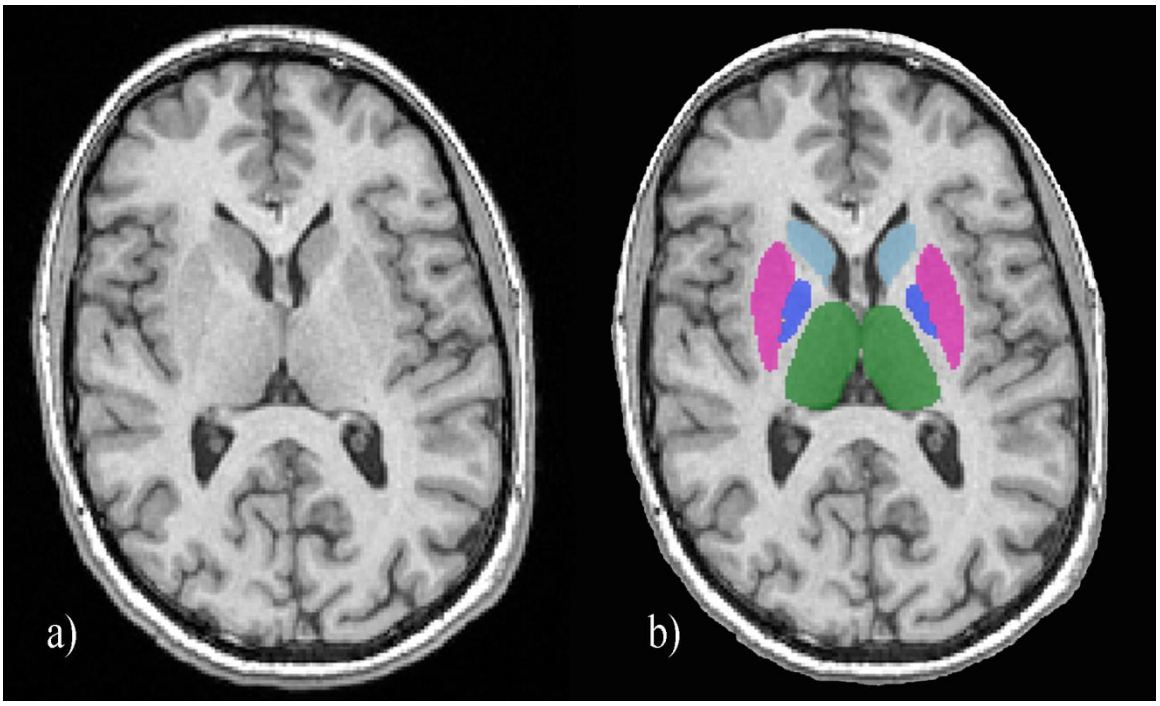

A representative 3D T1-weighted image acquired on a 1.5T scanner, as part of the current study, is shown in a). The resulting segmentation using FIRST is shown in b). Note that the lateral border of the thalamus is particularly difficult to accurately identify in a).
Color coding: thalamus = green; putamen = magenta; caudate = light blue;
globus pallidus = dark blue

One common method which is conceptually straightforward is to use nonlinearly registered probabilistic atlases (again based on manual segmentations by an expert) for voxelwise classification. This is the approach taken by FreeSurfer, although in this case a separate processing stream[6] is utilized than the surface-based one already described. A novel approach included as part of the FSL software package is FMRIB's Integrated Registration and Segmentation Tool (FIRST)[7]. The FIRST method still relies on training data but rather than mapping a probabilistic atlas, it uses 3D deformable mesh models. The trained models are based on manual segmentations parameterized as surface meshes, which are composed of a fixed

number of vertices per structure. The training dataset consists of over three-hundred individual MRIs with of a wide range of subject characteristics (e.g. healthy controls, schizophrenia, Alzheimer's disease, prenatal cocaine exposure). Once initialized via an affine registration, the models are iteratively deformed via displacement of the vertices. Shape and intensity information make up the actual models; both aspects will be briefly discussed. For the former, the average shape from all vertex locations is parameterized. The modes of variation about the mean are also captured within the model using principal components analysis. Taken together, the mean and mode represent the prior probability distribution within a Bayesian framework. The modes of variation are then iteratively searched in a linear fashion to find the best match in image to be segmented. This is achieved by sampling the image intensity along the surface normal and compared to the corresponding intensity information stored in the trained models (Figure 4). Thus, the procedure provides an efficient means of describing the most typical shape variations.

Figure 4

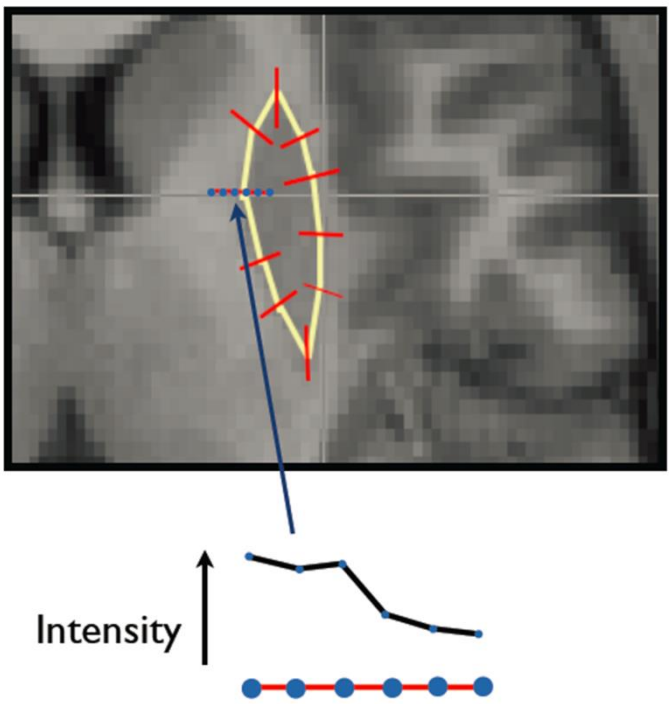

The figure shows a representation of sampling image intensities along the surface normal (red lines) of the putamen (yellow outline). Note that only a limited number of vertices are shown for demonstrative purposes; many more are used in the actual implementation. The lower figure represents the sampling of the intensities along a given surface normal. The sampled intensities are then compared to the corresponding intensities for that mode of variation in the training dataset. (Adapted from FSL course materials http://fsl.fmrib.ox.ac.uk/fslcourse/lectures/)

FIRST also maintains vertex correspondence across subjects during segmentation. This opens the door to the possibility of performing group-based, vertexwise analyses to reveal localized shape changes. As no smoothing is required, this approach potentially provides a more sensitive method to characterize the localization of atrophy. This is in contrast to techniques such as voxel-based morphometry (VBM) whereby data is smoothed, often with relatively large kernels, before performing any statistical inferences. Although VBM has received an enormous amount of attention in the literature, the smoothing step, by definition, results in the mixing of

areas with potentially disparate signal characteristics. As a consequence, it is likely much more difficult, if not impossible, to precisely characterize atrophy within a given structure. For example, the thalamus contains many different sub-nuclei[41], each with their own afferent/efferent connections, function and possibly different susceptibilities to pathological processes. Thus, traditional volumetric methods are unlikely to capture the exact localization. On the other hand, testing the individual vertices that make up the structural surface provides a means to overcome the limitations imposed by the traditional voxel-based approach.

Despite the advantages offered by FIRST for subcortical segmentation, it is important to consider that it was not explicitly trained nor tested during development with imaging data from MS patients. Thus, there is no guarantee that it will necessarily perform accurately in the presence of focal WM pathology. This problem is aggravated by WM lesions having a high predilection for periventricular areas[42], which also happen to be close to several of the DGM structures. As WM lesions often result in T1 intensities more similar to that of GM, it is likely that they may bias the overall final results. There have been some investigations into the effect of WM T1 hypointensities on subcortical segmentation of data from MS patients using FIRST. However, the results have been conflicting with respect to whether or not correcting for lesions prior to segmentation is required or not. Some have demonstrated a clear effect[43] while others have reported that they do not make a significant difference on the quality of the segmentations[44]. In the case of the former study, the authors did not explore in detail how WM lesions potentially exert their influence on FIRST (i.e. whether the effect is driven by registration or model fitting inaccuracies).

FIRST has been developed as a cross-sectional tool. However, it has been used in the literature for longitudinal studies as well. The general approach in these studies has been to

perform post-hoc modelling of data acquired at each time point. While conceptually simple, a potential drawback is that there are multiple sources of measurement error. Thus, the availability of improved methods for longitudinal processing would be likely to provide measures with more reliability and overall precision. A subsequent increase in statistical power could improve the ability to detect biological changes or reduce the required sample sizes to detect an effect.

Diffusion-weighted imaging

Diffusion-weighted imaging (DWI) exploits the physical process governing the Brownian motion of water molecules within tissue. The technique, as most commonly implemented, uses a spin echo. DWI is made sensitive to the movement of water molecules via the application of diffusion-sensitizing gradients. Specifically, a pair of strong gradient pulses is inserted around the 180 refocusing pulse. Thus, stationary spins remain unaffected by the gradient pair since the effects of the first half are subsequently undone by the second. On the other hand, spins which have diffused elsewhere in between the gradients will lose their phase coherence, ultimately leading to reduced intensity in the measured signal. Due to its inherent ability for rapid acquisitions, echo planar imaging (EPI) is most commonly used for DWI sequences. The use of EPI reduces the sensitivity to motion artifacts otherwise present with long acquisitions. Just as important, it opens the door to the possibility of acquiring many gradient-directions, which is required for a more precise characterization of the underlying diffusion processes.

Diffusion tensor imaging (DTI) is a widely used model for describing the random motion of water molecules in brain tissue. The key concept is that that tissue characteristics such as its type (i.e. GM or WM), architecture, inter-/intra-cellular barriers and overall integrity will ultimately influence the diffusion of water molecules. In general, diffusion within WM tends to

be the most restrictive due to the axonal membrane and surrounding myelin. As a natural consequence, WM diffusion is largely anisotropic, as water molecules will preferentially diffuse along the direction of the axon. On the other hand, diffusion within the GM tends to be more isotropic in nature and within the CSF it is essentially completely unrestricted. For modeling these characteristics, the diffusion tensor model can be adopted which is described mathematically as a symmetric 3x3 matrix:

$$\begin{matrix} D_{XX} & D_{XY} & D_{XZ} \\ D_{XY} & D_{YY} & D_{YZ} \\ D_{XZ} & D_{YZ} & D_{ZZ} \end{matrix}$$

Quantification of tissue microstructure properties

Diagonalization of the diffusion tensor results in the eigenvalues (λ_1, λ_2 and λ_3) as well as the eigenvectors ($\hat{e}_1$, $\hat{e}_2$, $\hat{e}_3$). Several quantitative parameters can thus be obtained from the obtained eigenvalues, including:

1. Mean diffusivity (MD), representing the average magnitude of the diffusion, is given by:

$$MD = \frac{\lambda 1 + \lambda 2 + \lambda 3}{3}$$

2. Axial diffusivity (AD), representing the magnitude of the diffusion along the principal eigenvector, is simply λ_1
3. Radial diffusivity (RD), representing the magnitude of diffusion perpendicular to the principal eigenvector, is given by:

$$RD = \frac{\lambda 2 + \lambda 3}{2}$$

4. Fractional anisotropy (FA), representing the degree of diffusion asymmetry and ranging from 0 (perfectly isotropic diffusion) to 1 (perfectly line-like), is given by:

$$FA = \sqrt{\frac{3}{2}} * \frac{\sqrt{(\lambda 1 - MD)^2 + (\lambda 2 - MD)^2 + (\lambda 3 - MD)^2}}{\sqrt{\lambda 1^2 + \lambda 2^2 + \lambda 3^2}}$$

The tensor-derived parameters have been used by many studies as a means to quantify underlying tissue microstructure integrity. Moreover, they have shown to be very sensitive to pathology that is otherwise not detectable using conventional imaging techniques[2, 10, 11, 45, 46]. For example, results from one murine model for studying WM pathology suggested that increased RD without any change in AD could be interpreted as a marker of demyelination[8]. Budde and colleagues reported that AD was the primary correlated of axonal image[47] in another murine model used specifically for emulating the effects of MS. FA is also often interpreted as an overall measure of tissue integrity. Despite such tantalizing findings, caution is warranted before considering these as truly specific pathological markers. This can be understood by considering the diffusion tensor model in the presence of multiple fiber populations in a given voxel. In this case, FA values will naturally be reduced since there is no single preferential diffusion direction. This is particularly discouraging considering that when using standard imaging acquisitions, the majority of WM voxels in the brain is characterized by crossing fibers[48]. Furthermore, it has been shown that changes in AD can result in spurious alterations of RD (and vice-versa) when multiple fiber tracts are present in a voxel[49]. Nonetheless, the aforementioned parameters have enjoyed widespread use in the literature. Indeed, the DTI-derived values are likely capturing some of the effects happening at the level of the microstructure even if the pathological specificity remains somewhat questionable. Thus, one needs to consider the aforementioned caveats when interpreting them.

Tractography

Beyond providing measures of the underlying tissue properties, DTI has also seen an enormous success in the realm of tractography. Tracrographic algorithms allow for the virtual reconstruction of WM bundles in vivo. A number of different approaches have been proposed, each with their own advantages. Deterministic DTI-based tractography is conceptually relatively simple. The key idea is to use the principal eigenvector as a surrogate measure for the orientation of the underlying fiber bundle. Thus, tracts can be reconstructed by iteratively following the direction given by the principal eigenvector in a given positon until certain criteria are no longer met. In this regard, examples include limiting reconstruction to voxels that have a minimum FA value (under the assumption that WM should be more anisotropic than GM), the bending angle does not exceed some threshold (to prevent anatomically implausible reconstructions) or ensuring that reconstructions pass through or begin in certain area(s) (to include a priori anatomical knowledge). The exact parameters will of course depend on the specifics of the algorithmic implementation as well as the overall aim of the experiment. Despite the simplicity of the approach, DTI-based tractography is inherently hampered by the fact that a given voxel is described by only a single tensor. As a consequence, there is a fundamental problem in any area where multiple fiber populations are present. In this case, the principal eigenvector no longer corresponds to the underlying tracts and smaller fiber tracts are likely to be difficult to reconstruct properly. Given that up to 90 percent of the voxels acquired in a standard diffusion-weighted experiment are estimated to have more than one fiber population[48], the single tensor approach clearly has its limitations.

Several alternative tractographic methods have been developed in recent years to overcome the limitations imposed by the single diffusion tensor model. For example, high

angular resolution diffusion imaging (HARDI) can be used for so-called q-ball imaging whereby multiple intravoxel orientations can be resolved without any a priori assumptions regarding Gaussianity (or multi-Gaussianity) of the diffusion process[50]. Nonetheless, as implied by the name of the acquisition scheme, HARDI requires many gradient directions, potentially limiting the utility within a clinical setting. On the other hand, the so-called "ball and stick" model does make some assumptions regarding intraxvoxel diffusivity[51]. Specifically, the model accounts for an isotropic component (the "ball") in addition to a single anisotropic direction (the "stick"). This approach has the benefit of resolving ambiguity with respect to the diffusivity profile and degree of uncertainty. In addition, the model naturally extends to multiple fibers within a single voxel via the inclusion of additional anisotropic components. The technique uses Markov Chain Monte Carlo sampling for estimating local probability density functions to create distributions of the diffusion parameters at each voxel. Armed with the voxelwise distributions of the principal diffusion directions, one can proceed with probabilistic tractography. While an increased number of gradient directions is certainly desirable in the ball and stick model as well, the approach has been successfully used with even relatively modest acquisition schemes[52-54]. In fact, one study found that having only twelve diffusion encoding directions still allows for a reproducible reconstruction of several key WM bundles[55].

In the case of focal WM damage, tractography algorithms often fail to properly reconstruct the underlying WM tract. In the case of MS, conventional T2-weighted WM lesions demonstrate heterogeneous pathological substrates. Regardless of the specific underlying pathology, the primary eigenvector may no longer reflect the correct orientation or FA values may end up below the stopping threshold. The practical consequence in either case may ultimately be an incorrect or aborted reconstruction of the fiber tract. Which scenario plays out

will depend on a combination of the tractography parameters used for reconstruction as well as the overall degree of pathology. For example, a WM lesion with a mild degree of inflammation might not pose significant problems. On average, probabilistic tractography approaches are more likely to be able to track through lesions but there is of course no guarantee in the event of severe tissue destruction, where also deterministic algorithms are all but certain to fail. To overcome these limitations, atlas-based methods have been proposed[12, 13]. In this context, tractography (deterministic or probabilistic) is used individually in healthy control subjects in order to generate an atlas. The result is then registered to patient data to extract the parameters of interest, thus bypassing the lesion problem altogether.

Susceptibility-weighted imaging

An increased degree of iron deposition, particularly within the DGM, is also a commonly reported feature of MS[14-17]. It is still a matter of debate as to whether iron deposition plays a role in the neurodegenerative aspects of the disease or is merely an epiphenomenon. Nevertheless, a number of iron-sensitive imaging markers have been developed and validated in the last several years. For example, phase imaging has seen an enormous success in recent years due to its sensitivity to local inhomogeneity in the presence of paramagnetic materials.

Historically, the phase component of the complex signal acquired during an imaging experiment was discarded[i]. An example of the magnitude and phase images from a T2* gradient echo (GRE) acquisition are shown in Figure 5.

[i] A notable exception is phase-contrast MRI, which has important applications for studying the flow of fluids such as blood and cerebrospinal fluid. Phase data has also been used in inversion recovery acquisitions.

Figure 5

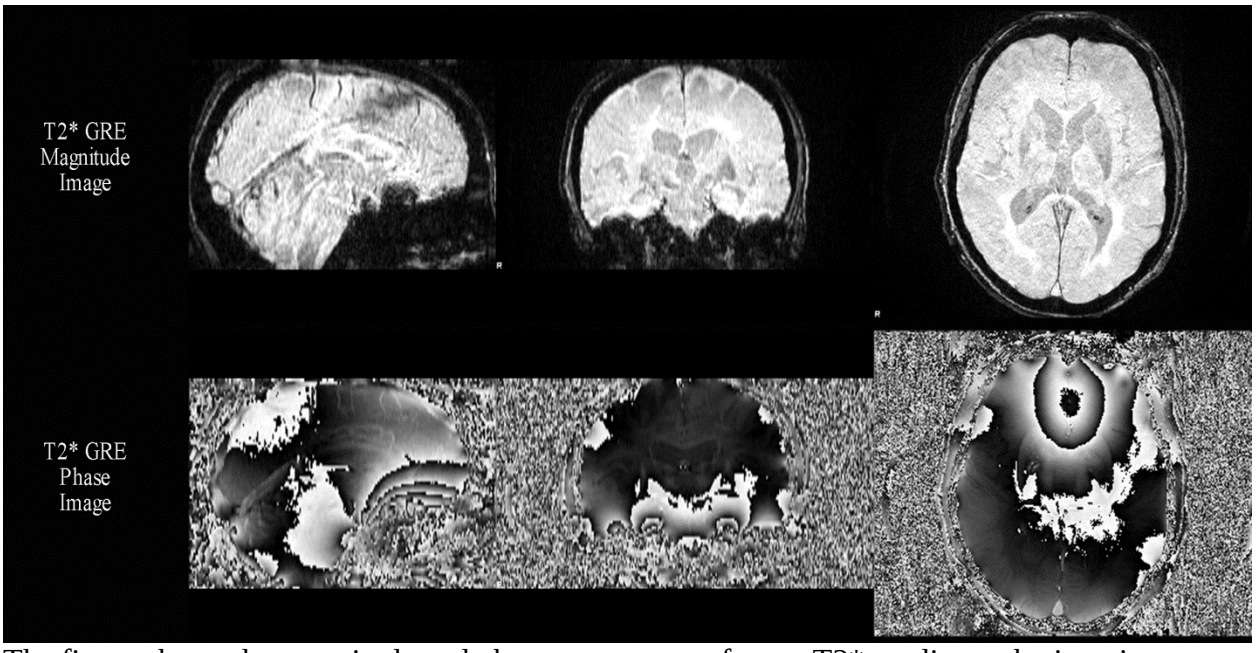

The figure shows the magnitude and phase components from a T2* gradient echo imaging experiment.

At first glance, it appears as though the phase image might be practically unusable due to the severe phase wraps. However, upon closer examination, it is clear that there is potentially interesting information present in the image which is complementary to that found in the magnitude image. Specifically, the contrast offered by the phase image provides a means to investigate susceptibility differences between tissues. In Figure 5, the phase image appears to show better GM/WM contrast with respect to the magnitude image. While the posterior areas are relatively free of artifact, the anterior portions are severely affected. These artifacts correspond to phase wraps as a result of macroscopic inhomogeneity of the B0 field. This explains why the anterior portion is so heavily affected – this corresponds to a primary area where there is an air/tissue boundary with very large susceptibility differences. In fact, susceptibility differences between tissue types within the brain are order of magnitudes smaller than air/tissue. However,

the B0 field is also affected by microscopic inhomogeneity stemming from paramagnetic sources such as iron depositions and deoxyhemoglobin or diamagnetic sources such as oxyhemoglobin and calcium.

Haacke et al. initially proposed the use of homodyne highpass filtering[56] to eliminate the bulk of effects due to macroscopic inhomogeneity[57]. This overall idea is to first generate a low pass filtered phase image and then complex divide the result into the original phase image in order to generate the final highpass filtered image. In practice, this is generally achieved via a 64 x 64 central k-space window. The exact size of the window used will of course alter the characteristics of the highpass filtered image. For example, a smaller window (e.g. 32 x 32) will yield better tissue contrast at the expense of worse performance in handling phase wraps. Haacke et al. proposed an additional post-processing step which combines in the magnitude and the phase image into a single susceptibility-weighted image (SWI). In practice, a fully flow-compensated (i.e. in all three directions) 3D GRE acquisition is used. In addition, a long TE is chosen such that susceptibility effects are maximized while maintaining a sufficient signal to noise ratio[57].

SWI images provide an excellent means for visualizing vasculature as well as iron deposits. However, for assessing the latter, SWI remains mostly useful for qualitative purposes. On the other hand, the SWI high-pass filtered phase image provides a means for semi-quantitatively, albeit indirectly, measuring iron levels. Figure 6 shows the result of the SWI-highpass filter applied to the phase image shown previously in Figure 5. As can be seen, the phase wraps have been effectively eliminated with the aid of the homodyne filter.

Figure 6

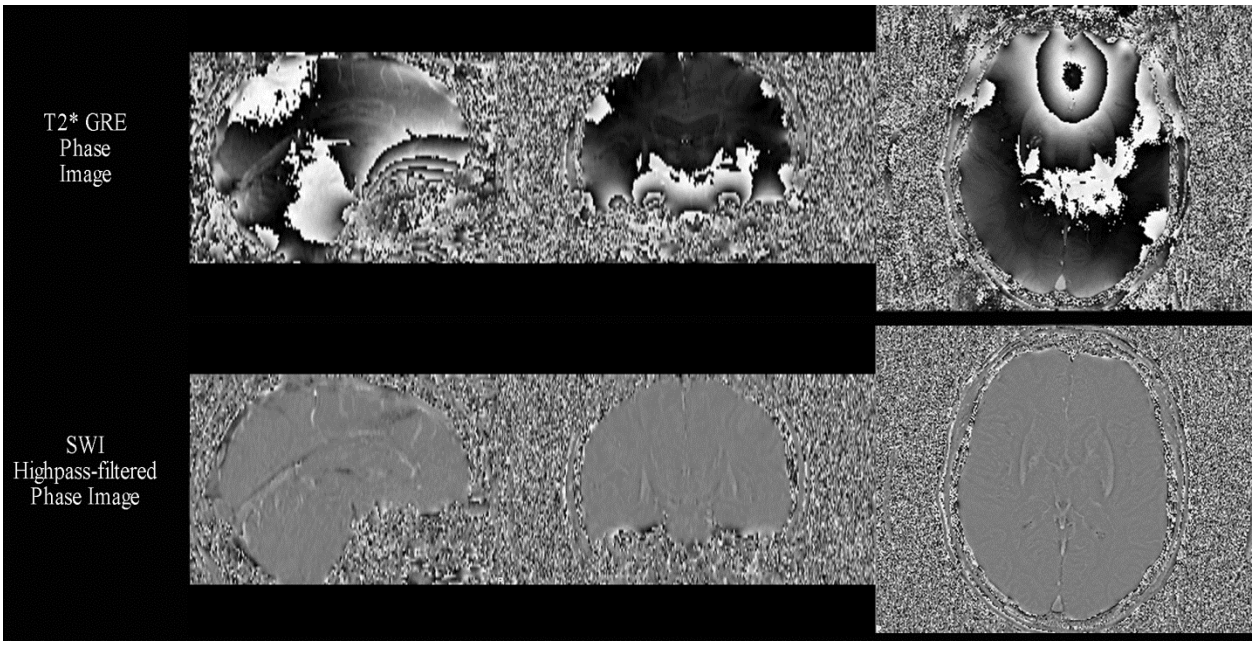

Despite the straightforward post-processing implementation of the highpass filter, the approach does have its limitations. Specifically, the resulting phase values still contain nonlocal effects and are orientation dependent. These drawbacks have motivated the development for truly quantitative measures of susceptibility in recent years. To this aim, quantitative susceptibility mapping (QSM) techniques have overcome many of the limitations of the SWI high-pass filtered phase approach and have opened the door even further to exploiting the unique contrast offered by phase imaging. However, it must be noted that QSM algorithms generally require the availability of the raw (i.e. not highpass filtered) phase data. On the other hand, a recently proposed method termed susceptibility weighted imaging and mapping (SWIM) does provide the potential to generate quantitative maps even when only the highpass filtered phase image is available[58]. Regardless, the SWI high-pass filtered phase approach has seen a tremendous amount of use in recent years for assessing putative iron content within the deep gray matter[59-62] as well as changes within white matter, particularly within lesions [59, 63-65]. While the

interpretation of phase changes within the white matter remains somewhat controversial, a strong relationship has been found between iron content and SWI high pass filtered phase values within the DGM. In fact, the latter has been shown using both synchrotron X-ray fluorescence[18] and comparisons with published reports of putative iron concentrations acquired from post-mortem data[19].

Multimodal imaging

The use of multiple MR imaging modalities for a given study has seen a dramatic rise in popularity in recent years. There are several advantages that stem from combining the often complementary information provided by different sequences or image weightings.

The overall sensitivity/reliability of imaging analyses can be significantly improved with respect to when using just one modality. For example, in the novel boundary-based registration (BBR) technique[66], tissue class separation is first performed on the reference scan via either surface reconstruction or volumetric segmentation. Next, the intensity gradient across tissue boundaries in the moving image is maximized as the registration cost function. While not strictly a multimodal technique per se, BBR has enjoyed widespread use in the registration of lower quality images with vastly different tissue contrasts. Thus in the context of functional MRI[67, 68], diffusion-weighted[69, 70] and perfusion[71, 72] experiments, BBR can help to achieve more accurate registrations than otherwise possible using traditional techniques.

Perhaps the biggest impact that multimodal imaging has had is on shedding further light on the underlying pathological substrates involved in neurodegenerative diseases, including MS. The integration of multiple techniques can be used to provide insight into the association between pathogenetic mechanisms or how damage in one tissue compartment might be related to

that in another. For example, DTI-derived measures of WM microstructure can be combined with structural segmentations/reconstructions of the GM to quantify associations between damage the two tissue compartments[20, 21]. Integrated post-processing pipelines can also aid in automated analyses whereby segmentations from high resolution structural data is used to extract quantitative measures from another acquisition type. Such approaches have been successfully utilized with a wide range of imaging techniques (e.g. SWI high-pass filtered phase measures within the DGM[16], T2* mapping within the cortex[73]).

Thesis structure and author's personal contribution

In this section, the structure of the remaining chapters is summarized, describing the overall aims and obtained results while highlighting the author's personal contribution.

Chapter 2 describes a multimodal imaging study combining diffusion-weighted imaging with high-resolution 3D T1-weighted acquisitions. The relationship between white matter and cortical gray matter damage was evaluated in a sample of 51 relapsing-remitting MS patients and 30 healthy controls. Part of the preliminary work included the acquisition of the MRI data itself for a portion of the sample. It should be noted though that some of the imaging exams had already been acquired before beginning the doctoral program. All MRI data was acquired on a 1.5T scanner at Fondazione don Carlo Gnocchi, IRCCS Santa Maria Nascente (Milano, Italy). The primary analysis pipelines used in this chapter were developed based on existing software, including FMRIB's Software Library (FSL) and FreeSurfer. Novel contributions included: 1) implementation of an optimized lesion filling pipeline 2) a preliminary analysis of the evaluation of WM lesions on morphological reconstructions of the cortex and 3) optimization of the process

for obtaining meaningful measures of the normal appearing white matter in the presence of focal pathology. The author performed all of the cortical reconstructions himself and implemented/optimized the processing pipelines. The author performed quality control at all intermediate and final steps of the analysis. Preliminary results of this study were presented as a conference proceeding (Bergsland N, Laganà MM, et al., ISMRM 2014) while the final work has been published (Bergsland N, Laganà MM, et al. Mult Scler.).

Chapter 3 assesses potential improvements to automated segmentation of the deep gray matter structures using FMRIB's Integrated Registration and Segmentation Tool (FIRST). Two groups of subjects were evaluated, all acquired at the Buffalo Neuroimaging Analysis Center in Buffalo, NY, USA. The first group, consisting of 152 relapsing-remitting MS subjects, was acquired on a 1.5T scanner and the effects of white matter lesions were evaluated. This aim was achieved by comparing both volumetric- and surfaced-based measures of several deep gray matter structures (thalamus, caudate, putamen, globus pallidus) obtained after a lesion filling pre-processing step (as implemented in chapter 2) with respect to the original images. The author performed and quality controlled all segmentations and surface-based analyses. The second group, consisting of 64 MS patients and 22 healthy controls, was acquired on a 3T scanner at baseline and again after 3 years. The author implemented a change to the processing pipeline in an attempt to account for the longitudinal nature of the MRI data with a final aim of obtaining more precise measures of atrophy. Ultimately, the proposed longitudinal approach failed to yield improved measures but did provide insights for future developments. Results from this study were in part presented as an abstract (Bergsland N, Dwyer MG, et al., ECTRIMS 2015) while additional experiments are still ongoing as part of the full paper to be submitted (Bergsland N, Dwyer MG, et al.)

Chapter 4 investigates the utility of surface-based analysis for more precisely quantifying both the localization and neuropsychological associations of deep gray matter atrophy. 64 MS patients and 22 healthy controls were acquired on a 3T scanner at the Buffalo Neuroimaging Analysis Center in Buffalo, NY, USA. The analysis presented in this chapter is a sub-study within a larger study at the University at Buffalo that investigated MRI and neuropsychological changes in a cohort of MS patients and demographically group-matched healthy controls. Pre-processing pipelines developed in the previous chapters combined with FSL were applied to the study of deep gray matter atrophy and its relation to cognitive deficits. The cohort as a whole remained remarkably stable over the course of three years. However, using a surface-based analysis, anterior thalamic atrophy was found to correlate with decreased cognitive processing speed over the follow-up. Such an effect was not seen with other imaging methodologies, thus highlighting the utility of the surface-based approach. All structural analyses were performed and quality controlled by the author. Results from this study were presented as an abstract (Bergsland N, Zivadinov R, et al., ECTRIMS 2015) while the final work has been published (Bergsland N, Zivadinov R, et al., Mult Scler.)

In chapter 5, a novel method is proposed for investigating the relationship between focal iron deposition within the deep gray matter and injury in the associated WM tracts. The pipeline was used in a cohort of 66 MS patients and 29 HCs acquired on a 1.5T scanner at Fondazione don Carlo Gnocchi, IRCCS Santa Maria Nascente (Milano, Italy). Part of the preliminary work included the acquisition of the MRI data itself for a portion of the sample. It should be noted though that some of the imaging exams had already been acquired before beginning the doctoral program. Publicly available neuroimaging software was integrated into pipelines developed and

implemented by the author. The author performed all of the image processing analyses. The methodology and results are currently under review (Bergsland N, Tavazzi E, et al., AJNR.)

Most of the methodology used in this thesis was developed using publicly available, widely used neuroimaging packages. However, these tools were not designed nor explicitly tested during development with imaging data from MS patients. As a result, processing often needs to be fine-tuned to prevent pathology from interfering with obtaining reliable and precise results. Moreover, different tools and software packages provide different functionality and need to be properly integrated as per the needs of the study. Thus, much of the methodology developed as part of this thesis was aimed at overcoming the challenges presented by MS pathology as well as combining multiple imaging techniques to extract targeted data for the author's specific hypotheses. A full list of the software used as part of this thesis is provided as an appendix. The author wrote customized scripts and developed utilities to combine the disparate software packages/tools into uniform analysis processing pipelines.

Scientific publications

Full papers based on this study

- **Bergsland N,** Lagana MM, Tavazzi E, Caffini M, Tortorella P, Baglio F, Baselli G, Rovaris M. Corticospinal tract integrity is related to primary motor cortex thinning in relapsing-remitting multiple sclerosis. Mult Scler. Dec;21(14):1771-80. [Epub 2015 Mar 19.]
- **Bergsland N**, Zivadinov R, Dwyer MG, Weinstock-Guttman B, Benedict RH. Localized atrophy of the thalamus and slowed cognitive processing speed in MS patients. Mult Scler. 2015 Nov 5. [Epub ahead of print]

- **Bergsland N**, Tavazzi E, Lagana MM, Baglio F, Cecconi P, Viotti S, Zivadinov R, Baselli G, Rovaris M. White matter tract injury is associated with deep gray matter iron deposition in multiple sclerosis patients. (Under review in American Journal of Neuroradiology)

Conference Proceedings

- **Bergsland N**, Dwyer MG, Baselli G, Rovaris M, Zivadinov R. The effect of lesions on automated deep gray matter segmentation. 31st Congress of the European Committee for Research and Treatment in Multiple Sclerosis (ECTRIMS). October 7 – 10 2015, Barcelona, Spain. [Poster presentation]
- **Bergsland N**, Horakova D, Uher T, Vaneckova M, Ramasamy DP, Tyblova M, Seidl Z, Dwyer MG, Krasensky J, Havrdova D, Zivadinov R. Assessing the relationship between white matter lesion accumulation and gray matter atrophy development: a serial 10-year voxel-based morphometry and lesion probability mapping follow-up study of early relapsing-remitting MS patients. 31st Congress of the European Committee for Research and Treatment in Multiple Sclerosis (ECTRIMS). October 7 – 10 2015, Barcelona, Spain. [Poster presentation]
- **Bergsland N**, Zivadinov R, Dwyer MG, Benedict RH. Localized atrophy of the thalamus is related to changes in cognitive processing speed in MS patients. 31st Congress of the European Committee for Research and Treatment in Multiple Sclerosis (ECTRIMS). October 7 – 10 2015, Barcelona, Spain. [Poster presentation]
- **Bergsland N**, Laganà MM, Tavazzi E, Baglio F, Tortorella P, Caffini M, Clerici M, Baselli G, Rovaris M. Corticospinal tract diffusivity is related to motor cortex surface area in healthy controls. 23rd Annual Meeting of the International Society for Magnetic

Resonance in Medicine (ISMRM). May 30 – June 5 2015, Toronto, Canada. [Poster presentation]

- **Bergsland N**, Laganà MM, Tavazzi E, Caffini M, Tortorella P, Rovaris M, Baselli G. Multimodal imaging analysis in the assessment of gray and white matter damage in multiple sclerosis. 22nd Annual Meeting of the International Society for Magnetic Resonance in Medicine (ISMRM). May 10 – 16 2014, Milan, Italy. [Oral presentation]

Scientific publications not part of the thesis

Full papers

- Tavazzi E, Laganà MM*, **Bergsland N***, Tortorella P, Pinardi G, Lunetta C, Corbo M, Rovaris M.. Grey matter damage in progressive multiple sclerosis versus amyotrophic lateral sclerosis: a voxel-based morphometry MRI study. Neurol Sci. 2015 Mar;36(3):371-7.
  *Equal contribution
- Scaccianoce E, Lagana MM, Baglio F, Preti MG, **Bergsland N**, Cecconi P, Clerici M, Papadimitriou G, Makris N. A method for quantitative assessment of connections and their peripheral cortical fields using combined DTI tractography and fMRI in verbal fluency. [Under review in Brain Topography]

Conference Proceedings

- **Bergsland N**, Tavazzi E, Cattaneo D, Gervasoni E, Laganà MM, Grosso C, Saibene F, Di Pasquale O, Baglio F, Rovaris M. Effects of gait training on brain plasticity in multiple sclerosis: a functional MRI study. 31st Congress of the European Committee for

Research and Treatment in Multiple Sclerosis (ECTRIMS). October 7 – 10 2015, Barcelona, Spain. [Winner of best oral presentation by a young researcher]

- Baselli G, **Bergsland N**, Di Pasquale O, Scaccianoce E, Laganà MM, Costantini I, Pelizzari L, Clerici M, Baglio F. Integrating Structural and Functional Brain Connectivity. AEIT International Annual Conference. October 14 – 15, 2015, Naples, Italy. [Oral presentation]
- Dipasquale O, Lagana MM, Griffanti L, Tavazzi E, **Bergsland N**, Grosso C, Baglio F, Rovaris M, Baselli G. Comparing Resting State fMRI Data Cleaning Approaches in Multiple Sclerosis Patients versus Healthy Subjects. 36th Annual International Conference of the IEEE Engineering in Medicine and Biology Society. August 26-30, 2014, Chicago, IL, USA. [Poster presentation]
- **Bergsland N**, Baglio F, Baglio G, Nemni R, Clerici M, Zanette M, Blasi V. Abnormal cortical and thalamic development in children with Borderline Intellectual Functioning. 22nd Annual Meeting of the International Society for Magnetic Resonance in Medicine (ISMRM). May 10 – 16 2014, Milan, Italy. [Poster presentation]
- **Bergsland N**, Laganà MM, Viotti S, Mendozzi L, Tavazzi E, Tortorella P, Grosso C, Pagliari C, Baselli G and Rovaris M. Relationship between manual versus automatic MRI-based iron quantification and clinical disability. Gruppo Nazionale Bioingegneria IV Congresso. 25 – 27 June 2014, Pavia, Italy. [Poster presentation]
- Laganà MM, **Bergsland N**, Clerici M, Cecconi P, Baselli G, Nemni R, Baglio F. A whole brain approach of multimodal neuroimaging techniques for in vivo investigation of brain tissue changes in Alzheimer's Disease. 22nd Annual Meeting of the International Society

for Magnetic Resonance in Medicine (ISMRM). May 10 – 16 2014, Milan, Italy. [Poster presentation]

- Baglio F, Laganà MM, **Bergsland N**, Cecconi P, Nemni R. Microbleeds topography in neurodegenerative diseases. XLIV Congress of the Italian Society of Neurology. November 2 - 5 2013, Milan, Italy. [Oral presentation]
- Tavazzi E, Laganà MM, **Bergsland N**, Tortorella P, Pinardi G, Lunetta C, Corbo M, Rovaris M. Patterns of Grey Matter damage in progressive MS: a voxel-based morphometry study versus motor neuron disorders. XLIV Congress of the Italian Society of Neurology. November 2 - 5 2013, Milan, Italy. [Poster presentation]
- Tavazzi E, Laganà MM, **Bergsland N**, Tortorella P, Pinardi G, Lunetta C, Corbo M, Rovaris M. Grey matter damage in progressive multiple sclerosis versus amyotrophic lateral sclerosis: a voxel-based morphometry MRI study. 29th Congress of the European Committee for Research and Treatment in Multiple Sclerosis (ECTRIMS). October 2 – 5 2013, Copenhagen, Denmark. [Poster presentation]

Chapter 2: Corticospinal tract integrity is related to primary motor cortex thinning in relapsing-remitting multiple sclerosis.

In this chapter, a multi-modal imaging approach is used to study the relationship between damage in the white matter and that in the gray matter (GM) in a sample of relapsing-remitting multiple sclerosis (MS) patients. The FreeSurfer software package was used for cortical morphological reconstruction whereas diffusion-weighted imaging was used for the assessment of structural integrity of the white matter (WM). Although MS causes widespread damage throughout the central nervous system, we hypothesized that damage within the WM would be more closely linked to an anatomically and functionally connected GM area with respect to an area which is not. To this aim, we investigated the relationship between WM injury in the corticospinal tract (CST) and cortical thickness of the primary motor cortex, whereas the primary auditory cortex was used as a control region for testing our hypothesis. We found that axial diffusivity within the normal appearing WM of the CST was the best imaging predictor of primary motor cortex thickness in RRMS patients whereas no relationships were seen with respect to the primary auditory cortex. Although the study was cross-sectional in nature, the results suggest a direct association between WM and GM injury in MS.

Preliminary results from this study were presented as an oral presentation (Bergsland N, Laganà MM, et al., ISMRM 2014). The final work was published in Multiple Sclerosis Journal. (Bergsland N, Laganà MM, et al. Corticospinal tract integrity is related to primary motor cortex thinning in relapsing-remitting multiple sclerosis. Mult Scler. 2015 Mar 19. [Epub ahead of print]). Additional data concerning the healthy control sample was presented at ISMRM 2015.

Abstract

Background: The relationship between white matter (WM) injury and cortical atrophy development in relapsing remitting-multiple sclerosis (RRMS) remains unclear.

Objectives: To investigate the associations between corticospinal tract (CST) integrity and cortical morphology measures of the primary motor cortex (PMC) in RRMS patients and healthy controls (HC).

Methods: 51 RRMS patients and 30 HC underwent MRI examination for cortical reconstruction and assessment of CST integrity. Partial correlation and multiple linear regression (MLR) analyses were used to investigate the associations of focal as well as normal appearing white matter (NAWM) injury of the CST with thickness and surface area measures of the PMC. Relationships between MRI measures and clinical disability as assessed by the Expanded Disability Status Scale and disease duration were also investigated.

Results: With respect to HC subjects, MS patients presented with significantly decreased PMC thickness ($p = .017$) and increased CST NAWM diffusivity parameters ($p < .0001$ for all measures investigated). In patients only, decreased cortical thickness was related to increased CST NAWM mean, axial and radial diffusivities in addition to CST lesion volume. Fractional anisotropy of the CST, although lower in MS patients with respect to HCs, did not correlate with PMC thickness. The final multiple linear regression model for PMC thickness retained only NAWM axial diffusivity as a significant predictor (adjusted $R^2=.270$, $p=.001$). Clinical measures were associated with NAWM CST integrity measures.

Conclusions: PMC thinning in RRMS is related to alterations in connected WM and is best explained by decreased NAWM integrity. Moreover, the relationship between measures of WM tissue properties and connected GM change as a result of the disease process.

Introduction

Multiple sclerosis (MS) is a chronic inflammatory disease affecting the central nervous system which is now accepted to have a neurodegenerative component as well. While white matter (WM) injury was historically the primary research focus, the role of gray matter (GM) pathology has increasingly come under closer scrutiny[20, 74, 75]. Cortical atrophy, primarily as evidenced by thinning of the cortical ribbon, is a widely recognized feature of MS and has been shown to occur early in the disease[5]. Moreover, disability progression[3] and cognitive impairment[4, 5] appear to be heavily dependent on irreversible GM loss.

The exact mechanisms that contribute to cortical atrophy in MS remain to be fully elucidated. There is clear evidence, though, of direct injury within the cortex, as evidenced by demyelination, neuronal loss, activated microglia[76], and neurite transection[77]. However, focal lesions within the WM itself, as well as injury within the so-called normal appearing WM (NAWM) are also likely to play a role via mechanisms such as retrograde myelinoaxonal degradation[74].

While several studies have investigated the global impact of WM-induced GM injury using different MRI techniques[78, 79], only a limited number[20, 80, 81] have assessed the relationship between functionally and anatomically connected areas and tracts. Diffusion tensor imaging (DTI) is a technique which allows for both the in vivo reconstruction of WM tracts[82] and the assessment of tissue integrity changes in the NAWM[79]. Meanwhile, advanced cortical

reconstruction methodologies have been developed for regional parcellation and measurement of cortical morphology. Against this background, we aimed to investigate the relationship between cortical changes in a specific region along with measures of WM integrity in a functionally and anatomically connected tract. As motor dysfunction is primarily responsible for irreversible disability in MS, we chose the primary motor cortex (PMC) and the corticospinal tract (CST), respectively. We hypothesized that altered WM integrity as measured in both focal lesions and NAWM within the CST would be related to cortical morphology.

Materials and Methods

Subjects

This study included 51 patients with relapsing remitting MS (RRMS). At the time of MRI acquisition, MS patients were relapse- and steroid-free within the last three months. RRMS patients with any other pre-existing medical condition were also excluded. Clinical disability in patients was quantified via the Expanded Disability Status Scale (EDSS). 30 HC were recruited from volunteers who had a normal neurological examination with no history of neurological, psychiatric, cardiovascular, or metabolic disorders. All study participants provided written informed consent. The study was approved by the ‘‘Don Carlo Gnocchi Foundation’’ ethics committee, Milan, Italy.

MRI acquisition

All scans were acquired on the same 1.5T MRI scanner (Siemens Magnetom Avanto, Erlangen, Germany) with a 12-channel head matrix coil. The following sequences were acquired: 1) dual-echo turbo spin echo PD/T2-weighted [repetition time (TR)= 2,650ms; echo time (TE)=28/113ms; echo train length=5; 50 contiguous 2.5-mm thick axial slices; 1mm^2 in-plane

resolution] ; 2) 3-dimensional T1-weighted magnetization-prepared rapid gradient echo (MP-RAGE) [TR=1,900ms; TE=3.37ms; inversion time (TI)=1100ms; flip angle=15; 176 contiguous, 1-mm thick axial slices; $1mm^2$ in-plane resolution] ; 3) diffusion weighted (DW) pulsed-gradient spin echo planar [TR=7,000ms; TE=94ms; 50 contiguous, 2.5-mm thick axial slices; $2mm^2$ in-plane resolution; diffusion gradients applied in 12 non-collinear directions with a b-value=900 s/mm^2 ; number of runs = 2] All sequences were acquired with full coverage of the brain and slices parallel to the subcallosal plane.

MRI Assessment

Unless otherwise specified, all steps were performed using the tools available in FMRIB's Software Library[83] (FSL, http://www.fmrib.ox.ac.uk/fsl) version 5.0.7.

Lesion segmentation

WM lesions were segmented by an experienced neurologist on the PD-weighted scans with JIM software (http://www.xinapse.com/) version 5, which utilizes a semi-automated, local thresholding technique. The corresponding T2-weighted scan was used to increase confidence in lesion identification.

Lesion filling

White matter lesions tend to be hypointense with respect to the surrounding normal appearing WM in T1-weighted images. Their effect on automated tissue segmentation techniques used in the MS literature has been investigated by a number of reports[84-86]. Examples of the original and lesion filled image, along with their corresponding volumetric tissue-class segmentations, are shown in Figure 1. In this case, two effects of lesion misclassification can be seen. In the first

case, WM intensities are reduced (i.e. hypointense) in the presence of lesions with respect to the NAWM. This has the effect of lesion intensities being more similar to those of GM, or as cerebrospinal fluid (CSF) in cases of severe tissue destruction. These misclassifications are clearly evident when examining the resulting segmentations. A more subtle effect though can also be detected with respect to classification of distal regions. While the case of focal misclassification is fairly intuitive, the effect in distal areas is perhaps somewhat more subtle. The problem can be understood by considering what happens when lesional tissue remains classified as WM. In this case, it is likely that despite correct classification as WM, the lesional areas still have somewhat reduced intensities with respect to the NAWM. As the commonly used algorithms for tissue segmentation model the underlying classes using Gaussian models, lesional voxels correctly classified as WM tend to extend the lower end of the tail. This has the consequence of pulling into the WM distribution some voxels that would otherwise be correctly classified as GM. Thus, the final consequence of this effect can be an underestimate of the true GM tissue volume. Whether focal or distal classification contributes the most to overall error will depend on the overall lesion load of a patient as well as the nature of the lesions themselves (i.e. the degree of injury and subsequent intensity values).

Figure 1

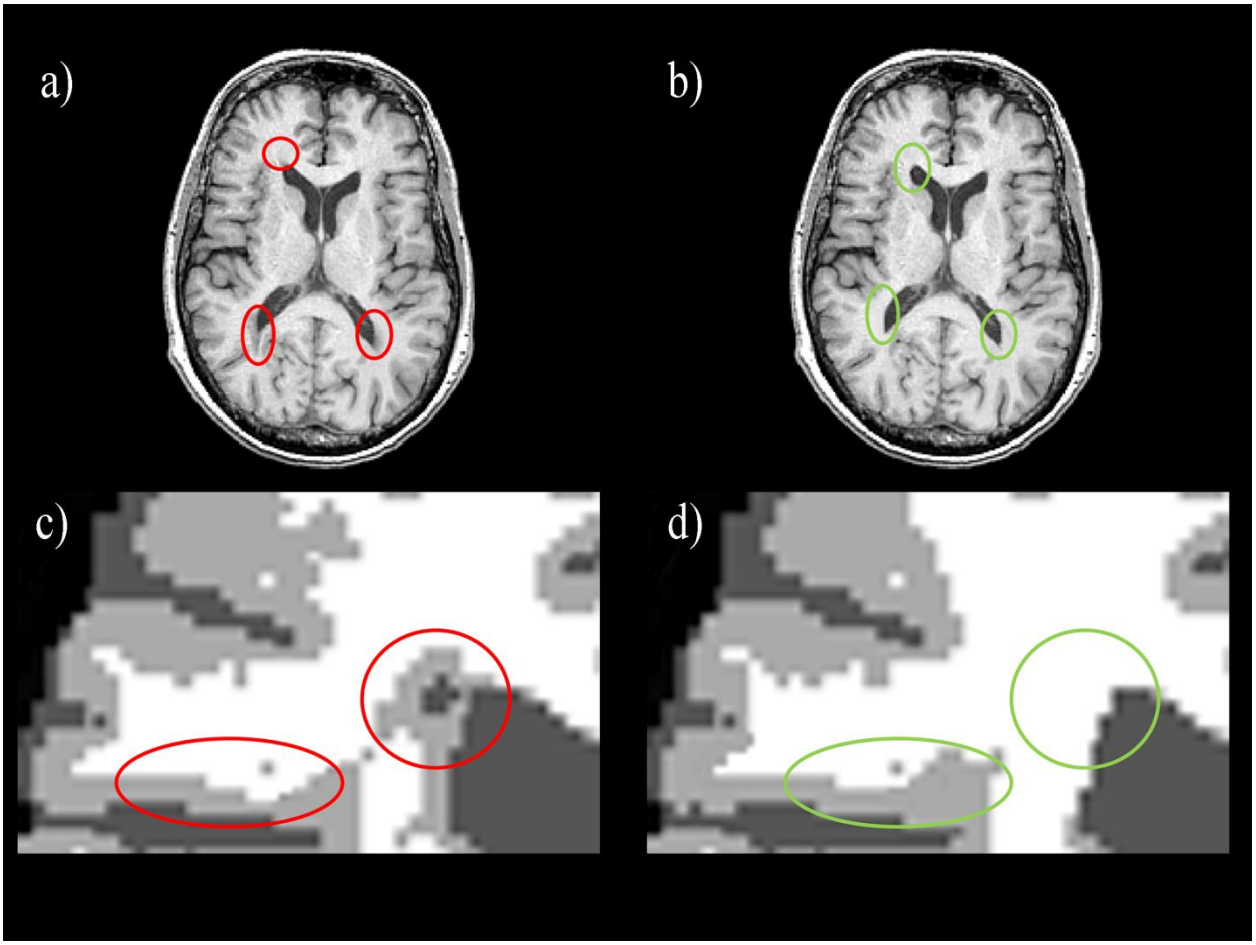

a) Representative T1-3D image of an RRMS patient
b) Lesion filled version of the image shown in a)
c) Tissue class segmentation of a). Note that the periventricular lesion is misclassified as cerebrospinal fluid in the core of the lesion whereas the surrounding area is misclassified as white matter. Distal misclassification is also seen whereby the estimates of the cortical gray matter are reduced.

d) Tissue class segmentation of b). Note that the lesion has now been properly classified as white matter. The estimate of cortical gray matter is also improved in the area remote from the lesion.

The effect of lesion filling as a preprocessing step for cortical thickness measures has also recently been investigated[87, 88]. As such, to avoid the impact of T1 hypointensities on tissue segmentation and cortical measures, 3D T1 images were preprocessed using the "lesion_filling" tool. This technique requires a mask of the lesions to identify the areas in the 3D T1 image which should be replaced with voxel values that simulate healthy tissue. The FSL "lesion_filling" tool by default will sample voxel intensities in the area immediately surrounding the lesions. Although conceptually simple, this often creates unsatisfactory results when lesions are periventricular or near gray matter boundaries. In these cases, the lesion filled areas tend to have intensities that fail to approximate the normal appearing WM and tends to yield a poor result overall. This is especially important when the overall aim is to accurately reconstruct the cortex. As it is a thin, convoluted ribbon by nature, sampling neighboring voxels may end up with lesional areas being replaced with intensities that correspond to the cortex. This may subsequently result in geometric inaccuracies or imperfect labeling of the WM surfaces. To overcome this problem, an optional WM mask can be supplied which provides additional information to the "lesion_filling" tool to help guide the intensity sampling for replacement values. Such an approach generally yields much better results but care is still needed to ensure that satisfactory results are obtained. This is particularly true in the case of juxtacortical lesions, for example. As such, the following approach was used:

1. A six degree of freedom (rigid body) transformation was used to register the PD-weighted image to the 3D T1.

2. The registration matrix from step 1 was then used to register and resample the binarized T2 lesion mask into the space of the 3D T1, using trilinear interpolation and subsequently thresholded at 0.5 and re-binarized.
3. The registered T2 lesion mask was then visualized on the 3D T1 and the lesion boundaries were inspected for accuracy. Corrections to the lesion masks (either removing or adding voxels) were made as appropriate.
4. Lesions were masked out of the 3D T1, which had previously been deskulled using BET
5. FMRIB's Automated Segmentation Tool (FAST)[89] was then used to segment the lesion-nulled 3D T1
6. The corrected lesion mask from step 3 and the WM segmentation from step 5, along with the original 3D T1, were passed to the lesion_filling tool.
7. All lesion filled 3D T1 images were visually inspected to ensure satisfactory performance.

Morphological reconstruction

Cortical reconstruction was performed on the 3D T1 images (lesion filled, in the case of MS patients) using the FreeSurfer package[6, 90] (http://www.freesurfer.net/) version 5.3 (Figure 2). The technical details of the FreeSurfer methodology have been extensively described. As such, only a brief overview of the processing steps is provided:

1. Motion correction and averaging of multiple T1-weighted volumes[91] (for a single session for a given subject), when available.
2. Removal of non-brain tissue via a hybrid watershed/surface deformation technique[92]
3. Automated registration to Talairach space

4. Automated volumetric segmentation of subcortical WM and DGM structures[6, 93]
5. Inhomogeneity intensity correction[94]
6. Tessellation of the gray matter white matter boundary, automated topology correction[95, 96]and surface deformation following intensity gradients to optimally place the gray/white and gray/cerebrospinal fluid borders at the location where the greatest shift in intensity defines the transition to the other tissue class[90, 97]
7. Surface inflation via deformable models[98] and registration to a spherical atlas based on individual cortical folding patterns[99] allowing for matching of cortical geometry across subjects.
8. Parcellation of the cerebral cortex into units with respect to gyral and sulcal structure[100, 101]. FreeSurfer provides several atlases which have been derived from the manual tracing of individual subjects.
9. Calculation of morphological measures (e.g. thickness, surface area, curvature). Of particular interest to the current study is the cortical thickness which is derived from the closest distance from the gray/white boundary to the gray/CSF boundary for each vertex on the tessellated surface.

It should also be noted that FreeSurfer does not rely solely on the voxel intensity for its estimation of cortical thickness calculation. Instead, it uses the intensity gradients across the tissue classes. This has the key benefit of allowing for the calculation of cortical thickness values at subvoxel resolution. Moreover, the FreeSurfer derived metrics have been validated against both histological data[102] and manual tracings of MRI data[103].

Quality control was performed at all steps of the pipeline and manual corrections were made as necessary. The DKT40 atlas[37] was then used to extract thickness and surface area

measures for the precentral gyrus (corresponding to the PMC) and transverse temporal gyri (corresponding to the primary auditory cortex (PAC)); the latter was used as a control region as it has no connections with the CST. Thalamic and total intracranial volumes (TIV) were also obtained. The former was calculated as part of the automated subcortical segmentation stream in FreeSurfer while the latter was estimated based on the determinant of the affine registration to Talairach space.

Figure 2

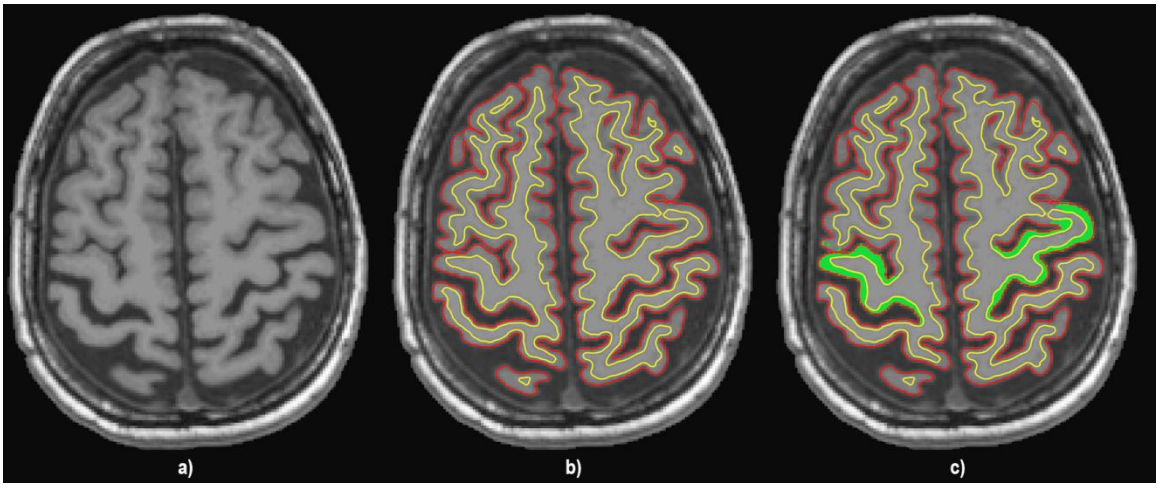

d) Representative T1-3D image of an RRMS patient
e) White matter and pial surfaces shown in yellow and red, respectively.
f) Parcellated primary motor cortex shown in green.

Although not the primary aim of the study, we also explored the effect of lesion filling as preprocessing step prior to cortical reconstruction in a sample of five RRMS patients. The FreeSurfer stream was run twice, once with lesion filling and once without (i.e. the original 3D T1 image).

Corticospinal tract measures

DW images were corrected for eddy current and patient motion induced distortions using the eddy_correct tool. Then, the tensor was calculated for each voxel using "dtifit" from which voxelwise maps of fractional anisotropy (FA), mean diffusivity (MD), axial diffusivity (AD), and radial diffusivity (RD) were obtained. As WM lesions may hinder conventional tractography[82], we used a previously generated in-house probabilistic CST atlas[104], derived from a completely separate sample of HC. Briefly, the CST of 25 HCs was reconstructed with deterministic tractography by placing inclusion masks in the precentral gyrus and the anterior half of the posterior limb of the internal capsule. The reconstructed tracts were then warped into standard MNI space using FNIRT[83] and averaged such that voxel intensities represent the probability of corresponding to the CST.

Using FNIRT[83], subject-specific FA images were warped to the FMRIB_58_FA image. Trilinear interpolation was used and lesions were excluded as part of the cost function. The calculated warp field was then used to bring along MD, AD, RD and binarized lesion maps. Warped lesion maps were thresholded at 0.5 and re-binarized. The CST atlas was then used to extract the aforementioned DTI-based parameters for all subjects (Figure 3). In the MS patients, we calculated measures within both the NAWM and lesions. CST measures were computed by weighting the DTI indexes by the probability of a given voxel corresponding to the CST in the atlas. Finally, we computed weighted lesion volumes within the CST in a similar manner as for the DTI parameters.

Figure 3

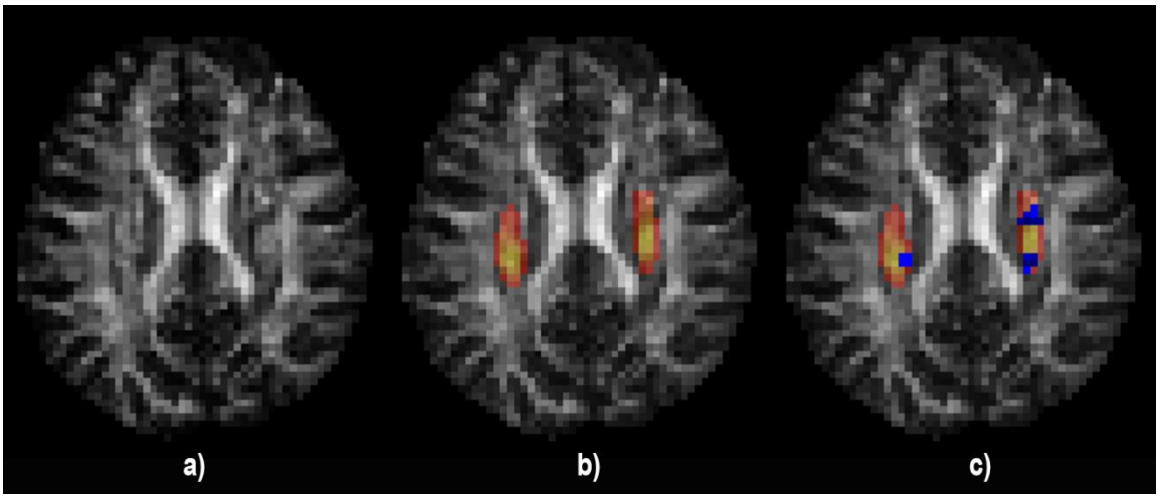

d) Representative FA image of an RRMS patient
e) The same FA image with the probabilistic CST atlas overlaid. Warmer colors represent an increased probability of corresponding to the CST in the atlas. Note that actual image analyses were performed in standard MNI space.
f) Segmented lesions within the CST atlas are shown in blue.

To provide confirmation of the atlas-based tractography results, we used the Tract Based Spatial Statistics (TBSS) pipeline (version 1.2)[105]. Briefly, subject FA maps were first nonlinearly aligned to standard space. An average FA image was then created and subsequently thinned, resulting in a mean FA "skeleton". This image represents the centers of all tracts common to the group. Each subject's aligned FA data was then projected onto this skeleton. We made modifications to the standard TBSS scripts such that lesions were excluded from the registration cost function. Rather than performing a full voxelwise analysis, we extracted mean DTI parameters within the CST portion of the TBSS skeleton[106].

Lesion probability maps

Lesion probability maps (LPM) within the CST were created as previously described[107]. Briefly, the T1 3D image for each subject was nonlinearly registered into MNI space using FNIRT[83]. As with the registration of the diffusion data, lesional areas were excluded from the registration cost function. The calculated warp was then used to bring individual lesion masks into MNI space. Registered lesions were then summed and average to create the final LPM. The resulting map corresponds to the probability of a given voxel corresponding to a lesion in the sample of MS patients. Permutation based inference testing with the randomise[108] tool was then used to test for voxelwise associations between the spatial positions of CST lesions and cortical thickness measures, with age and sex included as nuisance covariates. The probabilistic CST atlas was binarized for use as a mask to restrict the LPM analyses only to lesions within the CST. Voxels with $p<.05$ corrected for family-wise error rate were considered significant.

Statistical analysis

Statistical analyses were performed using SPSS (version 21; IBM Corp., Armonk, NY, USA). Differences in demographic characteristics between the groups were assessed using the Student's t-test and Chi-squared, as appropriate. Normality of the distribution of variables was assessed using the Kolmogorov-Smirnov method. T2 lesion volumes were logarithmically transformed due to positive skew. Although measures for the left and right hemispheres were obtained separately, total or average values, as appropriate, were calculated to reduce the number of comparisons.

Group differences between CST measures were assessed using an ANCOVA model, controlling for age and sex. For surface area measures, $\sqrt[\frac{2}{3}]{TIV}$ was also included as a covariate[ii]. The same covariates were included when examining partial correlations between cortical, CST, and clinical outcomes. Next, multiple linear regression (MLR) analyses were used to assess the contribution of variables showing univariate correlations with cortical measures and clinical measures. Covariates were input into first block (enter method) and MRI measures in the second (forward-stepwise method) with cortical and clinical outcome measures as the dependent variables. We also assessed for interactions between group and NAWM CST indices when predicting cortical measures. As the disease duration and EDSS distributions were positively skewed, we repeated all analyses using the following sub-groups to exclude potential effects due to outliers: i) disease duration<20 years; ii) EDSS< 6; iii) disease duration<20 years and EDSS<6. P-values <.05 were considered significant using two-tailed tests.

[ii] The choice to use $\sqrt[\frac{2}{3}]{TIV}$ was based on recommendations made on the FreeSurfer listserve from Bruce Fischl, one of the FreeSurfer FreeSurfer (https://www.mail-archive.com/freesurfer@nmr.mgh.harvard.edu/msg22048.html) In the end, the same results were obtained using either $\sqrt[\frac{2}{3}]{TIV}$ or the entire TIV.

Results

Demographic, Clinical, and MR Imaging Characteristics

30 HC and 51 RRMS patients were enrolled in this study. Table 1 provides an overview of the demographic and clinical characteristics. No significant demographic differences between the two groups were found.

Table 1: Demographic and clinical characteristics of healthy controls and relapsing remitting multiple sclerosis patients

	HC (n = 30)	RRMS (n = 51)	*p*
Age in years, mean (SD)	41.9 (10.3)	42.0 (10.9)	.881
Sex, female, N (%)	17 (56.6)	28 (54.9)	1.0
Disease duration – mean in years (SD) / median (range)	-	10.4 (8.4) / 8 (1 – 33)	-
EDSS – median (range)	-	4 (0 – 7)	-

Legend: HC = healthy controls; RRMS = relapsing remitting multiple sclerosis; N = number ; SD = standard deviation ; EDSS = Expanded Disability Status Scale

Demographic differences were tested using the Student's *t*-test and Fisher's exact test for age and sex, respectively.

Table 2 shows the imaging characteristics of the groups. No HC presented with T2 lesions. RRMS presented with a mean global T2 lesion volume (LV) of 12.23 ± 13.37mL (median 6.94mL, range 0.79 – 61.16mL). For CST DTI indices in the NAWM, RRMS patients presented with significantly lower FA, higher MD and RD. RRMS patients presented with significantly decreased PMC thickness.

Table 2: CST and cortical measures in HC and RRMS.

	HC (N = 30)	RRMS (N = 51)	*p*
CST Measures			
NAWM			
FA_{ATLAS}	.50 (.02)	.47 (.02)	< **.0001**
FA_{TBSS}	.54 (.02)	.51 (.02)	<**.0001**
MD_{ATLAS}	.77 (.02)	.81 (.05)	<**.0001**
MD_{TBSS}	.73 (.01)	.76 (.03)	<**.0001**
AD_{ATLAS}	1.22 (.02)	1.25 (.05)	**.013**
AD_{TBSS}	1.23 (.02)	1.23 (.03)	.885
RD_{ATLAS}	.54 (.02)	.60 (.05)	< **.0001**
RD_{TBSS}	.49 (.02)	.52 (.04)	< **.0001**
T2 Lesion			
Volume	-	.49 (.80) .20 (.01 – 3.2)	-
FA_{ATLAS}	-	0.37 (.07)	-
MD_{ATLAS}	-	0.98 (.15)	-
AD_{ATLAS}	-	1.37 (.16)	-
RD_{ATLAS}	-	0.79 (.16)	-
Cortical Measures			
Thickness			
Primary motor cortex	2.39 (.14)	2.23 (.26)	**.017**
Primary auditory cortex	2.41 (.27)	2.32 (.28)	.305
Surface area			
Primary motor cortex	9647 (983)	9576 (1071)	.998
Primary auditory cortex	781 (132)	731 (109)	.075

Legend: HC = healthy controls; RRMS = relapsing remitting multiple sclerosis; N = number; CST = corticospinal tract; NAWM = normal appearing white matter ; FA = fractional anisotropy ; MD = mean diffusivity ; AD = axial diffusivity ; RD = radial diffusivity ; TBSS = tract based spatial statistics

All cells are presented as mean (standard deviation) except for CST T2 volume where the median (range) is also provided. FA is a dimensionless index. MD, AD, and RD are given in $mm^2/s * 10^{-3}$. Lesion volume is given in milliliters. Thickness measures are given in mm whereas surface area measures are in mm^2. *p* values were calculated using ANCOVA, controlling for age and sex; total intracranial volume was included as well for surface area comparisons. Significant differences are shown in bold.

Relationships with cortical measures in healthy controls and patients

Partial correlations between cortical measures and other MRI parameters are shown in Table 3.

In the HC group, PMC surface area, but not cortical thickness, correlated with MD and AD within the CST. With MLR, the final model retained as significant predictors: TIV (β = .689, p=.001), age (β=-.460, p=.004) and AD (β=-.355, p=.021) (F(3,20)=11.789, p<.001, adj. R^2=.652).

In the RRMS group, PMC thickness, but not surface area, correlated with all three CST diffusivity measures and with the volume of CST lesions. CST FA was not related to PMC thickness. With MLR, the final model retained as a significant predictor only NAWM AD (β=-.426, p=.001) (F(3,47)=7.167, p<.0001, adj. R^2=.270).

When investigating the entire cohort, the interaction term between group and NAWM CST AD was significant (p=.028) in predicting PMC thickness. For PMC surface area, significant interaction terms between group and NAWM CST MD (p=.025) and RD (p=.026) were found.

Thalamic volume was not associated with cortical outcomes. PAC measures were not related with any other MRI measures.

Table 3: Partial correlations with cortical measures in HC and RRMS

	HC				RRMS			
	Primary motor cortex		Primary auditory cortex		Primary motor cortex		Primary auditory cortex	
	Thickness	Surface area	Thickness	Surface area	Thickness	Surface area	Thickness	Surface area
Thalamic volume	-.156 (.488)	-.150 (.515)	.140 (.533)	.007 (.975)	.276 (.055)	.067 (.653)	.165 (.258)	.085 (.564)
	NAWM CST measures							
FA	.072 (.749)	.236 (.304)	.190 (.397)	.346 (.125)	.264 (.067)	-.064 (.667)	.084 (.566)	.062 (.677)
MD	.219 (.328)	**-.476 (.029)**	-.065 (.773)	-.313 (.167)	**-.440 (.002)**	.038 (.797)	-.104 (.476)	-.154 (.295)
AD	.411 (.057)	**-.500 (.021)**	.128 (.571)	-.131 (.570)	**-.448 (.001)**	.025 (.867)	-.104 (.479)	-.174 (.237)
RD	.106 (.638)	-.372 (.097)	-.114 (.614)	-.332 (.142)	**-.426 (.002)**	.048 (.746)	-.104 (.479)	-.139 (.347)
	Lesional CST measures							
FA	-	-	-	-	.148 (.317)	-.051 (.734)	-.086 (.560)	.077 (.605)
MD	-	-	-	-	-.190 (.196)	.004 (.979)	-.026 (.858)	-.287 (.050)
AD	-	-	-	-	-.150 (.308)	-.007 (.964)	-.086 (.560)	-.276 (.061)
RD	-	-	-	-	-.191 (.194)	.010 (.949)	.008 (.959)	-.264 (.073)
Volume	-	-	-	-	**-.327 (.022)**	-.039 (.791)	-.173 (.234)	-.265 (.482)

Legend: HC = healthy controls; RRMS = relapsing remitting multiple sclerosis; N = number ; CST = corticospinal tract ; NAWM = normal appearing white matter ; FA = fractional anisotropy ; MD = mean diffusivity ; AD = axial diffusivity ; RD = radial diffusivity ;

Partial correlations were calculated controlling for age and sex; TIV was included as well for surface area comparisons. Significant correlations are shown in bold.

Relationships between clinical and MRI measures in patients

Partial correlations with clinical outcomes are shown in Table 4. Both disease duration and EDSS correlated with measures of CST NAWM FA and all three diffusivity measures. In addition, EDSS, but not disease duration, correlated with both increased CST lesion volume and decreased PMC thickness. With MLR, the final model for EDSS retained as significant

predictors: age (β=.302, p=.008), CST LV (β=.458, p<.0001) and PMC thickness (β=-.254, p=.033) (F(4,46)=13.007, p<.001, adj. R^2=.490).

PAC thickness and surface area were not related to either of the clinical measures.

Table 4: Partial correlations with clinical outcomes in RRMS patients

	Disease duration	EDSS
NAWM CST:		
FA	**-.432 (.002)**	**-.405 (.004)**
MD	**.362 (.011)**	**.467 (.001)**
AD	**.290 (.044)**	**.437 (.002)**
RD	**.386 (.006)**	**.475 (.001)**
Lesional CST:		
FA	.006 (.968)	-.061 (.681)
MD	.013 (.928)	.116 (.434)
AD	.058 (.695)	.119 (.422)
RD	-.010 (.949)	.102 (.489)
Volume	.272 (.059)	.594 (< .0001)
Primary motor cortex		
Thickness	-.188 (.196)	**-.429 (.002)**
Surface area	-.022 (.883)	.017 (.906)
Primary auditory cortex		
Thickness	-.149 (.306)	-.250 (.084)
Surface area	.078 (.599)	.003 (.986)

Legend: RRMS = relapsing remitting multiple sclerosis;
N = number ; CST = corticospinal tract ; NAWM = normal appearing white matter ; FA = fractional anisotropy ; MD = mean diffusivity ; AD = axial diffusivity ; RD = radial diffusivity
Partial correlations were calculated controlling for age and sex; TIV was included as well for surface area comparisons. Significant correlations are shown in bold.

Lesion probability mapping

Within the CST, lesion probability was highest (43.1%) in the left CST (MNI standard coordinate: x=-20, y=-24, z=28). PMC thickness correlated with lesion probability throughout several areas of the CST (Figure 4 and Table 5). No significant voxels were found for the PAC.

Figure 4

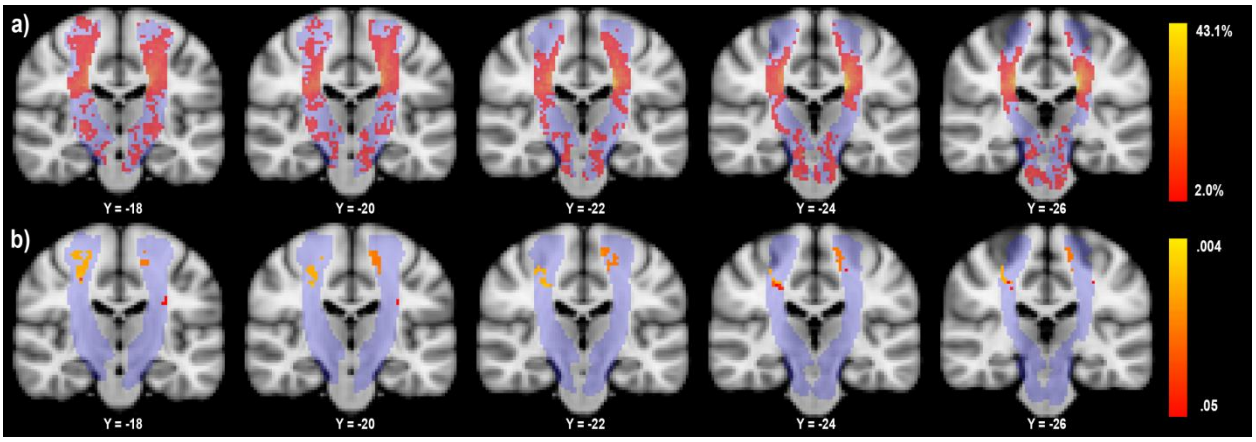

c) The T2-lesion probability map (LPM) shows the percentage of patients with a lesion in a given voxel. The probabilistic CST atlas is shown in light blue.
d) Lesional voxels that significantly correlate with primary motor cortex thickness are shown in red-yellow. The probabilistic CST atlas is shown in light blue.

Table 5: Lesion probability mapping within the CST in RRMS patients

Number of voxels	Peak X	Peak Y	Peak Z	p
185	22	-28	42	.004
99	-12	-22	58	.022
8	-30	-20	26	.048
3	-6	-32	-34	.048

Local maxima within each significant cluster ($p < .05$, family-wise error corrected) where lesion probability in the CST was correlated with primary motor cortex thickness.

TBSS results

With the exception of NAWM AD, group differences were of a similar magnitude between results obtained with both TBSS and atlas-based tractography (Table 2).

Sub-group analyses

Sub-group analyses with disease duration <20 years retained 39 patients; EDSS <6 retained 36 patients; disease duration <20 years and EDSS <6 retained 33 patients. Results obtained with the reduced cohorts were in line with those of the full cohort (data not shown).

Discussion

In this cross-sectional study of patients with RRMS, we showed that MRI measures of WM integrity are related to cortical thickness of an anatomically and functionally connected cortical area. Although the link between GM and WM damage in MS has been the subject of intense study, most reports have either examined global relationships[20, 79, 109] or only connected WM-GM regions [80]. Thus, we included the primary auditory cortex as a control region since it has no connections with the CST. While stronger relationships between CST integrity and morphological measures of the PMC are more plausible than with the PAC, the complete lack of any correlations with the latter may be somewhat surprising considering the widespread damage caused by MS throughout the brain, including within the auditory cortex[110]. One might expect a relationship between anatomically distinct areas merely due to overall disease burden. In this context, our results underline the fact that regional investigations are likely to be more informative when studying the interplay between GM and WM pathology.

We found robust relationships between PMC and CST integrity measures in RRMS patients. While no DTI metrics within the CST lesions were associated with PMC thickness, all of them (i.e. FA, MD, RD, AD) were significantly correlated with it in the NAWM. This is in line with whole brain associations recently reported by Steenwijk et al.[20]. The finding of very similar correlation coefficients may suggest that the degree of tract-specific integrity and its relationship to thinning in connected cortical areas may be similar throughout the brain. On the other hand, the rate of cortical thinning should scale with the relative degree of connectivity for a given area if it is in part due to axonal transection following focal WM injury[109]. Thus, the investigation of other tracts and corresponding cortical regions may help elucidate this question. It should be noted though that while lesion volume and location was related to PMC thickness in both univariate correlation and LPM analysis, NAWM AD was the only MRI variable retained in

the regression analysis. Thus, NAWM, rather than focal measures may capture more of the overall tissue injury. Finally, we did not find any associations between CST integrity and PMC surface area, contrary to previously published data.[80] However, while cortical thinning has been widely described in MS, differences in surface area have not been consistently reported[5, 80].

Although FA was significantly reduced in the NAWM of the CST in RRMS patients with respect to HCs and in lesions with respect to NAWM, it was not related to PMC measures. Few studies have investigated the relationship between WM tract FA and cortical thickness, with conflicting findings[20, 80, 81] likely due to patient cohort differences. Indeed, the longer disease duration reported in other studies might have led to increased tissue microstructure damage. This lends support to the notion that FA may be less sensitive than diffusion coefficient indices to the amount of underlying tissue damage[111]. In addition, one should keep in mind that FA will remain relatively stable in the event that there is no preferential change in AD or RD. Finally, one longitudinal study reported that DTI indices in the CST did not change in a consistent pattern in MS patients[112]. Thus, additional longitudinal studies are needed to better understand the evolution of diffusion coefficient and FA changes in both lesions and the NAWM and their relation to cortical thinning.

Furthermore, increased EDSS was related to PMC thinning to a similar degree as has been previously reported[110, 113]. Such a relationship might be expected considering that EDSS is heavily weighted towards motor dysfunction. The fact that the FreeSurfer PMC parcellation is larger than the area responsible for motor/lower limb function may explain why the relationship is not stronger. Thus, the application of other clinical scales, including those able to capture upper limb dysfunction, may indeed improve the relationships we found between MS disability and cortical damage.

In the HC sample, we unexpectedly found correlations between MD and AD in the CST and PMC surface area, but not thickness. Age was included as a covariate as it has been shown to correlate with both increased WM diffusivity[114] and decreased cortical surface area and thickness[115]. Sex was also included due to expected differences[116]. A residual nonlinear effect of sex after covariation can be excluded as these relationships were still evident when investigating males and females separately. Meanwhile, no such relationships were found in the MS sample despite not differing in PMC surface area. It is important to consider that several of the interaction terms between group and diffusivity indices were significant when predicting cortical measures in the cohort as a whole. This suggests that the relationship between measures of WM and connected GM change as a result of the disease process. These findings warrant further investigation in a larger sample to better understand the underlying dynamics.

The exploratory analysis investigating the effect of WM lesions on cortical reconstruction revealed a significant effect in terms of the lesion filling step. This is perhaps not so surprising given the way in which the FreeSurfer reconstructs the surfaces based on the intensity gradient. Indeed, this was seen visually whereby the cortical ribbon tended to incorrectly expand into the WM in the presence of juxtacortical lesions. A recent multi-center study examined the effect of lesion filling in FreeSurfer-derived cortical thickness measures[88]. The authors concluded that although there was a significant effect, it was relatively modest with a mean difference of about two percent. It was also reported that effects were regionally dependent, more prominent at 1.5T with respect to 3T and the difference between using lesion filling or not was correlated with lesion load. It was postulated that the stronger effect at 1.5T is due to a decreased contrast to noise ratio relative to that at 3T. It must be noted though that the authors do acknowledge the lesion presence has a larger impact in patients with high lesion volumes (defined as > 6 mL in

their study). Although not formally tested, the increased likelihood of juxtacortical lesions with larger lesion volumes is likely to be at least in part of the explanation for this finding. This is in line with the exploratory analysis done for the current study. The RRMS patients in our study had a mean T2 lesion volume of more than 12 mL and many presented with juxtacortical lesions. Moreover, while the two percent difference reported by the authors may seem relatively small, it is important to consider that yearly atrophy rates in MS may be as low as 0.5%. Thus, the use of non-lesion filled images may yield inaccurate results in longitudinal studies where new or enlarging lesions develop with respect to the baseline. In this case, the effect of lesions on the cortical thickness measures may dwarf any biological effect due to atrophy. These results are in line with another recent study which found that lesion filling improved the accuracy of cortical thickness measurements in a longitudinal sample of MS patients[87]. In sum, lesion filling does in fact appear to be an important step in studies aiming to use cortical morphology reconstruction techniques such as FreeSurfer.

There are a number of limitations in this study that need to be considered. As with any cross-sectional study, it is not possible to draw any firm conclusions regarding the temporal evolution between the investigated measures. It should also be noted that the FreeSurfer precentral gyrus parcellation is larger than the area to which the CST connects. Thus, damage in connecting tracts that we did not consider may also contribute to PMC injury. Moreover, we only considered a single WM tract and associated cortical region. As such, studies investigating a larger number of tracts/regions are warranted to better understand the interplay between WM-GM damage. Furthermore, longitudinal studies should aid in better characterizing the temporal dynamics of injury between the two tissue compartments. Additionally, the number of acquired diffusion directions in this study was quite small by current standards[117]. These sequences were

acquired during clinical examinations though, limiting the available amount of time. Regardless, all participants were scanned using the same protocol, minimizing any systematic bias in the results. Moreover, the CST atlas used in this study was generated from a separate HC sample and we subsequently confirmed our findings with TBSS. Consequently, despite the limited DTI protocol, the overall interpretability of the results should not be affected. However, it is important to remember that we utilized a probabilistic atlas for extracting the DTI-derived parameters within the CST. This was due to the difficulty in reconstructing the CST in our patient cohort due to focal WM lesions. Recent tractographic developments, such as TRACULA[118] (TRActs Constrained by UnderLying Anatomy), may yield better subject-specific reconstructions even in the presence of patient pathology. For example, TRACULA uses a combined approach consisting of probabilistic tractography and anatomical priors. Thus, it may be that the case that the addition of anatomical information can help overcome the difficulties traditionally encountered in the presence of focal lesions where existing methods often fail. Future studies should compare such methods with the approach used in the current study. It should also be noted that our study focused primarily on the relationship between GM atrophy and damage in the WM. While we did not find clear evidence of thalamic atrophy being related to PMC thinning, cortical pathology is likely explained as well in part by primary causes such as neuronal/axonal damage within the cortex itself. We lacked a method to visualize cortical lesions and could not assess their contribution to cortical thinning. Finally, beyond our exploratory analysis investigating the effects of lesion filling, we did not distinguish between juxtacortical and "pure" WM lesions in our analysis. A more fine-grained analysis of WM lesion types may provide further insight into the relationship between focal WM injury and cortical thinning.

In conclusion, the present study demonstrated that focal as well as diffuse tissue microstructure alterations in the CST are associated with thinning of the PMC in RRMS. This finding highlights the importance of studying anatomically and functionally related areas of the brain for a better understanding of the pathogenesis of the damage in MS. Serial MRI studies are needed to unravel the temporal-spatial dynamics of WM injury and cortical atrophy.

Acknowledgements

The authors gratefully acknowledge all the study volunteers as well as the developers of both the freely available FSL and FreeSurfer software packages.

Chapter 3: Improving the quality of automated deep gray matter structural segmentations in multiple sclerosis

In this chapter, the effect of multiple sclerosis white matter (WM) lesions on automated deep gray matter (DGM) segmentation is investigated. We compared volumetric- and surface-based analyses of several DGM structures by analyzing lesion filled images with respect to the original ones. WM lesions were found to bias thalamic and caudate volumes when using FMRIB's Integrated Registration and Segmentation Tool (FIRST). After lesion filling, thalamic and caudate volumes were significantly smaller with respect to the original segmentations. This effect was also confirmed via shape-based analysis of the DGM surfaces. Our findings highlight the importance of correcting for WM lesions when using automated segmentation techniques for measuring DGM atrophy. As registration to standard space is a key step in the FIRST algorithm, we also investigated the effect of using a common transformation for longitudinal FIRST analyses. Ultimately, the proposed longitudinal modification to the FIRST pipeline yielded inferior results compared to running the analyses fully independently at baseline and follow-up time points.

Results from this study were in part presented at ECTRIMS 2015 (Bergsland N, Dwyer MG, et al.). Based on the insights gained from the work presented in this chapter, additional research into improving FIRST for longitudinal studies is still ongoing.

Abstract

Background and purpose: White matter (WM) lesions are known to impact MRI-based tissue segmentation and cortical reconstruction techniques. However, there are conflicting reports regarding their effect on automated segmentation of the deep gray matter (DGM) structures. Moreover, longitudinal studies investigating DGM atrophy have generally relied on post-hoc comparisons of cross-sectional segmentations, which subsequently introduces multiple sources of measurement error. More precise longitudinal measures are thus needed to better characterize DGM atrophy.

Material and methods: FMRIB's Integrated Registration and Segmentation Tool (FIRST) was used for automated segmentation of the thalamus, caudate, globus pallidus and putamen. Two groups of subjects were analyzed. The first group consisted of 152 MS patients imaged on the same 1.5T scanner whereas 64 MS patients and 22 healthy controls were examined on a 3T scanner as part of the second group. The effect of WM lesions was assessed using the first group by comparing segmented structural volumes and surface-based analysis, before and after lesion filling. In the second group, the use of common registration to standard space was investigated as a potential means for reducing intra-subject variability.

Results: Thalamic and caudate segmentations were shown to be affected by the presence of WM lesions. The use of lesion filling before segmentation resulted in significantly smaller volumes of these structures when using FIRST. Focal WM lesions exerted local as well as nonlocal effects on the final segmentations as evidenced by vertex-wise shape analysis of the thalamus and the caudate. The proposed longitudinal modifications to the pipeline yielded poorer results as evidenced by smaller effect sizes and slightly worse reproducibility when compared to running FIRST fully independently at baseline and follow-up.

Conclusions: Lesion filling is recommended as a preprocessing step before using FIRST for DGM segmentation. Additional research is needed to improve FIRST for longitudinal analyses.

Introduction

Obtaining reliable segmentations of the deep gray matter (DGM) is an area of active research in the study of neurodegenerative diseases. The inherent difficulties in this regard stem in large part from the relatively poor contrast between GM/WM and signal variability in subcortical areas. FMRIB's Integrated Registration and Segmentation Tool (FIRST)[7] is a widely used and freely-available tool which helps overcome these challenges. FIRST has been utilized in a large number of reports investigating DGM atrophy in numerous neurological diseases[119, 120], including several studying MS[16, 121].

One of the key aspects of FIRST is its use of trained shape data. These models are provided as part of the algorithm and incorporate manually segmented data from a large number of subjects (see next paragraph for more information.) The method incorporates Active Shape and Appearance Models into a Bayesian framework which allows for both intensity and shape information to be used probabilistically for segmentation. FIRST creates a surface mesh for each segmented structure using a deformable mesh model. Each mesh is made up of a set of triangles and the apex of connecting triangles is called a vertex. The number of vertices for each structure is fixed and vertex locations are standardized, allowing corresponding vertices to be compared across individuals. Segmentation itself is carried out via the registration of previously trained shape models to the input image. A two stage registration technique is utilized. Initially, the pipeline performs a linear, affine registration to standard MNI space. Next, a secondary registration is performed whereby the cost function is weighted by the DGM structures, as defined in MNI space. The inverse of the final transformation is then computed and the trained models are brought into the native space of the input image. Based on the observed intensities,

the posterior probability of the shape is maximized via an iterative search. The resulting subject-specific meshes are then used to obtain three-dimensional volumes for each structure.[7]

The manual labels used for the construction of the FIRST models incorporate data from 336 subjects with a wide age range (4 – 87 years) and different cohorts (including but not limited to healthy controls, Alzheimer's disease, schizophrenia). However, the training data does not include any brains from people with MS. This is of potential importance considering that MS, in addition to GM atrophy, is also characterized by the presence of focal WM pathology which may interfere with accurate GM segmentation. Although subjects with Alzheimer's disease (which yields to some degree a similar pattern of WM lesion as in MS[122]) are part of the trained models, they represent a relatively small number of the total sample. Thus, it is reasonable to assume that the algorithm, which was neither trained nor tested during development on imaging data from MS subjects, may not be fully optimized for imaging data of patients with this disease.

In the case of FIRST, lesions may potentially interfere with the automated segmentation in the registration step, the model fitting step or in both. The effect on registration can be appreciated by recalling the two-stage registration approach it uses. Even in the presence of WM lesions, the initial registration is expected to perform reasonably well considering the total volume of WM lesions will still be a relatively small percentage of the total brain volume. However, the second stage of registration is optimized by weighting the subcortical structures in MNI space. As there is considerable individual variation in terms of brain structure sizes, the weighting mask actually encompasses a larger area than just the subcortical areas seen on the MNI image. Thus, lesions in the vicinity of the subcortical structures may potentially impact the quality of the registration. Of course the effect will depend on the level of WM lesion load as well as degree of pathology (i.e. more severe tissue destruction will be more dissimilar to the

MNI template). At this point, the learned models are fit to the data via the inverse of the registration, as described above. During this step, lesions may also negatively impact the segmentation during the model fitting as FIRST works on the principle of matching observed modes of variation in the training model with that seen in the input image. Thus, a lesion that would result in an "unnatural" (i.e. not seen in the training data) shape is likely to be effectively ignored. On the other hand, a lesion that borders an atrophic area may result in the final segmentation incorrectly including it in order to "restore" the expected shape variation. To what degree this occurs will depend on the specific localization of the lesions as well as the pattern of atrophy in a given subcortical structure.

As currently implemented, FIRST is inherently cross-sectional. Longitudinal studies using FIRST have generally processed each time point separately and then used post-hoc analyses (e.g. repeated measures modeling[123], calculation of changes scores[3, 124, 125]) to measure effects over time. Such approaches have certainly provided additional insight into the course of DGM atrophy and demonstrated the utility of measuring this aspect of the disease. Moreover, scan-rescan tests of FIRST have demonstrated the excellent reproducibility of the technique[16]. However, a key disadvantage of performing two separate measurements is that it entails two sources of measurement errors. In addition, direct measures of brain atrophy, such as SIENA[126] and SIENAX multi-time point[127], generally account for factors such as patient positioning differences and scanner drift that otherwise introduce additional variability in longitudinal measurements. Thus, such approaches tend to yield results that are generally both more precise and more robust compared to serial applications of cross-sectional measures. In the case of FIRST, variability in the initialization of the search procedure might be reduced by using a common registration to standard space procedure used to match the shape models.

Against this background, the aims of the current study were twofold. The first aim was to assess the impact of lesions on FIRST-based DGM segmentation. The second aim was to evaluate whether the use of a common registration to standard space could improve the sensitivity of FIRST for longitudinal analysis.

Materials and Methods

The current study was approved by the University at Buffalo Health Sciences Institutional Review Board.

Subjects

Two separate groups of subjects were analyzed for the aims of the study.

Group 1

One-hundred and fifty-two (152) MS patients with a relapsing-remitting disease course were included. MS patients underwent a full neurological evaluation and clinical disability was quantified via the Expanded Disability Status Scale (EDSS). At the time of MRI acquisition, MS patients were relapse- and steroid-free within the last three months. This group of subjects was used to assess the impact of WM lesions on DGM segmentation.

Group 2

Sixty-four (64) MS patients and twenty-two (22) healthy control (HC) subjects were included. MS patients underwent a full neurological evaluation and clinical disability was quantified via EDSS. At the time of MRI acquisition, MS patients were relapse- and steroid-free within the last three months. HC subjects were group matched for age and sex to the patient sample. All HCs

denied any history of medical or neurological illness. This group of subjects was used to evaluate the impact of using a common registration to standard space for longitudinal analyses.

MRI acquisition

Group 1

All scans were acquired on the same 1.5T MRI scanner (General Electric, Signa Excite 12.0, Milwaukee, WI USA). The following axial sequences were acquired: 1) dual-echo spin echo PD/T2-weighted [repetition time (TR)=3,000ms; echo time (TE)=12/90ms; flip angle(FLIP)=90° ; echo train length(ETL)=12; 48 contiguous 3-mm thick slices; $1mm^2$ in-plane resolution] ; 2) fluid attenuated inversion recovery (FLAIR) [TR=8002ms; TE=128ms; inversion time (TI)=2000ms; 48 contiguous 3-mm thick slices] 3) 3-dimensional (3D) T1-weighted spoiled gradient echo [TR=24ms; TE=7ms; FLIP=30°; 128 contiguous, 1.5-mm thick slices; $1mm^2$ in-plane resolution]

Group 2

All scans were acquired on the same 3T MRI Scanner (General Electric, Signa Excite 12.0, Milwaukee, WI USA). The following axial sequences were acquired: 1) dual fast spin echo PD/T2-weighed [T2=5,300ms; TE=9/98ms, FLIP=90°, ETL=14] 2) FLAIR [TR=8,500ms, TE=120ms, TI=2,100ms, FLIP=90°] 3) 3D high resolution T1-weighted images using a fast spoiled gradient echo with magnetization-prepared inversion recovery pulse [TR=5.9ms, TE=2.8ms, TI=900ms, FLIP=10°]

MRI analysis

All steps were performed using the tools available in FMRIB's Software Library (FSL, http://www.fmrib.ox.ac.uk/fsl) version 5.0.7[83] unless otherwise stated.

Lesion segmentation

WM lesions were segmented on FLAIR scans with JIM software (http://www.xinapse.com/) version 5, which utilizes a semi-automated, local thresholding technique. The corresponding PD/T2-weighted scans were used to increase confidence in lesion identification.

Assessing the impact of lesions

Assessing the impact of lesions was done using the subjects from Group 1. FIRST was used to segment the thalamus, caudate, globus pallidus and putamen (left and right separately). The 3D T1 image was preprocessed using the "lesion_filling" tool as described in detail in Chapter 2. FIRST was subsequently run four times:

1. Original 3D T1 image
2. Lesion filled 3D T1 image
3. Original 3D T1 image using the registration matrix from run 2
4. Lesion filled 3D T1 image using the registration matrix from run 1

Vertex analysis of surfaces and lesion probability mapping (LPM) was also performed to assess the impact of lesion presence on DGM segmentations. LPM analysis was performed as described in detail in Chapter 2.

Assessing the impact of a common registration to standard MNI space for longitudinal analysis

For longitudinal experiments, we used the subjects from Group 2. In an attempt to derive a more consistent registration between baseline and follow-up 3D T1 images, we first calculated the midway transform for each pair. To this aim, FMRIB's Linear Image Registration Tool (FLIRT)[128, 129] was used to calculate the transformation in both directions. An unbiased halfway transformation was then calculated using the "midtrans" tool. Next, both images were resampled into the halfway space using trilinear interpolation. The average of the two images was then calculated and the result was used as the input into "flirt_flirt", to derive the subcortical-optimized registration to standard MNI space. The resulting matrix was then combined with the inverse of the corresponding halfway space registration matrix. Finally, FIRST was run with this registration matrix along with the original image. Thus, baseline and follow-up images were analyzed separately, but using a common registration to standard MNI space. All MS cases were preprocessed using the lesion filling approach previously described in Chapter 2.

Reproducibility analysis

To evaluate the reproducibility of the proposed longitudinal approach, we performed a scan-rescan analysis in a subset of 3 MS and 3 HC participants. Subjects were rescanned within at most one week after the original scan. These subjects were processed using the standard cross-sectional FIRST pipeline and then with the common registration to standard MNI space.

Statistical analysis

Analyses were performed using SPSS 21.0 (IBM Corp., Armonk, NY) and R 3.2.2 [130]. Demographic characteristics were compared between HCs and MS patients using Student's t-test Fisher's exact test for age and sex, respectively. Normality of the data was assessed via visual

inspection of histograms and the Shapiro–Wilk test. All investigated MRI-derived parameters were considered normally distributed.

For analysis assessing the impact of lesions, differences in segmented volumes were tested using a one-way repeated measures ANOVA with Bonferroni correction for pairwise comparisons.

We first assessed the reproducibility of the original and the modified methods for investigating DGM changes over time. Reproducibility of the two methods was first assessed in the scan-rescan dataset using intraclass correlation (ICC). Next, for each method, the MS patient and HC groups were compared using Student's *t*-tests and then effect sizes were calculated.

Results:

Subject characteristics

Demographic data and clinical characteristics of the study subjects in Groups 1 and 2 are summarized in Table 1 and Table 2, respectively. All of the enrolled subjects completed the full MRI examination and were included in the analysis.

Table 1: Demographic and clinical characteristics multiple sclerosis patients in Group 1

	RRMS (n = 152)
Mean age in years (SD)	34.9 (8.2)
Female, n (%)	112 (73.7)
Mean disease duration in years (SD)	9.6 (5.5)
Median EDSS (range)	2.0 (0 – 6.5)

Legend: HC = healthy controls; RRMS = relapsing-remitting multiple sclerosis; n = number; SD = standard deviation; EDSS = Expanded Disability Status Scale

Table 2: Demographic and clinical characteristics multiple sclerosis patients in Group 2

	MS (n = 64)	**HC (n = 22)**	**p-value**
Mean age in years (SD)	46.1 (8.5)	43.1 (10.8)	.18
Female *n* (%)	43 (67)	14 (64)	.80
Mean follow-up length in days (SD)	1166 .9 (85.5)	1147 (45)	.180
Mean disease duration in years (SD)	11.6 (8.5)	-	-
Median EDSS (range)	3.5 (0 - 6.5)	-	-

Legend: MS = relapsing-remitting multiple sclerosis; n = number; HC = healthy controls; SD = standard deviation; EDSS = Expanded Disability Status Scale

Demographic differences were tested using the Student's *t*-test and Fisher's exact test for age and sex, respectively.

Assessing the impact of lesions

A representative case showing the original and lesion filled segmentation is shown in Figure 1.

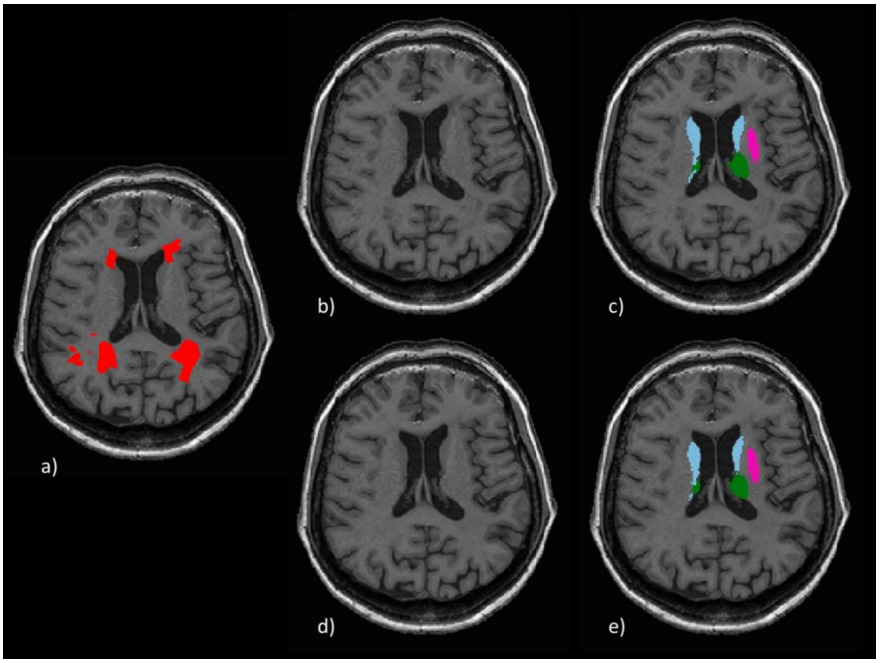

a) Representative 3D T1image with co-registered lesions shown in red. b) Original 3D T1 image
c) FIRST segmentation of original 3D T1 image d) Lesion filled 3D T1 image
e) FIRST segmentation of lesion filled 3D T1 image

Caudate are shown in light blue, thalami are shown in green and putamens are shown in magenta.

Comparisons between the four different FIRST analyses are presented in Table 3. With respect to the original segmentations, lesion filled structural volumes were significantly smaller for both left and right thalami ($p < .015$) and caudates ($p < .0001$). Globus pallidus and putamen volumes were not significantly different between the four methods. Thalmic volumes were dependent on the registration while they were independent of the image used for segmentation ($p = .999$ and $p < .01$, for the same image and same registration comparisons, respectively). Caudate volumes were dependent on the image used for segmentation while they were independent of the

registration while they were independent of the registration used for segmentation ($p < .0001$ and $p = .999$ for same image and same registration, respectively).

Table 3: Comparison between FIRST-derived segmentations using four different methods

	Original segmentation	**Lesion-filled segmentation**	**Original image (lesion filled registration)**	**Lesion-filled image (original registration)**	**p**
L. thalamus	6948 (933)	6928 (940)	6929 (941)	6948 (931)	.014
R. thalamus	6765 (911)	6738 (926)	6741 (913)	6765 (910)	.004
L. caudate	3146 (478)	3063 (505)	3146 (468)	3072 (500)	< .0001
R. caudate	3307 (456)	3201 (505)	3302 (463)	3193 (491)	< .0001
L. putamen	4507 (666)	4510 (657)	4504 (665)	4511 (653)	.556
R. putamen	4426 (619)	4434 (606)	4431 (615)	4433 (613)	.753
L. globus pallidus	1618 (237)	1624 (240)	1621 (241)	1619 (237)	.235
R. globus pallidus	1702 (250)	1701 (243)	1702 (250)	1704 (246)	.567

Legend: FIRST = FMRIB's Integrated Registration and Segmentation Tool; L. = Left; R. = Right

Cells represent mean volume in mm^3 (standard deviation). Differences in segmented volumes were tested using a one-way repeated measures ANOVA. See main text for pair-wise comparisons.

Vertex-wise analysis of the subcortical surfaces yielded similar results as the volumetric analysis but showed that large portions of the surface were affected beyond just areas of focal WM lesions (Figure 2).

Figure 2

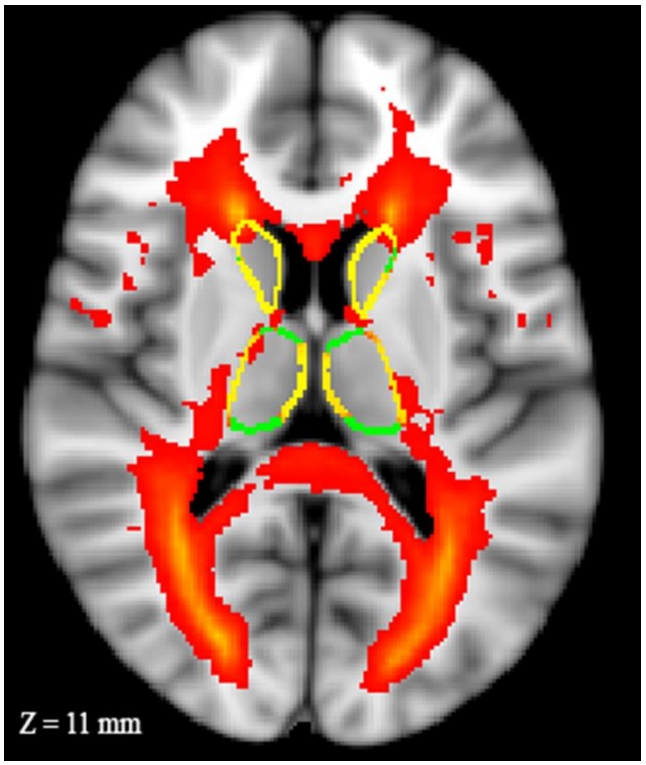

Vertex-wise analysis of the thalami and caudates. Surfaces are shown in green and significant differences where lesion filled segmentations are smaller are shown in yellow ($p < .01$). Vertex-wise analysis of the putamens and globus pallidi did not yield any significant differences along the surface. The lesion probability map is shown in red-yellow, with yellow indicating higher lesion probability. The peak probability is 51%.

Assessing the impact of a common registration to standard space for longitudinal analysis

Table 4 shows the results of the comparisons between running FIRST independently with respect to using a midspace registration to standard space. Results are presented as percent changes in volume between baseline and follow-up. In both methods and for all structures investigated, MS patients exhibited larger degrees of atrophy. However, only the right caudate and bilateral globus pallidi were significantly different between the groups when running the two FIRST analyses fully separately. In terms of midspace registration approach, the right caudate was no longer

significant while the bilateral globus pallidi remained so. The effect size was greater in magnitude for the standard method with respect to the common registration one for all investigated structures.

Table 4: Comparison between standard and midspace registration for post-hoc comparisons of FIRST-derived segmentation

	Standard method				**Midspace registration method**			
	MS (n =64)	HC (n = 22)	p	Cohen's d	MS (n =64)	HC (n = 22)	p	Cohen's d
L. thalamus	-2.54 (2.52)	-1.96 (2.01)	.331	-.254	-1.38 (2.52)	-1.14 (2.61)	.709	-.094
R. thalamus	-2.76 (2.55)	-2.17 (2.31)	.321	-.243	-1.67 (2.76)	-1.43 (1.97)	.705	-.100
L. caudate	-3.87 (8.35)	-1.10 (9.05)	.193	-.318	-3.36 (8.30)	-1.41 (8.44)	.348	-.233
R. caudate	-3.01 (4.88)	.19 (5.06)	.010	-.644	-3.20 (4.82)	-1.36 (4.38)	.119	-.400
L. putamen	-3.89 (4.46)	-3.32 (3.24)	.582	-.146	-3.50 (4.45)	-3.40 (3.76)	.867	-.024
R. putamen	-4.31 (4.11)	-3.24 (2.87)	.263	-.302	-3.90 (4.28)	-2.88 (2.89)	.216	-.280
L. globus pallidus	-4.93 (4.67)	-.07 (4.04)	<.0001	-1.113	-3.98 (6.03)	-.29 (4.36)	.010	-.701
R. globus pallidus	-4.10 (4.73)	-.95 (3.97)	.006	-.721	-2.72 (4.79)	.41 (4.14)	.008	-.699

Legend: FIRST = FMRIB's Integrated Registration and Segmentation Tool; MS = multiple sclerosis; HC = healthy controls; L. = Left; R. = Right

Data are shown as mean (standard deviation) percent changes in volume between baseline and follow-up. Differences in mean values between the MS and HC groups were tested using Student's *t*-test. Effect sizes are given as Cohen's d, in which the difference between means is divided by the pooled standard deviation.

Reproducibility

ICC results of the FIRST-derived segmentation volumes using the two different methods are reported in Table 3. All volume measurements were highly reliable, regardless of the method used. The midspace registration method consistently yielded slightly smaller ICC values.

Table 3: Intra-class correlation (ICC) for FIRST-derived volumes

	Standard method	**Midspace registration method**
L. thalamus	.989 (< .001)	.977 (<.001)
R. thalamus	.990 (< .001)	.978 (<.001)
L. caudate	.919 (<.001)	.899 (<.001)
R. caudate	.917 (<.001)	.901 (<.001)
L. putamen	.931 (< .001)	.930 (<.001)
R. putamen	.925 (< .001)	.918 (< .001)
L. globus pallidus	.987 (< .001)	.972 (< .001)
R. globus pallidus	.985 (<.001)	.981 (<.001)

Data are shown as ICC value (p).

Discussion

The present work assessed two methods with the aim of improving the precision and reliability of DGM segmentation via FIRST. We demonstrated a clear effect of WM lesions for thalamic and caudate nuclei segmentations. Our proposed approach for improving the sensitivity of longitudinal analyses, however, was not successful.

We found that the use of lesion filling as preprocessing step resulted in significantly smaller volumes for the caudate and the thalamus (bilaterally). However, the differences were driven by separate aspects of the FIRST pipeline. In the case of the thalamus, the effect of registration drove the observed differences. This is likely due to the fact that there is already naturally low GM/WM contrast along the border of the thalamus. In fact, the lateral border of thalamus is considerably difficult to identify on T1-weighted images. In the presence of MS-related pathology, distinguishing the thalamic border is likely to be even more challenging. Thus, it may be the case that FIRST relies more on the learned shape models at this point. If this is indeed true, then one would expect that the segmentation is more heavily dependent on the initialization procedure for fitting the models. In the case of FIRST, this is derived from the registration and thus might explain the observed effects. On the other hand, the caudate is considerably easier to identify on a T1-weighted image and has a more clearly defined border. Thus, it is likely that the intensity information plays a more substantial role in deriving the final segmentation. In this case, the registration is less important and the shape models just need to be brought close enough to a reasonable starting position for proper segmentation. At this point, image intensity differences due to presence of/lack of lesions in the vicinity of the caudate will have the strongest effect on the overall segmentation.

In the case of both the thalamus and the caudate, the surface-based analysis revealed that lesions exerted an influence on the segmentation beyond areas of focal WM injury. This is also of particular importance for studies investigating shape changes of the DGM in MS as it suggests that WM lesions, if not corrected for, may explain the findings to some degree. The same argument can be made for longitudinal studies where new or enlarging lesions occurring at follow up may confound the interpretation of shape changes over time if not corrected for in preprocessing.

Our results are somewhat conflicting with respect to those of another study which employed similar methods for assessing the impact of lesions on DGM segmentations. Gelineau-Morel et al.[43] found that, with the exception of the hippocampus, the use of lesion filling resulted in larger DGM volumes. The exact reason for this discrepancy is not entirely clear at this time. However, a key methodological difference is the way in which lesions were filled. In the current study, we utilized the procedure described in Chapter 3 whereby lesions were filled with voxel intensities sampled from the normal appearing white matter. In the work of Gelineau-Morel et al., only neighboring voxels were utilized (including potential GM or CSF voxels). While this minimizes the possibility of filling voxels with dissimilar intensities due to inhomogeneity of the magnetic field, it does potentially increase the risk of sampling voxels corresponding to so-called dirty appearing white matter (i.e. areas with abnormal signal intensity but not outlined as a lesion). We attempted to mitigate the effects of inhomogeneity by first using the N3 algorithm for bias field correction. Additional studies, including the use of simulation lesions as was done in the other study, might shed further light on the observed discrepancy with respect to the work of Gelineau-Morel et al.

We failed to demonstrate a positive benefit of using a midspace registration for longitudinal FIRST analysis. Indeed, the proposed longitudinal modification appears to actually have performed worse than the standard method of running FIRST fully independently from one another. This was evidenced by a consistent decrease in the measured effect size between the MS patient and HC group for all investigated measures. Moreover, the reliability analysis revealed slightly reduced ICC values for the midspace registration method with respect to those obtained when using independent FIRST runs.

Despite not having achieved an improvement for longitudinal FIRST-based analyses in the current study, there are still other potential changes that may have a positive impact and warrant further investigation. One possibility is to pursue an approach similar to that used in the longitudinal FreeSurfer processing stream. In this case, individual time points are first analyzed separately and subsequently used in the generation of an unbiased template volume[131]. The template volume is then processed with the FreeSurfer stream and the results are propagated back to the individual time points for initialization purposes of the individual steps in the pipeline. This has the benefit of reducing variability across time points for a given subject, resulting in an overall increase in reliability and statistical power to detect biological changes[132]. Such an approach could conceivably be implemented within the existing FIRST framework. In this case, the midspace average image would not only be used for registration to standard MNI space but would be fully processed by the FIRST pipeline. The resulting segmentations would then be propagated back to the original images and used to initialize the individual segmentations. It should also be noted that there is the possibility that differences in patient positioning have an effect on volumetric measurements[133] over time. We did not account for this in our method as segmentations ultimately occurred in native imaging spaces. However, as the

DGM structures are centrally located within the brain, they should remain relatively close to the isocenter of the magnet across time points. Thus, patient positioning differences between a baseline and follow-up exam should have less of an effect on volumetric measures of the DGM structures than they have on the cortex. The use of nonlinear registration may also help but one would need to be very careful to ensure that it does not effectively "undo" any real biological changes. Regardless, a more detailed assessment of patient positioning differences in the context of longitudinal investigations is need to properly address this question.

In conclusion, we investigated two methods in attempt to obtain more precise segmentations of the DGM. The presence of WM lesions appear to bias both volumetric- and surface-based measures of the thalamus and caudate as segmented by FIRST. Thus, lesion filling is recommended as a pre-processing step prior to segmentation. On the other hand, the proposed longitudinal modification yielded poorer results compared to processing individual time points separately. Despite this, future research is warranted for the development of longitudinal pipelines for more precise DGM segmentation. Improved quantification of DGM atrophy will aid in furthering our understanding of the temporal/spatial dynamics of neurodegeneration.

Chapter 4: Localized atrophy of the thalamus and slowed cognitive processing speed in MS patients.

In this chapter, a surface-based approach is used to study the relationship between deep gray matter (GM) atrophy and cognitive deficits in a sample of multiple sclerosis (MS) patients. Cross-sectionally, a more precise localization of the associations between atrophy of the thalamus, putamen and caudate versus cognitive deficits were revealed than has been previously reported in the literature. Moreover, longitudinally, the study revealed that focal, anterior atrophy in of the left thalamus is associated with decreased cognitive processing speed over three years of follow-up. Of particular note is that imaging techniques widely used in the literature (region of interest and voxel-based morphometry) were not sufficient to detect this relationship. Rather, the correlation between localized thalamic atrophy and cognitive decline was only seen when using vertex-wise based analysis of the thalamic surface. Our findings highlight the role that surface-based analyses may play in furthering the knowledge of pathogenetic mechanisms in MS. Results from this study were presented at ECTRIMS 2015 (Bergsland N, Zivadinov R et al.). The optimized longitudinal voxel-based morphometry method was described in a presentation at ECTRIMS 2015 (Bergsland N, Horakova D, et al.). The final work was published in Multiple Sclerosis Journal. (Bergsland N, Zivadinov R et al. Localized atrophy of the thalamus and slowed cognitive processing speed in MS patients. Mult Scler. Dec;21(14):1771-80.

Abstract

Background: Deep gray matter (DGM) atrophy is common in MS, but no studies have investigated surface-based structure changes over time with respect to healthy controls (HC).

Moreover, the relationship between cognition and the spatio-temporal evolution of DGM atrophy is poorly understood.

Objectives: To explore DGM structural differences between MS and HCs over time in relationship to neuropsychological (NP) outcomes.

Methods: The participants were 44 relapsing remitting and 20 secondary progressive MS patients, and 22 HCs. All were scanned using 3T MRI at baseline and 3-year follow-up. Neuropsychological (NP) examination emphasized consensus standard tests of processing speed and memory. We performed both volumetric and shape analysis of DGM structures and assessed their relationships with cognition.

Results: Compared to HCs, MS patients presented with significantly smaller DGM volumes. For the thalamus and caudate, differences in shape were mostly localized along the lateral ventricles. NP outcomes were related to both volume and shape of the DGM structures. Over 3 years, decreased cognitive processing speed was related to localized atrophy on the anterior and superior surface of the left thalamus.

Conclusions: These findings highlight the role of atrophy in the anterior nucleus of the thalamus and its relation to cognitive decline in MS.

Introduction

Cognitive impairment, a core deficit in multiple sclerosis (MS),[134, 135] is associated with reduced volume of the cerebral gray matter.[136] Of the gray matter structures, cognitive performance is most readily explained by volume of the deep gray matter (DGM),[137, 138] especially the thalamus.[139] In addition, the striatum (i.e. putamen and caudate) has also been implicated in MS cognitive decline[140].

Robust correlations are consistently found using a wide variety of techniques, including manual tracing of structure volume correcting for intracranial volume,[141] automated segmentation,[137, 138] and voxel-based morphometry.[142] These approaches, however, make it somewhat difficult to identify the precise location where such changes occur and whether certain sub-regions or within-structure nuclei are more preferentially related to cognitive impairment. Shape-based analysis has the potential to advance the field via measuring geometric surface changes without the need of smoothing, which by definition results in blurring of the data.[7] Moreover, while full structure volumetric analysis treats the entire structure as a homogeneous unit, the DGM structures possess substantial fine structure heterogeneity - the thalamus is composed of many discrete sub-nuclei with differing function, architecture, and connectivity. These sub-regions may lose volume at different rates, with variable functional consequences. Vertex-wise shape analysis provides a means to study these spatially separate changes individually. Given its potential advantage to more precisely characterize the regional predilection of DGM atrophy, the technique was recently utilized in MS patients.[54] The authors examined 57 healthy controls and 52 relapsing-remitting patients. Widespread thalamic atrophy in MS patients was seen with respect to healthy controls. Moreover, a larger degree of atrophy

was found in the anterior thalamic region for cognitively impaired MS patients with respect to those that were cognitively preserved.

Few longitudinal studies have attempted to associate changes in DGM volume with clinical status.[3, 143] Preliminary findings suggest that DGM atrophy is a risk factor for disease worsening and that reduction in thalamus[125] and putamen[143] is correlated with worsening disability. However, these studies did not include a cognitive outcome measure, and did not compare MS patients to healthy controls. Moreover, longitudinal studies assessing focal atrophy of the DGM as measured by shape-based techniques are currently lacking.

Against this background, our primary aim of this study was to describe the localization of thalamic and striatum atrophy and its relation to neuropsychological outcomes. We endeavored to replicate a recent cross-sectional study[54] and extend the findings to a longitudinal framework. For this purpose, we performed a 3-year, longitudinal study enrolling a cohort of MS patients along with a group of healthy controls (HC) and utilized both volumetric and shape-based analyses of the aforementioned structures.

Methods

Subjects

The study[124] was approved by the University at Buffalo Health Sciences Institutional Review Board. The participants were reduced to a smaller subset for whom complete shape analysis was available (see below). MS patients (n=64) met revised McDonald criteria for clinically definite MS[24] and had either a relapsing-remitting (RR) or secondary-progressive (SP) course.[144] All patients were free of relapse or steroid treatment for 8 weeks prior to the study. Exclusion criteria for all participants were as follows: failure to complete a full battery of tests, previous or current

substance abuse, developmental delay, other major medical, neurological, or psychiatric disorder. Mood disorders emerging after MS onset were permitted in patients except for current major depressive episode. We also evaluated 22 HC volunteers, group matched to the patient sample on demographic characteristics. All participants denied history of medical or psychiatric illness that could affect cognitive function (e.g. depression, anxiety disorder, concussion, learning disability).The Beck Depression Inventory-Fast Screen was used to evaluate depression. All participants were evaluated by a clinical neurologist (BWG), board-certified and specializing in MS, and blinded to MRI findings. For MS patients, neurological disability, as quantified via the Expanded Disability Status Scale (EDSS), and disease course were assessed. Only participants that had all available data at both baseline and 3-year follow-up were included in this study.

Neuropsychological assessment

A neuropsychologist (RHBB), board-certified and specializing in MS, and blinded to MRI findings, supervised the Brief International Cognitive Assessment for MS (BICAMS).[145] Specifically, the Symbol Digit Modalities Test (SDMT),[146] California Verbal Learning Test-Second Edition (CVLT-2),[147] and the Brief Visuospatial Memory Test-Revised (BVMT-R)[148] were administered. Raw test scores were normalized based on normative data that account for demographics, such as age and education[149].

MRI acquisition

All scans were acquired on the same 3T General Electric, Signa Excite HD scanner, with a maximum slew rate of 150 T/m/s and maximum gradient amplitude in each orthogonal plane of

50mT/m. The protocol included the following sequences: [a] 2D dual fast spin echo proton density (PD) and T2-weighted images, [b] fluid-attenuated inversion recovery (FLAIR), [c] 3D high resolution T1-weighted images using a fast spoiled gradient echo with magnetization-prepared inversion recovery pulse. Scans were acquired in an axial-oblique orientation, parallel to the sub-callosal line. All sequences were acquired with a 256x192 matrix (frequency x phase), field-of-view of 25.6cm x 19.2cm (256x256 matrix with Phase FOV=0.75), for an in-plane resolution of 1mm x 1mm. For PD/T2 and FLAIR sequences, 48 slices were collected, thickness of 3mm, and no gap between slices. For the 3D T1-weighted sequence, 128 locations were acquired, 1.5 mm thick. Other relevant parameters were as follows: for dual FSE PD/T2, echo and repetition times (TE and TR) E1/TE2/TR=9/98/5300ms, flip angle (FLIP)=90°, echo train length (ETL)=14; for FLAIR, TE/TI/TR=120/2100/8500ms (TI-inversion time), FLIP=90°, ETL=24; for SE T1-WI, TE/TR=16/600ms, FLIP=90° and for 3D T1 TE/TI/TR=2.8/900/5.9ms, FLIP=10°.

MRI Assessment

Lesion segmentation

We calculated T2 lesion volume (T2-LV) using a local thresholding segmentation technique (JIM 5.0, Xinapse Systems) on the FLAIR, using the PD/T2 sequence to increase confidence in lesion identification. Lesions in the DGM were counted on the FLAIR images with the PD/T2 acquisition used for confirmation. All reading of MRI data was performed in a blinded manner.

Tissue class segmentation

Baseline regional tissue volumes were calculated using the SIENAX tool from FSL. Percent whole brain volume change was calculated using the SIENA method[150] while for GM, WM, cortical, and lateral ventricle volume changes, we applied a modified SIENAX multi-time point algorithm.[127] A lesion filling algorithm was used as a pre-processing step prior to tissue segmentation to avoid the impact of T1 hypointensities on tissue segmentations.[84] Specific details of the lesion inpainting process are provided in Chapter 2.

Deep gray matter structural segmentation

To segment the DGM structures (thalamus, caudate, putamen) of interest for volumetric region of interest analyses, we applied FMRIB's Integrated Registration and Segmentation Tool (FIRST)[7] to the lesion-filled 3D-T1WI. Further details concerning the algorithm are provided in Chapter 3, which describes the methods used for improving DGM segmentation with FIRST. All segmentations were verified for accuracy. Subpar registrations resulting in inaccurate segmentations were corrected and FIRST was then re-run. This was needed for a limited number of cases (6). As described in Chapter 3, using the registration matrix derived the average midspace image yielded significantly worse segmentations. As such, baseline and follow-up images were processed independently. To reduce the number of comparisons, the volumes obtained from each hemisphere were added to represent total structural volume. DGM volumes were normalized by the SIENAX derived volumetric scaling factor as previously described[121].

Surface-based shape analysis of deep gray matter structures

To assess whether localized structural alterations may provide further insight into the underlying pathology and relations with clinical outcomes, we also performed vertex-wise shape analysis of

the thalamus, caudate and putamen surfaces. For this aim, the average shape of the cohort was first calculated. Next, vertexes corresponding to the individual DGM structures were projected onto the surface normal of the mean shape. The projected value for each vertex thus represented the perpendicular distanced from the mean surface. A positive value for a given vertex position meant that the position was outside (i.e. larger) than the mean surface whereas a negative value was inside (i.e. smaller). Left and right structures were analyzed separately. Surfaces were reconstructed in MNI space, which normalizes for head size. The effects of age and sex were regressed out for all analyses. For longitudinal shape analyses, the mean shape was calculated from the baseline and follow-up segmentations of all subjects in the study. Pairwise subtractions were then calculated for each baseline and follow-up pair such that positive values corresponded to "growth" whereas negative ones represented atrophy. Additional exploratory analyses were conducted by including either baseline T2-LV or normalized brain tissue volume as an additional covariate in longitudinal assessments. Significance of group differences between HC and MS participants and correlations with neuropsychological measures (MS patients only) were tested using the FSL tool "randomise" with threshold-free cluster enhancement.[151] We used 5000 permutations for all tests. Shape differences between HC and MS groups were tested at $p < .05$ corrected for family wise error (FWE). For correlations between shape and the three neuropsychological outcomes, the FWE rate due to multiple testing was controlled using Bonferroni correction, resulting in a final threshold of $p < .0167$. We did not control for the number of DGM structures tested.

Voxel-based morphometry of the deep gray matter structures

To further evaluate the sensitivity of shape-based analyses for detecting pathological changes over time that are otherwise not possible using volumetric approaches, we also performed a

voxel-based morphometry (VBM) analysis. We implemented an optimized VBM pipeline for longitudinal analyses based on the standard FSL-VBM protocol[152]. The key modifications were as follows:

1. 3D T1 images for baseline and follow-up were registered into an unbiased mid-space and averaged (T1-average)
2. The 3D T1average was deskulled using FSL's Brain Extraction Tool (BET) [153] and the subsequent brain mask was transformed back to the native space of the baseline and follow-up 3D T1s
3. Baseline and follow-up 3D T1s were segmented into cerebrospinal fluid, GM and WM using FMRIB's Automated Segmentation Tool (FAST)[89]
4. Native GM segmentations were registered into T1average space and subsequently averaged (GM-average)
5. The group template was created using the GM-average images
6. Native GM segmentations were then aligned into the space of the group template and modulated by the Jacobian determinant of the GM-average to template warp
7. Pairwise difference images were calculated such that negative values corresponded to a decrease in GM concentration (i.e. atrophy)

The rest of the FSL-VBM pipeline was left as is (e.g. flipping template along x-axis to create left-right symmetry, nonlinear registration using FNIRT[154]). The modulated grey matter difference images were then smoothed with an isotropic Gaussian kernel. Three separate kernels of 1.5 mm, 2 mm and 2.5 mm were used. To be comparable with the structural volume and shape-based approaches, VBM analyses were restricted to the thalamus, caudate, putamen (based on masks derived from the Harvard-Oxford Subcortical Structural Atlas). Significance of group

differences between HC and MS participants and correlations with neuropsychological measures (MS patients only) were tested using the FSL tool *randomise* with threshold-free cluster enhancement.[151] The effects of age and sex were regressed out for all analyses. We used 5000 permutations for all tests.

Statistical Analysis

The MS and NC groups were compared on demographics, MRI and neuropsychological variables using Chi-square and t-tests, as appropriate. In all subsequent comparisons between the two groups, age and sex were included as covariates. Baseline differences between the groups were assessed using ANCOVA models. Partial correlations were used to assess the relationship between normalized volumes of the DGM structures and neuropsychological outcomes. For longitudinal analyses, differences between HCs and MS patients in terms of change over time were assessed using either 1) the interaction term in mixed-factor models with group the between factor and time the within-subjects factor or 2) ANCOVA models for measures that are inherently longitudinal (e.g. SIENA and SIENAX- multi-time point). Additional exploratory analyses were performed by including either baseline T2-LV or normalized brain tissue volume as an additional covariate. An alpha level of $p < 0.05$ was used for comparisons between HC and MS patients. For correlations between structural volume and the three neuropsychological outcomes, the FWE rate due to multiple testing was controlled for by using Bonferroni correction, resulting in a final threshold of $p < .0167$. We did not control for the number of DGM structures tested.

Results

Baseline characteristics and clinical changes over 3 years

Of the 64 patients, 44 were diagnosed with a RR course and the remainder had SP disease. The mean disease duration was 11.6 ± 8.5 years. The median EDSS was 3.5 (range 0-6.5). Seventy-five percent of the MS cohort was treated with disease modifying therapies. No significant differences in demographic characteristics were found between the two groups.

At baseline, MS patients performed worse on all neuropsychological tests; tissue volumes were also smaller while lateral ventricle volume was increased (Table 1). The median (range) lesion counts within the thalamus, caudate and putamen were 0 (0 – 3), 0 (0 -2) and 0 (0 – 1), respectively. At follow-up, the median EDSS of the MS cohort was 3.25 (range 0 to 8), which was not significantly different from baseline. One RR MS patient converted to SP course. There were no significant group changes in NP outcomes over follow-up.

Table 1: Baseline demographic, clinical, neuropsychological and MRI characteristics

	MS (n = 64)	**HC (n = 22)**	**p-value**	**Cohen's d**
Mean age in years (SD)	46.1 (8.5)	43.1 (10.8)	.18	
Female *n* (%)	43 (67)	14 (64)	.80	
Mean education in years (SD)	14.7 (2.4)	15.3 (2.1)	.29	
Mean follow-up length in days (SD)	1166 .9 (85.5)	1147 (45)	.180	
Mean disease duration in years (SD)	11.6 (8.5)	-	-	
Median EDSS (range)	3.5 (0 - 6.5)	-	-	
Disease course (RR / SP)	44 / 20	-	-	
BDI-FS	2.7 (3.1)	2.1 (2.0)	.415	0.235
[a]SDMT total (SD)	-0.89 (1.33)	0.37 (1.00)	< .0001	-1.06
[a]BVMT-R total (SD)	-0.93 (1.18)	0.06 (0.78)	< .0001	-0.99
[a]CVLT-2 total (SD)	-0.38 (1.16)	0.83 (0.98)	< .0001	-1.13
T2-LV in mL (SD)	13.4 (14.4)	1.5 (1.8)	< .0001	1.16
Normalized WBV in mL (SD)	1464.3 (76.2)	1525.6 (65.4)	.001	-0.86
Normalized GMV in mL (SD)	742.8 (47.6)	770.9 (44.1)	.017	-0.61
Normalized WMV in mL	721.5 (47.1)	754.6 (28.8)	< .0001	-0.85
Normalized cortical GMV in mL (SD)	603.8 (41.2)	627.0 (39.0)	.023	-0.58
Normalized LVV in ML (SD)	46.5 (19.4)	35.0 (16.8)	.015	0.63
Normalized thalamus volume in mL	19.1 (2.2)	21.0 (1.2)	< .0001	-1.07
Normalized putamen volume in mL	12.4 (1.4)	12.8 (1.3)	.230	-0.30
Normalized caudate volume in mL	8.5 (1.2)	9.2 (1.0)	.006	-0.63

[a]Normalized values based on normative data that account for demographics, such as age and education[149]

Notes:

MS = multiple sclerosis ; HC = healthy control; EDSS = Expanded Disability Status Scale ; RR = relapsing remitting ; SP = secondary progressive ; BDI-FS = Beck Depression Inventory – Fast Screen ; SDMT = Symbol Digit Modalities Test ; BVMTR = Brief Visuospatial Memory Test - Revised ; CVLT-2 = California Verbal Learning Test – Second Edition ; T2-LV = T2-lesion volume ; WBV = whole brain volume ; GMV = gray matter volume ; WMV = white matter volume ; LVV = lateral ventricle volume

Effect sizes are given as Cohen's d, in which the difference between means is divided by the pooled standard deviation.

Volume and shape differences between HC and MS

For both left and right thalami, significant differences between HCs and MS patients were seen with regards to shape. In both cases, shape differences, corresponding to localized atrophy in MS patients, spanned more than half of the thalamic surface, including the anterior, medial, and posterior portions of the thalamus. For the left putamen MS patients showed more atrophy along the inferior and lateral surface, whereas no shape differences were found for the right structure. A single cluster showing shape differences along the medial caudate surface was found bilaterally. An additional cluster in the anterior head of the caudate was found on the left side. No significant clusters on the surface indicative of MS > HC were found for any of the structures investigated. A correspondence between presence of DGM lesions and localized atrophy was not seen. Further details regarding the clusters are given in Figure 1 and Table 2

Table 2: Shape analysis differences between multiple sclerosis patients and healthy controls at baseline

Structure	Cluster index	X	Y	Z	Extent (% of surface)	p-value
Left thalamus	1	-3	-5	-3	2141 (68.9)	< .0001
Right thalamus	1	5	-14	-4	1886 (61.3)	.001
Left putamen	1	-17	12	-13	267 (9.6)	.024
Left caudate	1	-8	17	4	621 (22.5)	.02
	2	-16	22	-8	76 (2.8)	.039
Right caudate	1	14	-8	20	888 (31.3)	.003

Notes:

Local maxima within each significant cluster ($p < 0.05$, family-wise error corrected) of significant clusters in the shape analysis comparison of healthy controls > multiple sclerosis patients. X, Y, Z coordinates refer to standard MNI space.

Figure 1

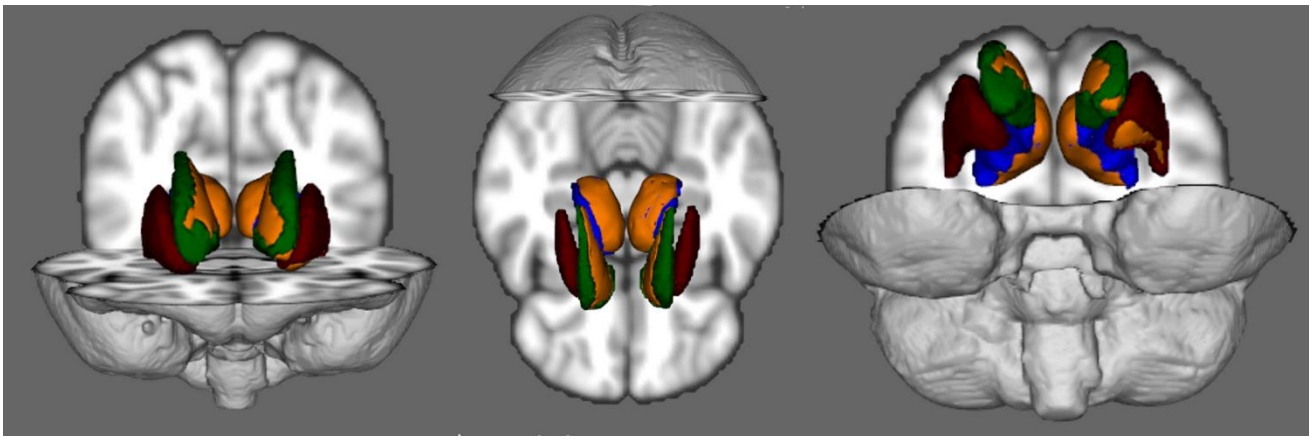

Shape differences between multiple sclerosis patients and healthy controls at baseline. The figure shows the mean shape of the thalamus (blue), caudate (green) and putamen (red). Significant clusters of shape difference, representing local atrophy, between the two groups are shown in orange.

Volume and shape differences between HC and MS over 3-year follow-up

Differences in the rates of change were in the expected direction over the course of the study, with MS patients exhibiting larger degrees of atrophy (Table 3). However, most of the comparisons did not reach statistical significance. The only significant interaction effect seen was for the putamen ($p = .034$) and with the caudate showing a trend ($p = .074$). In terms of the VBM analyses, no significant differences were found regardless of the smoothing kernel used. With respect to shape changes over time, a significant group by time interaction effect was not seen for any of the examined structures. Controlling for baseline T2-LV or normalized brain volume yielded similar findings, with the exception of the caudate which was subsequently significant in both cases (Table 3).

Table 3: Rates of volumetric change in MS and HC over 3-year follow-up

	MS (n = 64)	**HC (n = 22)**	**p-value ***	**p-value #**	**p-value ^**
WBV percent change	-1.37 (1.46)	-.78 (1.39)	.111	.227	.189
GMV percent change	-1.17 (2.65)	-0.40 (3.7)	.367	.805	.914
WMV percent change	0.63 (3.83)	1.30 (3.52)	.617	.551	.883
Cortical GMV percent change	-0.81 (2.96)	-0.33 (3.58)	.566	.736	.653
LVV percent change	1.40 (7.55)	2.42 (12.84)	.436	.009	.059
Caudate volume percent change	-3.87 (5.58)	-1.27 (5.83)	.074	.021	.021
Putamen volume percent change	-3.87 (5.58)	-1.27 (5.83)	.034	.103	.032
Thalamus volume percent change	-2.37 (2.17)	-2.29 (1.79)	.192	.050	.125

Notes:
MS = multiple sclerosis; HC = healthy control; WBV = whole brain volume ; GMV = gray matter volume ; WMV = white matter volume ; LVV = lateral ventricle volume; T2-LV = T2-lesion volume; NBV = Normalized brain volume
* = corrected for age and sex
# = corrected for age, sex and T2-LV
^ = corrected for age, sex and NBV

Data are shown as mean (standard deviation).

Relationships between structural and neuropsychological outcomes in MS patients

At baseline, cross-sectional correlations between neuropsychological tests and shape tended to yield consistent results in terms of both localization and extent across tests (i.e. percentage of surface showing significant relationships). Areas on the surface correlating with SDMT and BVMT-R performance overlapped to a large degree while associations with CVLT-2 performance yielded somewhat smaller clusters (Figure 2 and Table 4).

Figure 2

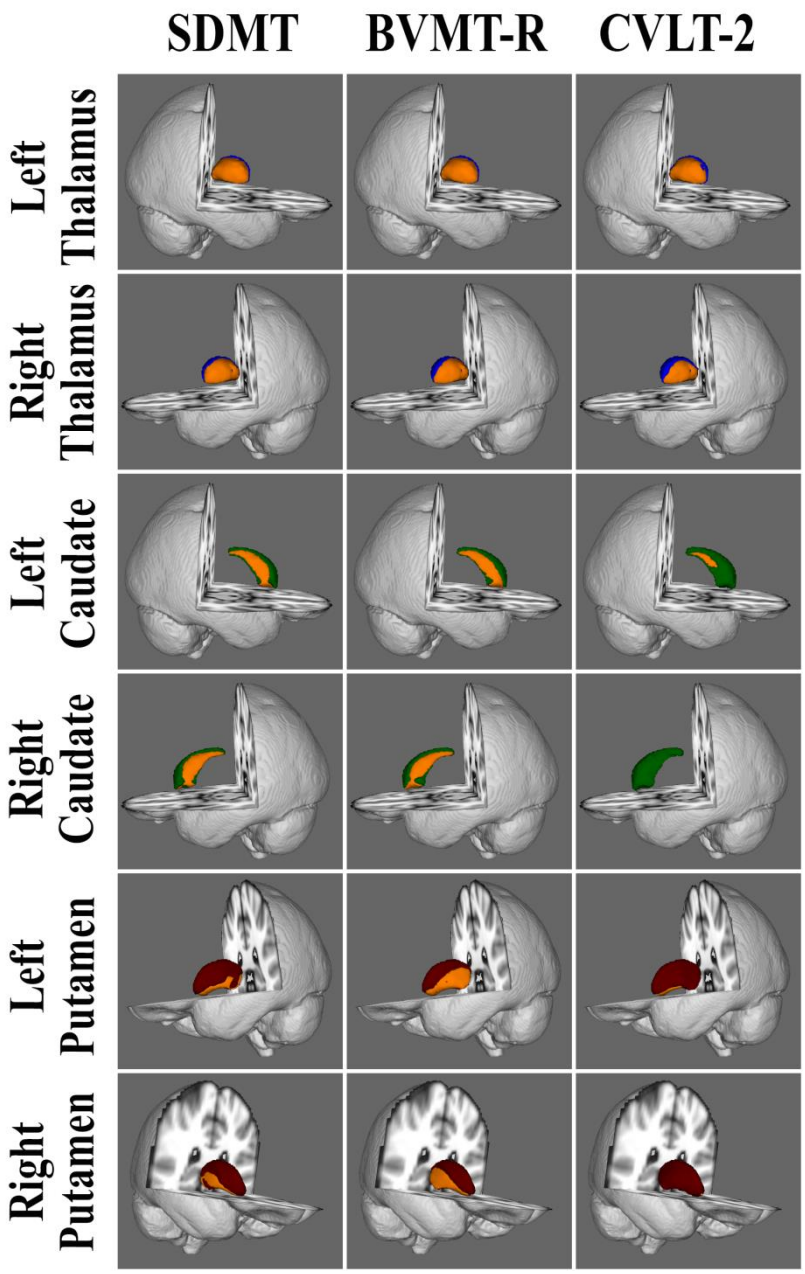

Correlation between localized atrophy and neuropsychological outcomes in multiple sclerosis patients. Significant clusters are shown in orange.
Columns from left to right: SDMT = Symbol Digit Modalities Test; BVMT-R = Brief Visuospatial Memory Test - Revised; CVLT-2 = California Verbal Learning Test - Second Edition

Table 4: Correlation between local atrophy and NP outcomes at baseline in in MS patients

	SDMT					
Structure	Cluster index	X	Y	Z	Extent (% of surface)	p-value
Left thalamus	1	-20	-31	-5	1872 (60.9)	<.0001
Right thalamus	1	22	-31	-4	1596 (52.9)	<.0001
Left putamen	1	-17	9	-13	398 (14.3)	<.0001
Left putamen	2	-31	-14	-10	23 (1.0)	.012
Right putamen	1	20	8	-12	395 (14.4)	.002
Left caudate	1	-7	10	5	858 (31.4)	<.0001
Right caudate	1	8	8	5	830 (29.4)	<.0001
Right caudate	2	15	22	-8	74 (2.6)	.01
	BVMT-R					
Structure	Cluster index	X	Y	Z	Extent (% of surface)	p-value
Left thalamus	1	-18	-33	-4	1823 (59.3)	<.0001
Right thalamus	1	18	-30	-4	1520 (50.4)	<.0001
Left putamen	1	-17	10	-13	881 (31.7)	<.0001
Right putamen	1	30	-3	-8	595 (21.6)	.003
Left caudate	1	-11	-1	16	846 (31.0)	<.0001
Right caudate	1	11	3	15	603 (21.3)	.0001
Right caudate	2	7	10	-5	179 (6.3)	.008
	CVLT-2					
Structure	Cluster index	X	Y	Z	Extent (% of surface)	p-value
Left thalamus	1	-15	-32	-4	1529 (49.8)	.001
Right thalamus	1	14	-21	-4	1151 (38.2)	.001
Left putamen	1	-17	9	-13	264 (9.5)	.002
Right putamen	1	20	8	-12	74 (3.0)	.007
Left caudate	1	-12	-6	17	176 (6.2)	.012

Notes:
NP = neuropsychological; MS = multiple sclerosis; SDMT = Symbol Digit Modalities Test;
BVMT-R = Brief Visuospatial Memory Test-Revised;
CVLT-2 = California Verbal Learning Test-Second Edition

Local maxima within each significant cluster ($p < 0.0167$, family-wise error corrected) of significant clusters in the shape analysis correlating neuropsychological outcomes. X, Y, Z coordinates refer to standard MNI space.

Over three years, volumetric decreases were not significantly related to changes in NP outcomes (Table 5). The same was true for the VBM analyses, where o significant relationships were detected regardless of the smoothing kernel used. However, alterations in left thalamic shape

were found to correlate with change in performance on the SDMT in a single cluster spanning 372 voxels (18.1 percent of the total surface) with a peak corrected p-value = .011. The cluster was localized to the anterior and superior areas of the thalamus (Figure 3). A similar cluster was found for change in shape of the right thalamus with SDMT change although these results did not survive Bonferroni correction. None of the other longitudinal outcomes were significantly correlated with change in shape over the three year follow-up. Including either baseline T2-LV or normalized brain volume as an additional covariate yielded similar findings as controlling for just age and sex when assessing correlations with volumetric change over time (Table 5).With respect to the shape analysis, including T2-LV or normalized brain volume as a covariate yielded similar results, with only results on the left thalamus being significant. Specifically, when including T2-LV, the cluster spanned 349 voxels (17.0 percent of the total surface) with a peak corrected p-value = .012, whereas for normalized brain volume it was 338 voxels (16.4 percent of the total surface) with a peak corrected p-value = 0.014.

Table 5: Correlation between rate of volumetric change and NP changes over follow-up in MS patients

	Controlling for age and sex			Controlling for age, sex and T2-LV			Controlling for age, sex and NBV		
	SDMT	BVMT-R	CVLT-2	SDMT	BVMT-R	CVLT-2	SDMT	BVMT-R	CVLT-2
Thalamus percent change	.085 (.510)	-.006 (.964)	.111 (.392)	.027 (.836)	-.061 (.643)	.089 (.501)	.088 (.500)	-.005 (.970)	.114 (.380)
Putamen percent change	.064 (.621)	.042 (.748)	.130 (.312)	.030 (.823)	.007 (.955)	.142 (.279)	.043 (.739)	.034 (.797)	.107 (.411)
Caudate percent change	.237 (.064)	.198 (.124)	-.072 (.577)	.209 (.108)	.172 (.188)	-.095 (.471)	.235 (.069)	.196 (.129)	-.077 (.556)

Notes: NP = neuropsychological; MS = multiple sclerosis;
SDMT = Symbol Digit Modalities Test; BVMT-R = Brief Visuospatial Memory Test- Revised;
CVLT-2 = California Verbal Learning Test-Second Edition;
T2-LV = T2-lesion volume; NBV = Normalized brain volume

Data are shown as r (p).

Figure 4

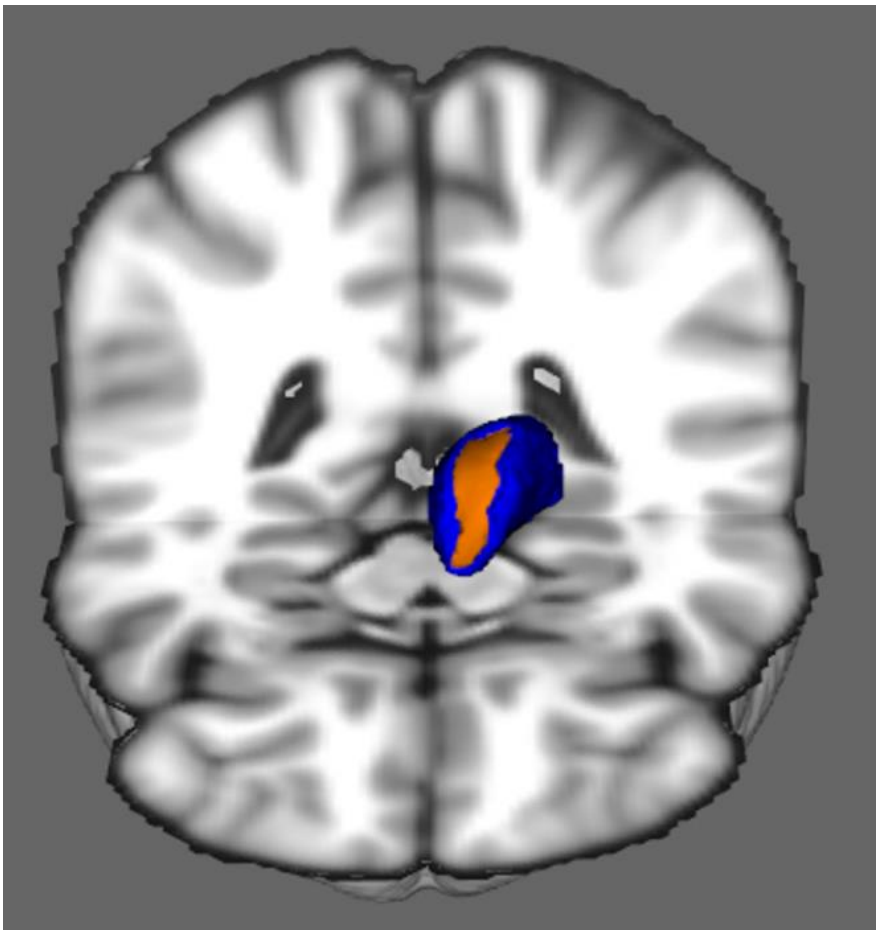

Correlation between localized atrophy over three years of follow-up and decreased performance on the Symbol Digit Modalities Test in multiple sclerosis patients. The figure shows the mean shape of the left thalamus in blue and the significant cluster, spanning 18% of the surface, in orange.

Discussion

The present work describes a 3-year follow-up study utilizing advanced structural MRI post-processing techniques to precisely describe and quantify the localization of thalamic and corpus striatum atrophy in MS. We combined volumetric and shape-based analysis of the DGM with validated neuropsychological tests that have been shown to be sensitive to assessing cognitive function in MS patients. One of the key findings is that localized atrophy of the left thalamus was correlated with decline in SDMT performance. The correlation involved the superior and anterior aspects of the thalamus, as would be anticipated, due to the eloquent function of these sub-regions for cognition.[155, 156] The anterior thalamus participates in key functional networks that mediate complex motor and cognitive operations[157] by virtue of its connections with the anterior cingulate and prefrontal cortex.[158] Moreover, it was recently shown that lesions in the anterior thalamus of rats impaired their ability to direct attention to task-relevant stimuli[155]. Our results are in line with this finding, given that the nature of the SDMT requires active participant attention. On the other hand, the exact cause(s) of the atrophy remain(s) unknown at this time. We did not find a relationship between focal atrophy and thalamic lesions. This is likely in part due to the scarcity of thalamic lesions that we are able to identify. However, it may be the case that we were limited in our ability to detect the latter as a much higher prevalence has been reported when using 7T MRI [159]. Retrograde neurodegeneration as a result of damage along efferent pathways also seems to be a probable candidate in explaining the longitudinal relationship between focal atrophy and cognitive impairment over time[139]. Although controlling for total baseline T2-LV did not alter our results, assessing tract-specific lesion volume may shed further light in this regard. While not surviving the correction for multiple comparisons, the fact

that a very similar pattern was found for the right thalamus appears to reduce the likelihood of this being a spurious finding.

The group effects for thalamus and caudate were generally localized along the medial surface of these structures. An important question is whether these findings represent true atrophy as opposed to mere expansion of the ventricles. If the latter were true, it would likely result in a spurious finding of tissue "growth" on the lateral side of the structure for MS patients as the DGM nuclei would be shifted in position. We did not find evidence of this, although we cannot rule out the possibility that increased pressure within the cerebral ventricles may lead to some degree of compression of the neighboring tissue. Be that as it may, it appears unlikely that such an effect could explain all of the differences that were seen, considering that DGM atrophy in MS has been confirmed in histopathological studies[160] and increased ventricular pressure is not known to be associated with MS. Moreover, shape differences were also seen in the left putamen as well, where ventricular expansion would have much less relevance. In sum, while preliminary, we believe these data support the hypothesis that shape-based changes actually reflect underlying tissue atrophy in this cohort.

Our findings support those from the Bisecco et al. cross-sectional study showing a relationship between cognitive impairment and more pronounced focal atrophy of the anterior thalamic region. However, shape analysis in that study compared MS patients after having been classified as either cognitively preserved or impaired. As such, spatial relationships with individual testing outcomes were not assessed, as was done in the current study. Unlike in the Bisecco et al. study, we did not see evidence of focal atrophy along the lateral sides of the thalami in addition to the medial sides. While the reason for the discrepancy is not entirely clear, there are some methodological differences that need to be considered. First, although the authors

state that lesion filled images were used for SIENAX-based tissue segmentation, they do not report as to whether or not lesion filled images were also used as inputs to FIRST. As shown in chapter 3 , the presence of lesions can significantly affect the shape analysis. Secondly, we did not implement the modifications to the FIRST processing pipelines as proposed by the authors. Briefly, Bisecco et al. suggest that the thalamic segmentation can be improved by using a fractional anisotropy (FA) image for the first stage of the FIRST registration. The rationale provided by the authors is that boundary between the thalamus and the internal capsule is better seen on an FA image, as opposed to a 3D T1 where the GM/WM border is less clear. However, it is difficult to evaluate whether the proposed modification actually yields better results as the authors do not provide any quantitative comparison with the standard registration method used by FIRST. Moreover, it is not clear that any theoretical gains in this regard will not be offset by the lower resolution of the FA maps or by the second stage registration of FIRST, which still utilizes the 3D T1 image. Despite such reservations, the possibility to improve automated segmentations using multiple modalities is clearly of great interest. In fact, the FSL group has recently demonstrated both the feasibility as well as gains in DGM segmentation quality as assessed by greater overlap with manual tracings and better consistency[161]. Regardless of the discrepancies and potential methodological differences, our longitudinal analysis did reveal an anterior region where volume loss over time was associated with cognitive dysfunction.

Given the longitudinal nature of our study, we expected to find more robust structural differences between the HC subjects and MS patient groups in global and localized atrophy rates. Even in terms of NP status, we did not detect evidence of cognitive decline over the course of three years in the MS cohort. As both imaging and NP metrics yielded similar conclusions (i.e. lack of clear changes at the group level over time), it might be the case that the relatively short

follow-up of three years hindered our ability to draw firm conclusions beyond the striking effect of thalamic atrophy in the anterior nuclei and cognitive decline. Moreover, we cannot exclude the possibility that disease modifying therapies and cognitive reserve factors reduced the amount of atrophy that would have otherwise been seen.

To the best of our knowledge, this is the first report detailing a comparison between several structural-imaging based techniques for assessing GM pathology in a longitudinal fashion. All three methods utilized (region of interest, VBM and shape-based) yielded similar findings when comparing changes over the three years of follow-up in MS and HC groups (i.e. a lack of clear differences longitudinally between the two). The only exception to this was for the putamen where MS patients were found to have a significantly increase rate of atrophy using the region of interest based approach. This may in part be explained by the fact that left and right volumetric measures were combined into a single measure for comparison purposes. This is supported by post-hoc tests where we did not find significant differences between the groups when testing left and right volumetric changes separately. On the other hand, only the vertex-wise analysis was able to detect an association between localized atrophy and cognitive decline. This highlights the role that shape-based analyses can have in localizing more precisely the regional predilection of GM pathology and its association with clinical outcomes. Although the various techniques can potentially yield complementary information, a key advantage of the shape-based technique is that no smoothing is needed, unlike in VBM. In the latter approach, signal intensities are blurred with neighboring voxels. However, there is no guarantee that this does not result in the mixing of signal from disparate structural regions. This aspect can be most easily appreciated by considering what happens in the cortex when two gyri are separate by a sulcus. In this case, the gyri may be anatomically and functionally independent but separated by

just a single voxel, corresponding to a sulcus. When smoothed, GM density estimates within the two gyri will be mixed due to being close to each other three dimensionally. However, if the cortex were flattened out like a sheet, the gyri would be much further apart. This fact lends support to the notion that surfaced-based measures may be more precise, and subsequently more informative, than traditional VBM-based approaches as was recently suggested in a comparative study with Parkinson's patients[162]. Although the DGM structures are not convoluted in nature the way the cortex is, the same principle applies with regards to the mixing of potentially separate signals. For example, the thalamus is composed of many different subnuclei with either own functionality and afferent/efferent connections[41, 163]. Thus in the presence of preferential atrophy affecting a given thalamic subregion, the smoothing step used in VBM may hinder the ability to detect it. This appears to have been confirmed by the fact that no association between atrophy and cognitive decline was seen even when using a conservative smoothing kernel of 1.5mm, in an attempt to maintain potential localized effects. Although smoothing is not part of the individual segmentation step in FIRST, treating the structure as a single region may result in any real effect being washed out by the overall tissue volume. Conceptually, this is similar to trying to assess thalamic atrophy by using brain volume as a surrogate measure, despite the likelihood of them being correlated with one another to a certain degree. Total thalamus volume contributes a relatively small amount to the total amount of tissue, rendering the latter as an impropriate proxy for the former. In this context, shape analysis overcomes the limitations inherent in voxel-based and volumetric region of interest based approaches. This claim is supported by the fact that shape analysis was indeed the only technique capable of detecting the relationship between cognitive decline and thalamic atrophy.

The present work is not without limitations. We only assessed the relationships between cognitive performance and DGM metrics in the MS cohort. Due to the small sample size, the cognitive testing in the HC cohort was only used to establish the degree of impairment in the patient group. Thus, we cannot say whether or not the finding of a longitudinal relationship between localized thalamic atrophy and decreased SDMT performance is unique to MS patients. Moreover, the MS cohort, which included both RR and SP MS patients, was analyzed as a whole. Although this was done to reduce the risk of committing a Type I error, it may very well be that the link between cognitive decline and tissue atrophy is magnified in SP disease[164]. Although we used Bonferroni correction when correlating structural measures with NP outcomes, we did not control for the number of assessed structures. Thus, our findings should be considered preliminary and warrant confirmation in larger studies with more targeted, a priori hypotheses. Finally, although FIRST-based shape analysis has not yet been directly validated, we have previously reported excellent scan-rescan reproducibility of volumetric measures using this technique with MS patients[16]. Moreover, it was recently shown that FIRST-derived caudate and putamen volumes in MS patients are comparable with those done manually by an expert rater (thalamic comparisons were not assessed)[44]. It should also be noted that the volumetric segmentation is based on the subject-specific meshes, which are used for the shape analysis itself. Thus, as all segmentations were deemed accurate, we believe that our results are both biologically plausible and clinically meaningful. Despite this, it would be worthwhile to assess whether the use of multimodal segmentation techniques yields results consistent with those presented in the current study. In this regard, the recently developed Multimodal Image Segmentation Tool[161] by the FSL group is an attractive choice. Specifically, the authors incorporate diffusion weighted and quantitative susceptibility mapping data to yield better

segmentation results than is possible using 3D T1 images alone. This is particularly intriguing in the context of the current study since although it was not analyzed, such data was acquired as part of the MRI protocol.

In conclusion, DGM alterations relate to cognitive decline in MS over time and the shape analysis approach allows a sensitive method to study localized atrophy in even finer detail. Future studies with larger sample sizes and a longer follow-up are warranted to provide additional insight in this regard.

Funding Acknowledgement

This work was supported by National MS Society (grant number RG4060A3/1).

Chapter 5: White matter tract injury is associated with deep gray matter iron deposition in multiple sclerosis patients

In this chapter, a novel, multimodal imaging method is implemented for better characterizing the relationship between white matter injury and increased iron deposition in multiple sclerosis (MS) patients. An unbiased, voxelwise approach is used to compare MS and healthy control groups for the identification of areas indicative of increased iron concentrations in the deep gray matter. These regions are subsequently used as seeds for probabilistic tractography for subsequent white matter integrity assessments in the anatomically connected tracts. The proposed approach of combining an iron-sensitive MRI technique with one that is able to quantify tissue microstructure damage may help shed further light on the pathogenetic mechanisms involved in MS.

The work is currently under review in the American Journal of Neuroradiology (Bergsland N, Tavazzi E, et al.).

Abstract

Background and purpose: With respect to healthy controls (HC), increased iron concentrations in the deep gray matter (GM) and decreased white matter (WM) integrity are common findings in multiple sclerosis (MS) patients. The association between these features of the disease remains poorly understood. The current study investigated the relationship between deep iron deposition in the deep GM (DGM) and WM injury in associated fiber matter tracts in MS patients.

Material and methods: 66 MS patients (mean age 50.0 years, median Expanded Disability Status Scale 5.25, mean disease duration 19.1 years) and 29 HCs, group matched for age and sex were imaged on a 1.5T scanner. Susceptibility-weighted imaging and diffusion-weighted images were used for assessing high-pass filtered phase values in the DGM and normal appearing WM (NAWM) integrity, respectively. Correlation analyses were used to investigate the associations between filtered phase values (suggestive of iron content) and diffusion tensor imaging (DTI) properties.

Results: Areas indicative of increased iron levels were found in the left and right caudates as well as in the left thalamus. Greater mean, axial and radial diffusivities were associated with increased iron levels in all three GM areas (r values ranging from .393 to .514 with corresponding p-values from .003 to < .0001). Global NAWM diffusivity measures were not related to mean filtered phase values within the DGM.

Conclusions: DTI properties within the NAWM of MS patients exhibited changes that correlated with increased iron concentrations in the connected DGM.

Introduction

Multiple sclerosis (MS) is a demyelinating, autoimmune-mediated disorder leading to widespread damage throughout the central nervous system. While historically considered a disease of the white matter (WM), MS is now widely understood as having a neurodegenerative component as well. The exact causes of neurodegeneration in MS remain to be fully elucidated. Although iron is an essential component for proper homeostatis in the CNS, it has been postulated that increased levels in MS patients end up being harmful[165]. This phenomenon has been evidenced utilizing both MRI[16, 19, 166, 167] and histopathology[165, 168] techniques, and may have a causative role in neurodegeneration, at least to some degree[17]. In this scenario, increased iron may lead to damage via promotion of proinflammatory mechanisms, induction of mitochondria dysfunction and generation of free radicals[169]. On the other hand, it may be the case that increased iron concentrations are secondary consequences stemming from WM injury. In this situation, neuronal loss or axonal transection may cause interruptions within the WM pathways and subsequently trigger neurodegenerative processes and/or altered metabolism of iron[169]. It might also be the case that even if WM injury is associated with iron deposition, the two phenomena reflect independent processes that occur in parallel rather than being directly related to one another.

Iron deposition in MS has been studied using a number of different MRI-based techniques, including T2 hypointensity[166], magnetic field correlation[170], R2* relaxometry[167], susceptibility-weighted imaging (SWI)[16, 17, 171] and quantitative susceptibility mapping[19, 172]. Due to its sensitivity to paramagnetic substances, SWI high-pass filtered phase imaging allows for the indirect characterization of iron deposition, primarily ferritin, within deep gray matter (DGM) structures[16, 171]. Meanwhile, diffusion weighted imaging acquisitions can be used for both in vivo

reconstruction of WM tracts[82] and assessment of tissue microstructure properties via quantification of the diffusion tensor[173].

A limited number of studies in the MS literature have combined imaging techniques to assess iron concentrations and WM tissue integrity. Ceccarelli et al.[166] reported that DGM T2 hypointensity, indicative of iron deposition, was moderately correlated with global white matter diffusion tensor derived metrics of WM tissue injury. On the other hand, a recent study utilizing magnetic field correlation did not detect any relationships between increased GM iron levels and decreased WM integrity[170].

Against this background, we aimed to investigate the potential relationship between WM injury and iron deposition within the DGM. To this aim, we implemented an unbiased, voxelwise analysis technique for assessing filtered phase differences between MS patients and healthy controls. We then reconstructed the associated WM fiber tracts and assessed the underlying tissue microstructure integrity. To the best of our knowledge, this is one of the first reports to incorporate a voxelwise analysis of filtered phase images along with tractography to more precisely characterize the relationship between DGM iron accumulation and WM integrity in MS patients. We hypothesized that DGM iron would be positively correlated with increased WM damage in anatomically connected tracts.

Materials and Methods

Subjects

Sixty-six (66) MS patients and twenty-nine (29) HC, group matched for age and sex, were included in the study. MS patients underwent a full neurological evaluation. Clinical disability in patients was quantified via the Expanded Disability Status Scale (EDSS). At the time of MRI

acquisition, MS patients were relapse- and steroid-free within the last three months. The HC sample was recruited from volunteers who had a normal neurological examination, with no history of neurological, psychiatric, cardiovascular or metabolic disorders. The study was approved by the "Don Carlo Gnocchi Foundation" ethics committee (Milan, Italy) and all participants provided written informed consent.

MRI acquisition

All scans were acquired on the same 1.5T MRI scanner (Siemens Magnetom Avanto, Erlangen, Germany) with a 12-channel head matrix coil. The following sequences were acquired: 1) dual-echo turbo spin echo PD/T2-weighted [repetition time (TR)=2,650ms; echo time (TE)=28/113ms; flip angle(FLIP)=90° ; echo train length=5; 50 contiguous 2.5-mm thick axial slices; $1mm^2$ in-plane resolution] ; 2) 3-dimensional (3D) T1-weighted magnetization-prepared rapid gradient echo (MP-RAGE) [TR=1,900ms; TE=3ms; inversion time=1100ms; FLIP=15°; 176 contiguous, 1-mm thick axial slices; $1mm^2$ in-plane resolution] ; 3) diffusion weighted (DW) pulsed-gradient spin echo planar [TR=7,000ms; TE=94ms; FLIP=90°; 50 contiguous, 2.5-mm thick axial slices; $2mm^2$ in-plane resolution; diffusion gradients applied in 12 non-collinear directions with a b-value=900 s/mm^2 and one b=0 s/mm^2 image ; number of runs = 2] ; 4) a long-TE, high-resolution, fully flow-compensated 3D gradient echo acquisition for susceptibility weighted imaging (SWI) [TR=49ms; TE=40ms; FA=15°; 80 contiguous,1.6-mm thick axial slices; 0.7 mm^2 in-plane resolution]. SWI high-pass filtered phase images were automatically processed on the console as per the MRI manufacturer's implementation. Briefly, a 96x96 low-pass filtered image was created. The next step then involved complex division of the original image with the low-pass filtered image to obtain the final SWI high-pass filtered phase image[171].

As the phase images are from a left-handed system, paramagnetic materials such as iron have positive phase.

MRI analysis

Unless otherwise specified, all steps were performed using the tools available in FMRIB's Software Library[83] (FSL, http://www.fmrib.ox.ac.uk/fsl) version 5.0.7.

WM lesions were segmented on the PD-weighted scans with JIM software (http://www.xinapse.com/) version 5, which utilizes a semi-automated, local thresholding technique, by a single reader. The corresponding T2-weighted scan was used to increase confidence in lesion identification. To reduce the impact of T1 hypointensities on tissue segmentation[43], 3D T1 images were preprocessed using FSL's "lesion_filling" tool with the processing described in Chapter 2.

The SIENAX cross-sectional software tool[126] was used to estimate normalized volumes of gray matter, white matter volume brain parenchyma. FMRIB's Integrated Registration and Segmentation Tool (FIRST)[7] was used to segment the caudate, pallidus, putamen and thalamus. All segmentations were quality controlled by an experienced rater. The SWI magnitude image for each subject was registered to the subject's 3D T1 image with FMRIB's Linear Image Registration Tool (FLIRT) using six degrees of freedom (rigid body). Mean SWI high-pass filtered phase values were subsequently calculated within the FIRST-derived segmentations.

Next, we generated an unbiased, group template from the 3D T1 data using the "buildtemplateparallel.sh" script provided as part of the ANTs software package (version 2.1)[174]. To avoid favoring one group over the other in terms of registration to template quality, we used

an equal number of subjects (29) from each group in the template construction. The 29 patients used for template construction were randomly selected from the total MS sample. The SWI high-pass filtered phase images were then registered into template space using a combination of the "SWI magnitude to 3D T1" rigid body transformation and "3D T1 to template" warp. Next, we utilized "randomise" with threshold-free cluster enhancement[151] to assess SWI high-pass filtered phase differences between MS and HC groups. 5000 permutations were used. Analysis was restricted to the DGM while age and sex were included as nuisance variables. Mean phase values within significant clusters were then extracted for each subject. As atrophy may potentially confound high-pass filtered phase measurements[175], we repeated the analyses with the inclusion of GM partial volume estimates from SIENAX (modulated by the Jacobian of the warp) as a voxelwise covariate. For visualization and reporting purposes, the resulting clusters are shown in MNI space.

Initial DTI processing was performed using FMRIB's Diffusion Toolbox[176]. Briefly, raw DW images were preprocessed using the "eddy_correct" tool to reduce effects of gradient-related geometric distortions and head motion. Then, "dtifit" was used to fit a tensor model at each voxel and scalar maps of fractional anisotropy (FA), mean diffusivity (MD), axial diffusivity (AD) and radial diffusivity (RD) were created. The b=0 image was linearly registered to the 3D T1 using the brain boundary registration cost function[66]. Diffusivity parameters within the normal appearing white matter were then calculated using SIENAX-derived segmentations while masking out lesional areas.

As the presence of WM lesions were found to interfere with successful tractographic reconstruction, we generated probabilistic tract atlases from the HC data. To this aim, voxelwise diffusion parameter distributions were first estimated using "bedpostx"[51]. Probabilistic

tractography was then performed with "probtrackx"[177] (5000 streamlines per voxel). The significant clusters obtained from the SWI high-pass filtered phase group analysis were used as seed regions. The resulting tract maps were then binarized after thresholding (0.3% of the total number of seeded streamlines) and then brought into the previously generated template space. Probabilistic atlases were subsequently created by averaging the individual maps. Finally, the resulting atlases were propagated to the native space of each subject to obtain weighted averages, based on atlas probability, of FA, MD, AD and RD within each tract. For visualization purposes, the resulting atlases are shown in MNI space.

Statistical analysis

Analyses were performed using SPSS 21.0 (IBM Corp., Armonk, NY) and R 3.2.2 [130]. Demographic characteristics were compared between HCs and MS patients using Student's *t*-test Fisher's exact test for age and sex, respectively. Normality of the data was assessed via visual inspection of histograms and the Shapiro–Wilk test. All investigated MRI-derived parameters were considered normally distributed except for lesion volumes, which were subsequently log-transformed to approximate normal distributions. Structural volumes, diffusivity parameters and DGM mean phase values were compared using Analysis of Covariance (ANCOVA) models, adjusting for age and sex.

Next, partial correlations were analyzed to investigate the association between cluster-wise phase values and the diffusivity parameters within the corresponding probabilistic atlas. For MS patients, we also assessed relationships between tract-specific lesion volumes and cluster-wise phase values. For all analyses, we controlled for age, sex and the mean value within the normal appearing WM (NAWM) for the respective diffusivity parameter. We also examined correlations between SWI high-pass filtered phase values of the DGM structures as whole and

global NAWM diffusivity parameters. Analyses were conducted separately for the HC and MS groups. Additional exploratory analyses were conducted in the patient group to assess relationships between EDSS and DTI-derived metrics within the NAWM.

Using two-tailed tests, p values < .05 were considered significant. Benjamini-Hochberg correction was used to control the false discovery rate[178].

Results

Subject characteristics

Demographic data and clinical characteristics (patients only) of the study subjects are summarized in Table 1. All of the enrolled subjects completed the full MRI examination and were included in the analysis.

Table 1: Demographic and clinical characteristics of healthy controls and multiple sclerosis patients

	HC (n = 29)	MS (n = 66)	*p*
Age in years, mean (SD)	45.5 (15.0)	50.0 (10.4)	.148
Sex, female, N (%)	17 (58.6)	39 (59.1)	1.0
Disease duration – mean in years (SD)	-	19.1 (9.8)	-
EDSS – median (range)	-	5.25 (0 – 8)	-
Disease course (RR / SP / PP)	-	32/25/9	-

Legend: HC = healthy controls; MS = multiple sclerosis; n = number; SD = standard deviation; EDSS = Expanded Disability Status Scale; RR = relapsing-remitting; SP = secondary progressive; PP = primary progressive

Demographic differences were tested using the Student's *t*-test and Fisher's exact test for age and sex, respectively.

Global and regional tissue measures

Table 2 presents differences between the HCs and MS group (as a whole) in terms of structural tissue volumes, diffusivity characteristics and mean phase values within the DGM structures. Overall, MS patients presented significantly increased tissue damage as evidenced by volumetric and diffusivity comparisons. There were no significant between-group differences in terms of SWI high-pass filtered phase values within the examined DGM structures as a whole.

Table 2: Structural brain volume, diffusion measures and phase measures in multiple sclerosis patients and healthy controls.

	HC (n = 29)	MS (n = 66)	*p*
Global and regional volumes			
Normalized brain vol.	1528 (87)	1420 (89)	< **.0001**
Normalized GM vol.	784 (62)	720 (58)	< **.0001**
Normalized WM vol.	744 (40)	700 (46)	< **.0001**
Normalized thalamus vol	20.6 (1.5)	17.5 (2.6)	< **.0001**
Normalized caudate vol.	9.1 (1.0)	7.9 (1.2)	< **.0001**
Normalized globus pallidus vol.	4.4 (0.5)	3.9 (0.7)	**.005**
Normalized putamen volume	12.5 (0.9)	11.0 (1.8)	< **.0001**
T2 lesion vol.	-	8.3 (5.6)	-
Diffusivity parameters			
NAWM FA	.34 (.01)	.32 (.02)	< **.0001**
Lesion FA	-	.28 (.04)	-
NAWM MD	.84 (.03)	.89 (.04)	< **.0001**
Lesion MD	-	1.19 (.14)	-
NAWM AD	1.15 (.03)	1.17 (.03)	**.002**
Lesion AD	-	1.54 (.14)	-
NAWM RD	.69 (.03)	.74 (.04)	< **.0001**
Lesion RD	-	1.02 (.14)	-
DGM phase measures			
Thalamus	.002 (.002)	.002 (.004)	.596
Caudate	.030 (.006)	.032 (.010)	.216
Globus pallidus	.020 (.011)	.025 (.017)	.133
Putamen	.009 (.009)	.014 (.014)	.138

Legend: HC = healthy control; MS = multiple sclerosis; vol. = volume; GM = gray matter; DGM = deep gray matter; WM = white matter; NAWM = normal appearing; FA = fractional anisotropy; MD = mean diffusivity; AD = axial diffusivity ; RD = radial diffusivity

Volumes are presented in milliliters. FA is a dimensionless measure. Diffusivity measures are presented as 10^{-3} mm^2/s. Phase values are shown in radians. As the phase images are from a left-handed system, paramagnetic materials have positive phase. *p* values were calculated using ANCOVA, controlling for age and sex. Benjamini-Hochberg correction was used to control the false discovery rate and p-values <0.05 were considered significant (bold).

Voxelwise analysis of high-pass filtered phase images

The 3D T1 template image is shown in Figure 2.

Figure 2

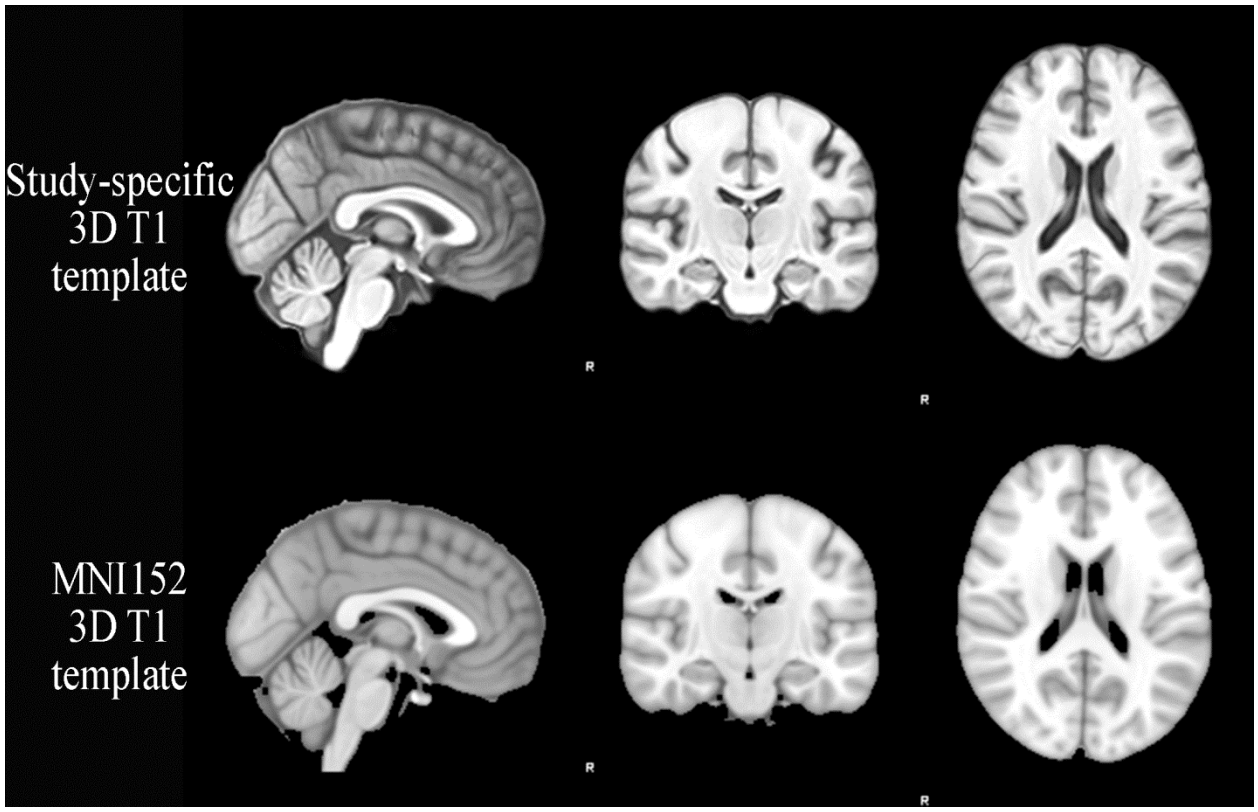

Representative sagittal, coronal and axial slices are shown of the study-specific 3D T1 and standard MNI 152 templates. The study-specific template has been aligned into the space of the MNI152 template for visualization purposes. The study-specific template was created using ANTs with 3D T1 images from 29 healthy controls and 29 MS patients. Note that the study-specific template has higher tissue contrast and borders are more sharply defined.

The voxelwise comparison of high-pass filtered phase images yielded three significant clusters within the DGM where MS patients presented with significantly increased SWI high-pass filtered phase values with respect to HCs (Figure 3 and Table 3). There were no areas of increased phase values in the HC group with respect to MS patients. The inclusion of GM partial

volume estimate images as a voxelwise covariate yielded the same localization of high-pass filtered phase differences.

Table 3: Voxelwise comparisons of increased SWI high-pass filtered phase values, indicative of iron deposition, in MS patients with respect to healthy controls

Structure	Cluster size	Peak X	Peak Y	Peak Z	Peak p value
Left caudate	556	-14	5	17	.029
Left thalamus	113	-7	-15	14	.035
Right caudate	18	13	-4	19	.035

Peak coordinates refer to standard MNI space. Voxelwise comparisons were family-wise error corrected at $p < .05$.

Figure 3

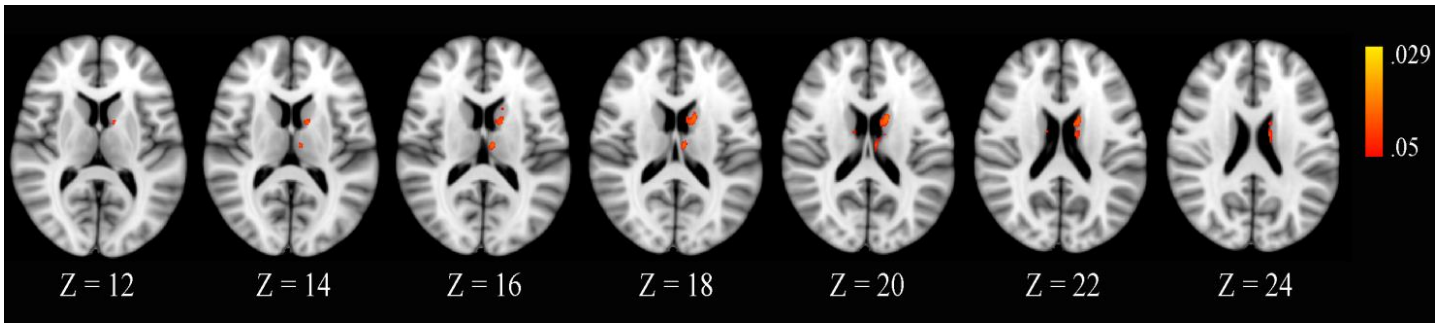

Voxelwise analysis of SWI high-pass filtered phase images within the deep gray matter. Red-yellow clusters are indicative of increased iron concentrations in MS patients with respect to healthy controls, with warmer colors representing smaller p-values. Slices are shown in MNI space for visualization purposes.

Probabilistic atlas generation

The probabilistic atlases generated from seeds within the caudates (left and right separately) consisted of the anterior thalamic radiations and the prefronto-caudate pathway. For the left thalamic seed region, there was considerable overlap for the generated atlas with respect to the one from the left caudate. However, the thalamic seed resulted in an atlas extending through a larger portion of the white matter throughout the brain, as might be expected (Figure 4).

Figure 4

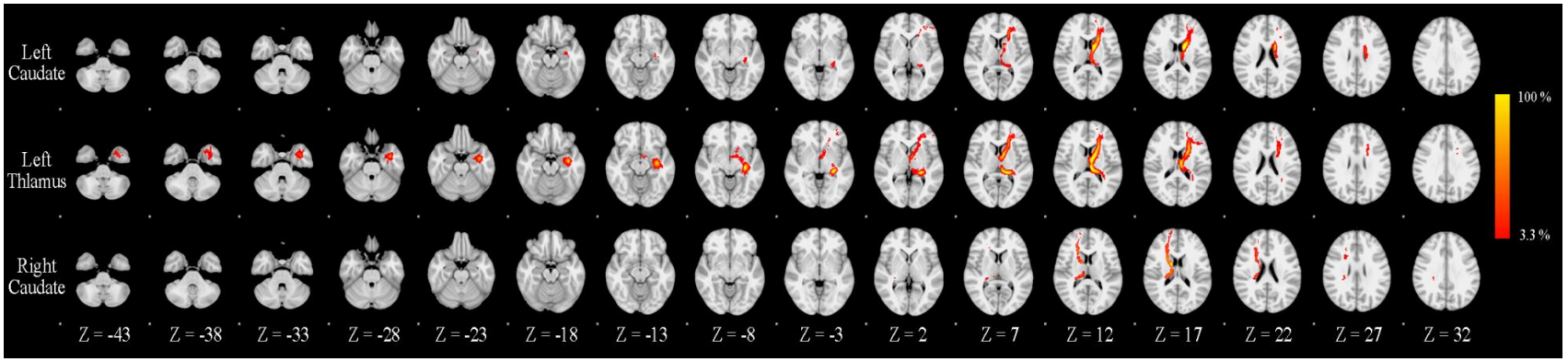

Probabilistic atlases constructed from the healthy control subjects. Probabilistic tractography was performed using seed points derived from the voxelwise SWI high-pass filtered phase analysis. Warmer colors represent an increased probability of a given voxel corresponding to the tract in the sample of healthy controls. Atlases are shown in MNI space for visualization purposes.

Correlations between filtered phase and white matter integrity

As regards the correlations between the cluster-derived SWI high-pass filtered phase values and the associated WM tracts, we consistently found relationships of similar magnitudes with all three measures of diffusivity (i.e. MD, AD and RD) in MS patients. Lesion volume within the tracts generated from the left thalamus and left caudate was also positively correlated with SWI high-pass filtered phase values. With the exception of fractional anisotropy of the tract originating from the seed in the left caudate, no relationships were seen in the HC group (Table 4). On the other hand, no significant correlations were seen in either group between phase values of DGM structures as a whole and any diffusivity measures of global NAWM.

Table 4: Correlations between mean SWI high-pass filtered phase values and diffusivity parameters / lesion volumes within associated white matter tracts

Phase cluster	Tract-specific measure								
	Fractional anisotropy		Mean diffusivity		Axial diffusivity		Radial diffusivity		Lesion volume
	HC	MS	HC	MS	HC	MS	HC	MS	MS
L. caudate	**-.467 (.036)**	-.034 (.822)	.193 (.467)	**.452 (<.0001)**	.118 (.639)	**.514 (< .0001)**	.234 (.357)	**.424 (.003)**	**.516 (< .0001)**
L. thalamus	-.008 (.970)	-.207 (.187)	.117 (.639)	**.408 (.003)**	.121 (.639)	**.439 (<.0001)**	.100 (.678)	**.393 (.003)**	**.345 (.012)**
R. caudate	-.363 (.131)	.163 (.321)	.243 (.348)	**.421 (.003)**	.138 (.639)	**.442 (< .0001)**	.293 (.248)	**.400 (.003)**	.230 (.131)

Legend: HC = healthy control; MS = multiple sclerosis; L. = left; R. =right

Partial correlations controlled for age, sex and respective mean diffusivity parameter within the entire normal appearing white matter. Data are shown as r (p). Benjamini-Hochberg correction was used to control the false discovery rate and p-values <0.05 were considered significant (bold). The associated tracts were constructed by seeding the tractography algorithm in HCs in areas where MS patients presented with significantly increased SWI high-pass filtered phase values.

Correlations between EDSS and tract-specific measures

Whereas mean DTI-derived metrics from the NAWM did not correlate with disability, tract-specific MD, AD and RD values significantly with MS patients' EDSS scores, albeit relatively modestly (Table 5).

Table 5: Correlations between EDSS and DTI-derived parameters

Parameter	Correlation (p)
NAWM FA	-.079 (.561)
NAWM MD	.161 (.249)
NAWM AD	.159 (.249)
NAWM RD	.152 (.255)
L. caudate tract NAWM FA	-.268 (.053)
L. caudate tract NAWM MD	**.401 (.008)**
L. caudate tract NAWM AD	**.367 (.010)**
L. caudate tract NAWM RD	**.442 (.003)**
L. thalamus tract NAWM FA	-.196 (.167)
L. thalamus tract NAWM MD	**.281 (.044)**
L. thalamus tract NAWM AD	.261 (.056)
L. thalamus tract NAWM RD	**.288 (.043)**
R. caudate tract NAWM FA	-.040 (.750)
R. caudate tract NAWM MD	**.307 (.032)**
R. caudate tract NAWM AD	**.315 (.032)**
R. caudate tract NAWM RD	**.309 (.032)**

Legend: EDSS = Expanded Disability Status Scale; NAWM = normal appearing; FA = fractional anisotropy; MD = mean diffusivity; AD = axial diffusivity; RD = radial diffusivity; L. = Left ; R. = Right

Benjamini-Hochberg correction was used to control the false discovery rate and p-values <0.05 were considered significant (bold). Data are shown as r (p).

Discussion

In the current study, we utilized a novel voxelwise-based technique for analyzing SWI high-pass filtered phase images which have been shown to be highly sensitive to the presence of iron in the deep gray matter[18]. We identified three areas where patients with MS showed significantly increased phase values, indicative of iron deposition[18], with respect to healthy controls**.** We subsequently used these areas as seeds for tractographic reconstruction with the final aim of constructing probabilistic atlases to be used for the extraction of quantitative parameters derived from the diffusion tensor. This novel approach allowed us to better assess the relationship between iron deposition and damage along the connected white matter tracts. Moreover, the results appear to be at least somewhat independent from GM atrophy, considering the voxelwise phase analysis results remained unchanged when including GM volume as a covariate.

The choice to use the ANTs package for generating the template was driven by it having been ranked number one (out of fourteen) in a comparison study of nonlinear deformation algorithms for human brain image registration[179]. A comprehensive evaluation of the commonly used tools in the neuroimaging community was beyond the scope of the current work. However, Figure 2 shows a qualitative comparison between the ANTs generated template and the standard MNI152 template. Although it was not investigated in the current study, ANTs does also have support for the creation of multivariate templates which combine multiple imaging modalities. Such an approach may be attractive for future studies whereby the additional contrast offered by the phase images may likely yield even better quality results. Indeed, such an approach was recently described whereby templates generated from T1 and quantitative susceptibility mapping data were superior than when using either image type independently[180].

A recent study reported that NAWM injury, as assessed using DTI-derived parameters, was not associated with increased iron deposition within the GM, as measured with magnetic field correlation[170]. It should be noted that Raz et al., investigated DTI-derived parameters within the overall NAWM and iron deposition within the entire GM. These results are in line with the current study where global NAWM diffusivity measures were not related to average SWI high-pass filtered phase values within DGM structures considered as a whole. On the other hand, the moderate correlations between clusters identified in the combined voxelwise SWI high-pass filtered phase and tract-specific analyses suggest that a more targeted approach is likely to better characterize the potential underlying relationship between WM injury and DGM iron deposition. We found that tract-specific measures of MD, AD and RD within the NAWM were all correlated with the phase values of their respective seed cluster in the GM. It should be noted that the exact interpretation of the AD and RD changes in terms of underlying tissue structure remains problematic[49]. Regardless of whether diffusivity alterations are a result of axonal damage, demyelination or perhaps even more likely, a combination of the two, these results do suggest that NAWM injury is associated with increased iron deposition in the DGM.

The high-pass filtered phase approach does not allow for a reliable estimation of iron within the WM due to the confounding effects of myelin[167]. Susceptibility contrast in the cortex is also thought to be driven primarily by differences in myelin contrast[167]. Thus, assessment of phase values was restricted to the DGM. Our findings of increased iron, bilaterally in the caudate, are in line with a number of studies using both phase measures[16, 181-183] as well as R2* mapping[183, 184]. There have also been several reports regarding the investigation of iron and the thalamus in multiple sclerosis. In this case, however, the results are somewhat more mixed. A recent study in which R2* mapping was used to longitudinally monitor iron concentrations found

evidence of decreased levels in the thalamus[181, 185] over time in subjects with clinically isolated syndrome (patients presenting for the first time with symptoms of MS). On the other hand, others have reported evidence of increased iron within the thalamus[16, 123, 184, 186]. Of note, the pulvinar nucleus appears to be the most consistent subregion of the thalamus associated with increased iron concentrations in MS[123, 184, 186, 187]. The reason for these discrepancies is not entirely clear at this time. However, it is important to remember the fact that there is considerable WM lamina between the thalamic nuclei. Thus, with respect to other DGM structures, myelin content may act more strongly as a relevant confound. In this context, one needs to consider the factors that affect susceptibility measures. Whereas iron is paramagnetic and results in an increase in phase (for a left-handed imaging system), myelin is diamagnetic, causing phase values to move in the opposite direction. Thus, an increase in phase values evidenced in MS patients may be attributed to an increase in iron concentration, a decrease in myelin content, or perhaps more likely, a combination of the two phenomena. On the other hand, reports of decreased susceptibility in the thalamus of MS patients with respect to healthy controls cannot be interpreted as increased myelin, considering the nature of the disease. Rather, this suggests that the temporal and spatial dynamics of iron deposition (and possibly iron clearance) within the thalamus might be more complex than other regions. Longitudinal studies with long-term follow up are likely required to resolve this question.

It should be noted that iron deposition has been reported to affect DTI-derived metrics within the DGM.[188, 189] Interestingly, however, the overall effect appears to potentially mask tissue damage as quantified by diffusivity parameters. This is evidenced by decreased MD and increased FA values in the presence of iron. Thus, there does not seem to be a potential bias in our findings. If anything, the effect of iron deposition may underestimate the true effect. To the

best of our knowledge though, no study has yet investigated the effect of iron on DTI parameters within the WM. As has been noted previously however, obtaining reliable measures of iron content within the WM using $R2^*$ or phase imaging is much more challenging (if not impossible) due to, in large part, the effects of myelin. While there are a number of reports suggesting that WM iron content can be assessed using phase[59, 190], quantitative susceptibility mapping[191] or $R2^*$[192], the inherent difficulty in disentangling the effect of demyelination is frequently given as a caveat in studies using such imaging modalities. Moreover, the interpretation of phase contrast in the WM as a sign of iron deposition has been further complicated by the work of Yablonskiy et al.[193] The specific type of WM tissue damage may be reflected by the change in phase behavior whereby myelin injury moves in the opposite direction with respect to neurofilament damage. While the expected behaviors in this case were derived primarily from theoretical considerations and need to be directly proven, the results certainly suggest that WM phase changes need to be interpreted with great caution. Thus, it seems that other approaches are needed in order to aid in accounting for myelin content. In this context, other MR imaging techniques such as myelin mapping[194] or ultrashort echo time[195, 196], could help in obtaining a more reliable measurement of iron outside of the deep gray matter. With these approaches, it seems likely that one could control for effects due to myelin and obtain a more direct measure of WM tissue iron content.

Although a number of reports have investigated associations between DTI-derived WM characteristics and patient disability, findings have not always been consistent. Such discrepancies are likely due to key differences in aspects such as post-processing methodology[46]and patient heterogeneity[197]. Regardless, our findings are in line with another study showing that atrophy of the anterior thalamic radiations is associated with increased EDSS

scores[198]. Although we did not assess tract-specific atrophy, decreased WM volume is likely to be linked with altered tissue diffusivity[199].

It should also be noted that we did not find any significant differences between MS patients and HCs when investigating the average SWI high-pass filtered phase values within structures as a whole. Several reports have found such an effect. However, it must be noted that these reports have generally relied on comparing the volume or mean value of voxels which are considered "abnormal" based on comparisons to normative values derived from HC data[16, 17, 190]. The most commonly used definition of abnormal in this context corresponds to filtered phase values which exceed more than two standard deviations of the mean value obtained in HCs. We did not implement such a technique in the current work as we aimed to use a purely data-driven approach. However, we would expect that the clusters we identified would correspond, at least in part, to areas retained after thresholding with the abnormal cut-off values.

We found evidence of increased iron content in the medial and anterior regions of the left thalamus in MS patients with respect to HCs. There have been other reports in the literature of increased thalamic iron content in MS patients. Using $R2^*$ mapping in a relatively small cohort of RRMS patients (n = 17), Walsh, et al. found increased iron concentrations both in the pulvinar nucleus of the thalamus as well as within the rest of the thalamus[184]. Phase imaging, however, only revealed differences within the pulvinar nucleus. With neither measure though was there a significant effect for time over the course of two years of follow-up. Increased iron content within the pulvinar nucleus and the thalamus as a whole has also been reported in a previous study using SWI high-pass filtered phase imaging. It must be noted though that in that study, non-pulvinar thalamic measures were not made, unlike in the Walsh, et al. study. Increased iron content within the pulvinar nucleus of the thalamus has been previously reported in a cohort of

adolescents with MS[187]. On the other hand, lower susceptibility values, indicative of less iron content, within the thalamus have recently been reported in a sample of 160 MS patients when using quantitative susceptibility mapping [200]. The reason behind this discrepancy is not clear at this time and requires further investigation.

The current study is not without its limitations. In recent years, there has been an enormous interest in quantitative susceptibility mapping for assessing iron deposition. This technique overcomes several issues that are inherent in the filtered phase approach (e.g. orientation dependence, non-local effects) [172]. Quantitative susceptibility mapping, however, require availability of the raw phase data, whereas we only had access to the high-pass filtered phase image. Additionally, the relatively coarse spatial and angular resolutions of the diffusion data prevented us from being able to fully separate the prefronto-caudate pathway from the anterior thalamic radiations[201]. However, we do not have reason to believe that this would bias the results one way or the other. Finally, as with any cross-sectional study, we were unable to assess the temporal dynamics between WM damage and iron deposition. Longitudinal studies are warranted to address this question.

In conclusion, an optimized, unbiased pipeline was successfully implemented for the combined analysis of filtered phase (indicative of iron deposition) within the DGM and tissue integrity in the associated WM tracts. The developed methodology was successfully applied to a cohort of healthy controls and MS patients. In this context, the study revealed an association between damage in the normal white matter and evidence of iron deposition within the associated DGM structures in MS patients. These findings may help shed further light on the pathogenetic mechanisms involved and the interplay between these two facets of the disease.

Acknowledgements

This research was supported by 2014 Ricerca Corrente (Italian Ministry of Health).

Chapter 6: Discussion and conclusions

The advent of MRI as a means for studying multiple sclerosis has significantly improved our understanding of the disease in a way that was only possible previously with histopathology. Despite all of the advances directly attributable to MRI though, there is still much to learn regarding the pathogenetic mechanisms, development, and damaged structures involved in the disease. Advanced MRI methods, such as fine-grained structural segmentation, DTI and iron-sensitive techniques, have demonstrated their utility in more precisely characterizing the multifaceted features associated with multiple sclerosis. The aforementioned imaging methods have yielded numerous insights even when used independently of one another. However, it appears to be more and more likely that it is only with combined, multimodal imaging assessments that we can fully understand the intricate relationships between different objective pathological features and also the cognitive impairment outcomes of the disease.

Addressing the aspect of focal WM pathology

Despite the attractiveness of using advanced imaging methods as described in this thesis, it is important to remember that most of the commonly used neuroimaging tools were not developed nor explicitly tested with data acquired from patients with MS. Thus, with respect to working with healthy control data, additional care is generally required to ensure that the obtained results are both accurate and biologically meaningful. For example, in the case of MS-related focal WM pathology such as that easily seen with conventional imaging techniques, tractographic and morphological analyses might be hampered. For the former, the reconstructed WM tracts might not reflect the true anatomy of the subject while WM lesions can result in artificially inflated GM volumes or cortical thickness for the latter. Such findings have motivated the use of additional pre-processing steps (such as lesion filling prior to segmentation) or

alternative methods (such as probabilistic WM atlases for template-based tractography) to obtain more reliable and reproducible patient specific measures. As regards the former, the effects of lesions on automated segmentation techniques were addressed qualitatively and quantitatively in Chapters 2 and 3, respectively. WM lesions were found to bias the results of both cortical reconstruction with FreeSurfer and FIRST-based, automated segmentation of the deep GM (DGM) structures. Moreover, the surface-based analysis of the DGM structures revealed that failing to correct for lesion presence may introduce non-local (i.e. distal from focal WM lesions) segmentation errors. These effects are likely to be particularly insidious given that many, if not most, users of the software are not experts in neuroanatomy and will simply trust the segmentations as being correct, barring any blatantly obvious errors. Focal lesions will of course also affect other steps, such as nonlinear registration, common to many processing pipelines. However, it must be noted that great attention was paid during the development and implementation of the analyses used in our studies and adjustments were made as necessary. In sum, the presence of pathology needs to be carefully considered in the design and planning of analyses used in a project utilizing advanced imaging techniques for the study of MS.

The role of tractography in characterizing WM damage

Two of the studies discussed in the current thesis utilized tractographic methods for the reconstruction of WM fiber bundles, as described in Chapters 2 and 5. In both cases, individual tractography in MS patients was found to be unsatisfactory. Deterministic tractography based on the manual placement of ROIs was used in the study involving the relationship between CST injury and motor cortex thickness. In this case, tractographic reconstruction tended to terminate prematurely in the presence of WM lesions for several of the MS subjects. On the other hand, we used probabilistic tractography in the study that investigated the relationship between putative

iron deposition and WM tract integrity. In this case, we also found that WM reconstructions were much more unreliable in the MS cohort with respect to the HC one. This was evidenced by incomplete reconstruction of fiber tracts as well as ones that were not consistent with known anatomy. Thus, we utilized probabilistic atlases derived from our HC data in both studies. This approach has enjoyed widespread use in the literature as a means to circumvent some of the well-documented difficulties with tractography of data from subjects with MS[11, 202].

It should be noted that there have been reports in the literature where tractographic techniques were successfully utilized directly in data from MS patients[54, 203, 204]. However, there are some important points that need to be considered in this regard. First, in both our studies, the diffusion protocol was relatively limited in that it utilized only twelve gradient directions, due to our clinical protocol limitations. It has been previously demonstrated that increased reliability as well as reproducibility of tractographic reconstructions can be obtained when using a larger number of directions[205]. Although the findings of that study were based on acquisitions acquired in a HC cohort, it is certainly reasonable to expect that a similar effect would be seen in MS patients, particularly in the case of focal WM lesions. The degree to which an increased number of diffusion encoding directions could help though would depend on the severity of the underlying pathological substrate. Areas of severe tissue destruction and axonal loss are unlikely to have a coherent diffusional preference whereas lesions characterized by relatively minor inflammation should not present too much of a problem. This aspect may also explain why some authors have found better success when using tractography directly with data from MS patients. For example, one study investigated patients in a much earlier stage of the disease[204] with respect to the patient cohorts in our studies. Although lesion load was not reported, the images shown by the authors reveal a much lighter degree of focal WM pathology. The use of higher field

strengths in other studies,[54, 203] using a direct tractographic approach, may also to play a role, at least to some degree. However, to the best of our knowledge, there have been no studies comparing the effect of field strength on tractographic reconstructions in the presence of MS lesions. Nevertheless, it is apparent that higher field strengths are not entirely sufficient to overcome the focal pathology problem in tractography studies; several studies utilizing diffusion data acquired at 3T have also exploited probabilistic atlases due to inaccurate/unreliable reconstructions of the fiber tracts in the presence of WM lesions[11, 104, 202, 206].

The relationship between WM pathology and GM injury

The aforementioned tractographic studies of this thesis examined the associations between WM injury and pathological processes in the GM. In the first study, we found that CST tract injury, as assessed by focal lesions and DTI-derived parameters, was associated with decreased cortical thickness in the anatomically and functionally connected primary motor cortex. As the study was cross-sectional in nature, we could not establish cause and effect, but both focal and NAWM injury is thought to contribute to GM pathology via retrograde myelinoaxonal degradation[74]. In the second study, we utilized a probabilistic tractography approach based on seed points derived from a voxelwise analysis of SWI high-pass filtered phase data, a putative marker of iron. To the best of our knowledge, we are the first to implement a method for quantitatively assessing the relationship between MRI markers of putative DGM iron deposition and injury in the associated WM tracts. Moreover, the approach is fully data-driven and unbiased. Although much remains to be learned with respect to DGM iron deposition, the results from our study may help shed further light on the possible role of WM injury. Finally, although we utilized SWI high-pass filtered phase data, the method itself is amenable to other

iron-sensitive acquisitions. Thus, it would be worthwhile to repeat the analysis using other imaging measures such as quantitative susceptibility mapping or R2* mapping.

We found that tract integrity in the MS patient cohort was related to focal iron deposition in the anatomically connected DGM. Conceivably, cortical thinning and iron deposition represent separate pathogenic mechanisms in MS. Indeed, it remains a matter of debate whether iron deposition is a cause[17] or a consequence[207], or perhaps a combination of the two, of neurodegenerative and inflammatory aspects in MS. Regardless, it is interesting to note that the magnitudes of the correlations were similar when investing the association between WM injury and 1) cortical thinning and 2) putative iron deposition in the DGM. The exact meaning of these similarities is unclear at this time but it might suggest that retrograde neurodegeneration following axonal transection plays a similar role in both phenomena. However, DTI-derived NAWM parameters are only partly related to WM lesion measures[1, 9]. These findings suggest that there may also be separate pathological processes within the NAWM beyond those occurring as a result of axonal transection following focal WM injury. Thus, a better characterization of NAWM pathology is needed to further our understanding of its relationship to both cortical thinning and iron deposition. Perhaps also somewhat surprisingly, in neither study was fractional anisotropy (FA) of the associated WM tracts related to either of the outcomes (i.e. cortical thinning or iron deposition). This is unlikely to be due to methodological issues as different processing streams were utilized in the two studies. Key differences between the cortical thinning and iron deposition studies include: tractography approach (deterministic versus probabilistic), nonlinear registration software (FNIRT[154] versus ANTs[174]) and choice of diffusion image for normalization (FA map versus b0 image). Taken together, our findings suggest that measures of diffusivity are more sensitive than FA in assessing the relationships

between WM pathology and that within the GM. This hypothesis is supported by a study which found that mean diffusivity was more sensitive than FA in terms of characterizing the degree of irreversible tissue damage in focal WM lesions[111].

The advantage of surface-based approaches in characterizing GM damage

The work presented in this thesis utilized advanced morphological techniques for reconstructing both cortical and DGM structures. Notably, these methods allow for the possibility to obtain sharper segmentations of the structures of interest. One of the key advances in the FreeSurfer and FIRST methodologies is the use of 2D surface-based representations as opposed to 3D volumetric ones. In the case of the cortex, it is quite natural to treat it as a surface given its inherent sheet-like nature. The benefit can be immediately appreciated by considering two points separated by a sulcus. In a 3D representation, the apparent distance between them will be much smaller than the true distance when measured in 2D. While subcortical structures are generally much more "blob like", a surface-based representation has its advantages here as well. In the case of FIRST, it represents the subcortical structure surface as a mesh of vertices, which are then iteratively deformed until the algorithm finds the best match with respect to its training data. For volumetric purposes, the mesh is then simply filled to yield the final segmentation. However, as the number of vertices is fixed for each structure and vertex correspondence is maintained throughout the segmentation process, individual vertices can be tested in a group-based analysis. As a consequence, the localization of atrophy, as well as its effects, can be characterized in a more fine-grained way when using surface-based techniques than is generally possible with voxel-based methods.

The advantage of the surface-based processing methods was demonstrated in both studies in which we utilized such techniques. This was first evidenced in the study investigating the

relationship between WM tract injury and cortical thinning. It is of course not possible to obtain a measure of cortical thickness without first separating the WM and pial surfaces from the image. In this context, the surface-based method has a distinct advantage over conventional 3D measures, which are inherently limited in that they can only quantify the total volume. However, the high dimensional nonlinear registration technique based on mapping the surface to a sphere also allows for a much more accurate parcellation of the individual cortical regions than is possible when using a volumetric registration. This is supported by very high Dice values of manual versus FreeSurfer-derived parcellations (mean ± standard deviation: 91 ± 6, range: 74–99)[37]. The primary motor cortex, which was the target of our study in which we used FreeSurfer, showed excellent overlap with a mean Dice value of over 96. It should be noted that FreeSurfer-derived cortical thickness values have also been validated with histological data[208]. Taken together, these results lend support to the conclusion that our analysis of fiber tract injury and cortical pathology is both biologically meaningful and relevant to characterizing the complex relationship between WM damage and GM atrophy.

Turning to the subcortical analysis, the group-based shape analysis revealed a more precise localization of GM atrophy both in terms of differences with respect to HCs and associations with cognitive measures than has typically been described in the literature. Moreover, it was only using the longitudinal shape-based analysis processing stream that we were able to characterize the effects of localized thalamic atrophy and its relation to cognitive decline. Given that atrophy was found in a relatively small area of the left thalamus, one of the most likely explanations is that the vertex-wise analysis was able to preserve this highly localized effect in a way that is inherently very difficult using volumetric methods. With a region of interest approach, the subtle effect of anterior thalamic atrophy is likely lost within the

variance of the entire structure. On the other hand, the smoothing step prior to statistical inference in the VBM analysis may have prevented us from detecting the effect. While we cannot rule out the possibility of a spurious finding, a similar pattern was found in the right thalamus but only at the level of a trend. Moreover, the localization of the atrophy to the anterior region of the thalamus is in line with other studies relating the thalamic subnuclei in this area to cognitive impairment[157, 209, 210]. So although our results should be confirmed in a separate study, the surface-based analysis technique appears to be a strong candidate for quantifying the effects of neurodegeneration within D GM as well.

Conclusion

The aim of this study was to implement and test objective methods for quantifying the relationships between GM and WM damage in multiple sclerosis. We consistently demonstrated the importance of paying close attention, in the preprocessing phase, to the confounding effects of WM lesions in terms of obtaining reliable results. In two separate studies, we found clear evidence of an association between WM injury and GM pathology. For the former, we used WM tractographic methodologies while for the latter we utilized both cortical morphological reconstruction and iron-sensitive acquisition/post-processing techniques. We found that both cortical thinning and a putative marker of increased iron deposition were related to increased NAWM injury in the connected tracts. We also showed for the first time that focal atrophy of the thalamus is associated with a decline in cognitive processing speed over three years of follow-up.

Taken together, the results obtained from the investigations performed as part of this thesis appear to be promising in leading to a better characterization of the association between structure-specific GM, both deep and cortical, and WM injury in multiple sclerosis. These

results, moreover, foster new insights yielded by multimodal imaging approaches for studying the multifaceted aspects of the disease.

References

1. Cercignani M, Inglese M, Pagani E, Comi G and Filippi M. Mean diffusivity and fractional anisotropy histograms of patients with multiple sclerosis. *AJNR American journal of neuroradiology*. 2001; 22: 952-8.
2. Senda J, Watanabe H, Tsuboi T, et al. MRI mean diffusivity detects widespread brain degeneration in multiple sclerosis. *Journal of the neurological sciences*. 2012; 319: 105-10.
3. Zivadinov R, Bergsland N, Dolezal O, et al. Evolution of cortical and thalamus atrophy and disability progression in early relapsing-remitting MS during 5 years. *AJNR American journal of neuroradiology*. 2013; 34: 1931-9.
4. Hulst HE, Steenwijk MD, Versteeg A, et al. Cognitive impairment in MS: impact of white matter integrity, gray matter volume, and lesions. *Neurology*. 2013; 80: 1025-32.
5. Nygaard GO, Walhovd KB, Sowa P, et al. Cortical thickness and surface area relate to specific symptoms in early relapsing-remitting multiple sclerosis. *Multiple sclerosis*. 2014.
6. Fischl B, Salat DH, Busa E, et al. Whole brain segmentation: automated labeling of neuroanatomical structures in the human brain. *Neuron*. 2002; 33: 341-55.
7. Patenaude B, Smith SM, Kennedy DN and Jenkinson M. A Bayesian model of shape and appearance for subcortical brain segmentation. *NeuroImage*. 2011; 56: 907-22.
8. Song SK, Sun SW, Ramsbottom MJ, Chang C, Russell J and Cross AH. Dysmyelination revealed through MRI as increased radial (but unchanged axial) diffusion of water. *NeuroImage*. 2002; 17: 1429-36.
9. Ciccarelli O, Werring DJ, Wheeler-Kingshott CA, et al. Investigation of MS normal-appearing brain using diffusion tensor MRI with clinical correlations. *Neurology*. 2001; 56: 926-33.
10. Fox RJ, Cronin T, Lin J, et al. Measuring myelin repair and axonal loss with diffusion tensor imaging. *AJNR American journal of neuroradiology*. 2011; 32: 85-91.
11. Steenwijk MD, Daams M, Pouwels PJ, et al. Unraveling the relationship between regional gray matter atrophy and pathology in connected white matter tracts in long-standing multiple sclerosis. *Human brain mapping*. 2015; 36: 1796-807.
12. Lawes IN, Barrick TR, Murugam V, et al. Atlas-based segmentation of white matter tracts of the human brain using diffusion tensor tractography and comparison with classical dissection. *NeuroImage*. 2008; 39: 62-79.
13. Lagana M, Rovaris M, Ceccarelli A, et al. Atlas-based vs. individual-based deterministic tractography of corpus callosum in multiple sclerosis. *Conference proceedings : Annual International Conference of the IEEE Engineering in Medicine and Biology Society IEEE Engineering in Medicine and Biology Society Annual Conference*. 2009; 2009: 2699-702.
14. Tjoa CW, Benedict RH, Weinstock-Guttman B, Fabiano AJ and Bakshi R. MRI T2 hypointensity of the dentate nucleus is related to ambulatory impairment in multiple sclerosis. *Journal of the neurological sciences*. 2005; 234: 17-24.
15. Bakshi R, Benedict RH, Bermel RA, et al. T2 hypointensity in the deep gray matter of patients with multiple sclerosis: a quantitative magnetic resonance imaging study. *Archives of neurology*. 2002; 59: 62-8.
16. Zivadinov R, Heininen-Brown M, Schirda CV, et al. Abnormal subcortical deep-gray matter susceptibility-weighted imaging filtered phase measurements in patients with multiple sclerosis: a case-control study. *NeuroImage*. 2012; 59: 331-9.

17. Hagemeier J, Weinstock-Guttman B, Bergsland N, et al. Iron deposition on SWI-filtered phase in the subcortical deep gray matter of patients with clinically isolated syndrome may precede structure-specific atrophy. *AJNR American journal of neuroradiology*. 2012; 33: 1596-601.
18. Hopp K, Popescu BF, McCrea RP, et al. Brain iron detected by SWI high pass filtered phase calibrated with synchrotron X-ray fluorescence. *Journal of magnetic resonance imaging : JMRI*. 2010; 31: 1346-54.
19. Schweser F, Deistung A, Lehr BW and Reichenbach JR. Quantitative imaging of intrinsic magnetic tissue properties using MRI signal phase: an approach to in vivo brain iron metabolism? *NeuroImage*. 2011; 54: 2789-807.
20. Steenwijk MD, Daams M, Pouwels PJ, et al. What explains gray matter atrophy in long-standing multiple sclerosis? *Radiology*. 2014; 272: 832-42.
21. Bergsland N, Lagana MM, Tavazzi E, et al. Corticospinal tract integrity is related to primary motor cortex thinning in relapsing-remitting multiple sclerosis. *Multiple sclerosis*. 2015; 21: 1771-80.
22. Poser CM. The multiple sclerosis trait and the development of multiple sclerosis: genetic vulnerability and environmental effect. *Clinical neurology and neurosurgery*. 2006; 108: 227-33.
23. Popescu BF, Pirko I and Lucchinetti CF. Pathology of multiple sclerosis: where do we stand? *Continuum*. 2013; 19: 901-21.
24. Polman CH, Reingold SC, Banwell B, et al. Diagnostic criteria for multiple sclerosis: 2010 revisions to the McDonald criteria. *Annals of neurology*. 2011; 69: 292-302.
25. Hackmack K, Weygandt M, Wuerfel J, et al. Can we overcome the 'clinico-radiological paradox' in multiple sclerosis? *Journal of neurology*. 2012; 259: 2151-60.
26. Pirko I, Lucchinetti CF, Sriram S and Bakshi R. Gray matter involvement in multiple sclerosis. *Neurology*. 2007; 68: 634-42.
27. Geurts JJ, Pouwels PJ, Uitdehaag BM, Polman CH, Barkhof F and Castelijns JA. Intracortical lesions in multiple sclerosis: improved detection with 3D double inversion-recovery MR imaging. *Radiology*. 2005; 236: 254-60.
28. Steenwijk MD, Vrenken H, Jonkman LE, et al. High-resolution T1-relaxation time mapping displays subtle, clinically relevant, gray matter damage in long-standing multiple sclerosis. *Multiple sclerosis*. 2015.
29. Klaver R, Popescu V, Voorn P, et al. Neuronal and axonal loss in normal-appearing gray matter and subpial lesions in multiple sclerosis. *Journal of neuropathology and experimental neurology*. 2015; 74: 453-8.
30. Popescu V, Klaver R, Voorn P, et al. What drives MRI-measured cortical atrophy in multiple sclerosis? *Multiple sclerosis*. 2015; 21: 1280-90.
31. Geurts JJ, Stys PK, Minagar A, Amor S and Zivadinov R. Gray matter pathology in (chronic) MS: modern views on an early observation. *Journal of the neurological sciences*. 2009; 282: 12-20.
32. Fisniku LK, Chard DT, Jackson JS, et al. Gray matter atrophy is related to long-term disability in multiple sclerosis. *Annals of neurology*. 2008; 64: 247-54.
33. Benedict RH, Bruce JM, Dwyer MG, et al. Neocortical atrophy, third ventricular width, and cognitive dysfunction in multiple sclerosis. *Archives of neurology*. 2006; 63: 1301-6.
34. Fisher E, Lee JC, Nakamura K and Rudick RA. Gray matter atrophy in multiple sclerosis: a longitudinal study. *Annals of neurology*. 2008; 64: 255-65.

35. Simon JH, Schiffer RB, Rudick RA and Herndon RM. Quantitative determination of MS-induced corpus callosum atrophy in vivo using MR imaging. *AJNR American journal of neuroradiology*. 1987; 8: 599-604.
36. Bermel RA, Bakshi R, Tjoa C, Puli SR and Jacobs L. Bicaudate ratio as a magnetic resonance imaging marker of brain atrophy in multiple sclerosis. *Archives of neurology*. 2002; 59: 275-80.
37. Klein A and Tourville J. 101 labeled brain images and a consistent human cortical labeling protocol. *Frontiers in neuroscience*. 2012; 6: 171.
38. Yushkevich PA, Amaral RS, Augustinack JC, et al. Quantitative comparison of 21 protocols for labeling hippocampal subfields and parahippocampal subregions in in vivo MRI: towards a harmonized segmentation protocol. *NeuroImage*. 2015; 111: 526-41.
39. Morey RA, Petty CM, Xu Y, et al. A comparison of automated segmentation and manual tracing for quantifying hippocampal and amygdala volumes. *NeuroImage*. 2009; 45: 855-66.
40. Makris N, Swaab DF, van der Kouwe A, et al. Volumetric parcellation methodology of the human hypothalamus in neuroimaging: normative data and sex differences. *NeuroImage*. 2013; 69: 1-10.
41. Jones EG. Functional subdivision and synaptic organization of the mammalian thalamus. *International review of physiology*. 1981; 25: 173-245.
42. Ge Y. Multiple sclerosis: the role of MR imaging. *AJNR American journal of neuroradiology*. 2006; 27: 1165-76.
43. Gelineau-Morel R, Tomassini V, Jenkinson M, Johansen-Berg H, Matthews PM and Palace J. The effect of hypointense white matter lesions on automated gray matter segmentation in multiple sclerosis. *Human brain mapping*. 2012; 33: 2802-14.
44. Amann M, Andelova M, Pfister A, et al. Subcortical brain segmentation of two dimensional T1-weighted data sets with FMRIB's Integrated Registration and Segmentation Tool (FIRST). *NeuroImage Clinical*. 2015; 7: 43-52.
45. Ontaneda D, Sakaie K, Lin J, et al. Identifying the start of multiple sclerosis injury: a serial DTI study. *Journal of neuroimaging : official journal of the American Society of Neuroimaging*. 2014; 24: 569-76.
46. Giorgio A, Palace J, Johansen-Berg H, et al. Relationships of brain white matter microstructure with clinical and MR measures in relapsing-remitting multiple sclerosis. *Journal of magnetic resonance imaging : JMRI*. 2010; 31: 309-16.
47. Budde MD, Xie M, Cross AH and Song SK. Axial diffusivity is the primary correlate of axonal injury in the experimental autoimmune encephalomyelitis spinal cord: a quantitative pixelwise analysis. *The Journal of neuroscience : the official journal of the Society for Neuroscience*. 2009; 29: 2805-13.
48. Jeurissen B, Leemans A, Tournier JD, Jones DK and Sijbers J. Investigating the prevalence of complex fiber configurations in white matter tissue with diffusion magnetic resonance imaging. *Human brain mapping*. 2013; 34: 2747-66.
49. Wheeler-Kingshott CA and Cercignani M. About "axial" and "radial" diffusivities. *Magnetic resonance in medicine*. 2009; 61: 1255-60.
50. Tuch DS. Q-ball imaging. *Magnetic resonance in medicine*. 2004; 52: 1358-72.
51. Behrens TE, Woolrich MW, Jenkinson M, et al. Characterization and propagation of uncertainty in diffusion-weighted MR imaging. *Magnetic resonance in medicine*. 2003; 50: 1077-88.

52. Lewis JD, Theilmann RJ, Townsend J and Evans AC. Network efficiency in autism spectrum disorder and its relation to brain overgrowth. *Frontiers in human neuroscience*. 2013; 7: 845.
53. Kumar V, Mang S and Grodd W. Direct diffusion-based parcellation of the human thalamus. *Brain structure & function*. 2015; 220: 1619-35.
54. Bisecco A, Rocca MA, Pagani E, et al. Connectivity-based parcellation of the thalamus in multiple sclerosis and its implications for cognitive impairment: A multicenter study. *Human brain mapping*. 2015; 36: 2809-25.
55. Heiervang E, Behrens TE, Mackay CE, Robson MD and Johansen-Berg H. Between session reproducibility and between subject variability of diffusion MR and tractography measures. *NeuroImage*. 2006; 33: 867-77.
56. Noll DC, Nishimura DG and Macovski A. Homodyne detection in magnetic resonance imaging. *IEEE transactions on medical imaging*. 1991; 10: 154-63.
57. Haacke EM, Xu Y, Cheng YC and Reichenbach JR. Susceptibility weighted imaging (SWI). *Magnetic resonance in medicine*. 2004; 52: 612-8.
58. Haacke EM, Tang J, Neelavalli J and Cheng YC. Susceptibility mapping as a means to visualize veins and quantify oxygen saturation. *Journal of magnetic resonance imaging : JMRI*. 2010; 32: 663-76.
59. Zivadinov R, Dwyer M, Markovic-Plese S, et al. A pilot, longitudinal, 24-week study to evaluate the effect of interferon beta-1a subcutaneous on changes in susceptibility-weighted imaging-filtered phase assessment of lesions and subcortical deep-gray matter in relapsing-remitting multiple sclerosis. *Therapeutic advances in neurological disorders*. 2015; 8: 59-70.
60. Modica CM, Zivadinov R, Dwyer MG, Bergsland N, Weeks AR and Benedict RH. Iron and volume in the deep gray matter: association with cognitive impairment in multiple sclerosis. *AJNR American journal of neuroradiology*. 2015; 36: 57-62.
61. Hagemeier J, Dwyer MG, Bergsland N, et al. Effect of age on MRI phase behavior in the subcortical deep gray matter of healthy individuals. *AJNR American journal of neuroradiology*. 2013; 34: 2144-51.
62. Haacke EM, Miao Y, Liu M, et al. Correlation of putative iron content as represented by changes in R2* and phase with age in deep gray matter of healthy adults. *Journal of magnetic resonance imaging : JMRI*. 2010; 32: 561-76.
63. Bozin I, Ge Y, Kuchling J, et al. Magnetic Resonance Phase Alterations in Multiple Sclerosis Patients with Short and Long Disease Duration. *PloS one*. 2015; 10: e0128386.
64. Hagemeier J, Heininen-Brown M, Gabelic T, et al. Phase white matter signal abnormalities in patients with clinically isolated syndrome and other neurologic disorders. *AJNR American journal of neuroradiology*. 2014; 35: 1916-23.
65. Haacke EM, Makki M, Ge Y, et al. Characterizing iron deposition in multiple sclerosis lesions using susceptibility weighted imaging. *Journal of magnetic resonance imaging : JMRI*. 2009; 29: 537-44.
66. Greve DN and Fischl B. Accurate and robust brain image alignment using boundary-based registration. *NeuroImage*. 2009; 48: 63-72.
67. Polimeni JR, Fischl B, Greve DN and Wald LL. Laminar analysis of 7T BOLD using an imposed spatial activation pattern in human V1. *NeuroImage*. 2010; 52: 1334-46.
68. Trachtenberg AJ, Filippini N, Ebmeier KP, Smith SM, Karpe F and Mackay CE. The effects of APOE on the functional architecture of the resting brain. *NeuroImage*. 2012; 59: 565-72.

69. Rosas HD, Lee SY, Bender AC, et al. Altered white matter microstructure in the corpus callosum in Huntington's disease: implications for cortical "disconnection". *NeuroImage*. 2010; 49: 2995-3004.
70. Ehrlich S, Geisler D, Yendiki A, et al. Associations of white matter integrity and cortical thickness in patients with schizophrenia and healthy controls. *Schizophrenia bulletin*. 2014; 40: 665-74.
71. Chen JJ, Rosas HD and Salat DH. Age-associated reductions in cerebral blood flow are independent from regional atrophy. *NeuroImage*. 2011; 55: 468-78.
72. Rickenbacher E, Greve DN, Azma S, Pfeuffer J and Marinkovic K. Effects of alcohol intoxication and gender on cerebral perfusion: an arterial spin labeling study. *Alcohol*. 2011; 45: 725-37.
73. Mainero C, Louapre C, Govindarajan ST, et al. A gradient in cortical pathology in multiple sclerosis by in vivo quantitative 7 T imaging. *Brain : a journal of neurology*. 2015; 138: 932-45.
74. Klaver R, De Vries HE, Schenk GJ and Geurts JJ. Grey matter damage in multiple sclerosis: a pathology perspective. *Prion*. 2013; 7: 66-75.
75. Muhlau M, Buck D, Forschler A, et al. White-matter lesions drive deep gray-matter atrophy in early multiple sclerosis: support from structural MRI. *Multiple sclerosis*. 2013; 19: 1485-92.
76. Kooi EJ, Strijbis EM, van der Valk P and Geurts JJ. Heterogeneity of cortical lesions in multiple sclerosis: clinical and pathologic implications. *Neurology*. 2012; 79: 1369-76.
77. Peterson JW, Bo L, Mork S, Chang A and Trapp BD. Transected neurites, apoptotic neurons, and reduced inflammation in cortical multiple sclerosis lesions. *Annals of neurology*. 2001; 50: 389-400.
78. Bendfeldt K, Blumhagen JO, Egger H, et al. Spatiotemporal distribution pattern of white matter lesion volumes and their association with regional grey matter volume reductions in relapsing-remitting multiple sclerosis. *Human brain mapping*. 2010; 31: 1542-55.
79. Cappellani R, Bergsland N, Weinstock-Guttman B, et al. Subcortical deep gray matter pathology in patients with multiple sclerosis is associated with white matter lesion burden and atrophy but not with cortical atrophy: a diffusion tensor MRI study. *AJNR American journal of neuroradiology*. 2014; 35: 912-9.
80. Gorgoraptis N, Wheeler-Kingshott CA, Jenkins TM, et al. Combining tractography and cortical measures to test system-specific hypotheses in multiple sclerosis. *Multiple sclerosis*. 2010; 16: 555-65.
81. Steenwijk MD, Daams M, Pouwels PJ, et al. Unraveling the relationship between regional gray matter atrophy and pathology in connected white matter tracts in long-standing multiple sclerosis. *Human brain mapping*. 2015.
82. Reich DS, Ozturk A, Calabresi PA and Mori S. Automated vs. conventional tractography in multiple sclerosis: variability and correlation with disability. *NeuroImage*. 2010; 49: 3047-56.
83. Smith SM, Jenkinson M, Woolrich MW, et al. Advances in functional and structural MR image analysis and implementation as FSL. *NeuroImage*. 2004; 23 Suppl 1: S208-19.
84. Battaglini M, Jenkinson M and De Stefano N. Evaluating and reducing the impact of white matter lesions on brain volume measurements. *Human brain mapping*. 2012; 33: 2062-71.
85. Chard DT, Jackson JS, Miller DH and Wheeler-Kingshott CA. Reducing the impact of white matter lesions on automated measures of brain gray and white matter volumes. *Journal of magnetic resonance imaging : JMRI*. 2010; 32: 223-8.

86. Sdika M and Pelletier D. Nonrigid registration of multiple sclerosis brain images using lesion inpainting for morphometry or lesion mapping. *Human brain mapping*. 2009; 30: 1060-7.
87. Magon S, Gaetano L, Chakravarty MM, et al. White matter lesion filling improves the accuracy of cortical thickness measurements in multiple sclerosis patients: a longitudinal study. *BMC neuroscience*. 2014; 15: 106.
88. Govindarajan KA, Datta S, Hasan KM, et al. Effect of in-painting on cortical thickness measurements in multiple sclerosis: A large cohort study. *Human brain mapping*. 2015; 36: 3749-60.
89. Zhang Y, Brady M and Smith S. Segmentation of brain MR images through a hidden Markov random field model and the expectation-maximization algorithm. *IEEE transactions on medical imaging*. 2001; 20: 45-57.
90. Dale AM, Fischl B and Sereno MI. Cortical surface-based analysis. I. Segmentation and surface reconstruction. *NeuroImage*. 1999; 9: 179-94.
91. Reuter M, Rosas HD and Fischl B. Highly accurate inverse consistent registration: a robust approach. *NeuroImage*. 2010; 53: 1181-96.
92. Segonne F, Dale AM, Busa E, et al. A hybrid approach to the skull stripping problem in MRI. *NeuroImage*. 2004; 22: 1060-75.
93. Fischl B, Salat DH, van der Kouwe AJ, et al. Sequence-independent segmentation of magnetic resonance images. *NeuroImage*. 2004; 23 Suppl 1: S69-84.
94. Sled JG, Zijdenbos AP and Evans AC. A nonparametric method for automatic correction of intensity nonuniformity in MRI data. *IEEE transactions on medical imaging*. 1998; 17: 87-97.
95. Fischl B, Liu A and Dale AM. Automated manifold surgery: constructing geometrically accurate and topologically correct models of the human cerebral cortex. *IEEE transactions on medical imaging*. 2001; 20: 70-80.
96. Segonne F, Pacheco J and Fischl B. Geometrically accurate topology-correction of cortical surfaces using nonseparating loops. *IEEE transactions on medical imaging*. 2007; 26: 518-29.
97. Fischl B and Dale AM. Measuring the thickness of the human cerebral cortex from magnetic resonance images. *Proceedings of the National Academy of Sciences of the United States of America*. 2000; 97: 11050-5.
98. Fischl B, Sereno MI and Dale AM. Cortical surface-based analysis. II: Inflation, flattening, and a surface-based coordinate system. *NeuroImage*. 1999; 9: 195-207.
99. Fischl B, Sereno MI, Tootell RB and Dale AM. High-resolution intersubject averaging and a coordinate system for the cortical surface. *Human brain mapping*. 1999; 8: 272-84.
100. Desikan RS, Segonne F, Fischl B, et al. An automated labeling system for subdividing the human cerebral cortex on MRI scans into gyral based regions of interest. *NeuroImage*. 2006; 31: 968-80.
101. Fischl B, van der Kouwe A, Destrieux C, et al. Automatically parcellating the human cerebral cortex. *Cerebral cortex*. 2004; 14: 11-22.
102. Rosas HD, Liu AK, Hersch S, et al. Regional and progressive thinning of the cortical ribbon in Huntington's disease. *Neurology*. 2002; 58: 695-701.
103. Kuperberg GR, Broome MR, McGuire PK, et al. Regionally localized thinning of the cerebral cortex in schizophrenia. *Archives of general psychiatry*. 2003; 60: 878-88.
104. Tortorella P, Lagana MM, Saresella M, et al. Determinants of disability in multiple sclerosis: an immunological and MRI study. *BioMed research international*. 2014; 2014: 875768.

105. Smith SM, Jenkinson M, Johansen-Berg H, et al. Tract-based spatial statistics: voxelwise analysis of multi-subject diffusion data. *NeuroImage*. 2006; 31: 1487-505.
106. Hua K, Zhang J, Wakana S, et al. Tract probability maps in stereotaxic spaces: analyses of white matter anatomy and tract-specific quantification. *NeuroImage*. 2008; 39: 336-47.
107. Bodini B, Battaglini M, De Stefano N, et al. T2 lesion location really matters: a 10 year follow-up study in primary progressive multiple sclerosis. *Journal of neurology, neurosurgery, and psychiatry*. 2011; 82: 72-7.
108. Winkler AM, Ridgway GR, Webster MA, Smith SM and Nichols TE. Permutation inference for the general linear model. *NeuroImage*. 2014; 92: 381-97.
109. Charil A, Dagher A, Lerch JP, Zijdenbos AP, Worsley KJ and Evans AC. Focal cortical atrophy in multiple sclerosis: relation to lesion load and disability. *NeuroImage*. 2007; 34: 509-17.
110. Sailer M, Fischl B, Salat D, et al. Focal thinning of the cerebral cortex in multiple sclerosis. *Brain : a journal of neurology*. 2003; 126: 1734-44.
111. Castriota-Scanderbeg A, Fasano F, Hagberg G, Nocentini U, Filippi M and Caltagirone C. Coefficient D(av) is more sensitive than fractional anisotropy in monitoring progression of irreversible tissue damage in focal nonactive multiple sclerosis lesions. *AJNR American journal of neuroradiology*. 2003; 24: 663-70.
112. Harrison DM, Caffo BS, Shiee N, et al. Longitudinal changes in diffusion tensor-based quantitative MRI in multiple sclerosis. *Neurology*. 2011; 76: 179-86.
113. Narayana PA, Govindarajan KA, Goel P, et al. Regional cortical thickness in relapsing remitting multiple sclerosis: A multi-center study. *NeuroImage Clinical*. 2012; 2: 120-31.
114. Bennett IJ, Madden DJ, Vaidya CJ, Howard DV and Howard JH, Jr. Age-related differences in multiple measures of white matter integrity: A diffusion tensor imaging study of healthy aging. *Human brain mapping*. 2010; 31: 378-90.
115. Lemaitre H, Goldman AL, Sambataro F, et al. Normal age-related brain morphometric changes: nonuniformity across cortical thickness, surface area and gray matter volume? *Neurobiology of aging*. 2012; 33: 617 e1-9.
116. Abe O, Yamasue H, Yamada H, et al. Sex dimorphism in gray/white matter volume and diffusion tensor during normal aging. *NMR in biomedicine*. 2010; 23: 446-58.
117. Mukherjee P, Chung SW, Berman JI, Hess CP and Henry RG. Diffusion tensor MR imaging and fiber tractography: technical considerations. *AJNR American journal of neuroradiology*. 2008; 29: 843-52.
118. Yendiki A, Panneck P, Srinivasan P, et al. Automated probabilistic reconstruction of white-matter pathways in health and disease using an atlas of the underlying anatomy. *Frontiers in neuroinformatics*. 2011; 5: 23.
119. Tondelli M, Wilcock GK, Nichelli P, De Jager CA, Jenkinson M and Zamboni G. Structural MRI changes detectable up to ten years before clinical Alzheimer's disease. *Neurobiology of aging*. 2012; 33: 825 e25-36.
120. Lett TA, Chakravarty MM, Felsky D, et al. The genome-wide supported microRNA-137 variant predicts phenotypic heterogeneity within schizophrenia. *Molecular psychiatry*. 2013; 18: 443-50.
121. Bergsland N, Horakova D, Dwyer MG, et al. Subcortical and cortical gray matter atrophy in a large sample of patients with clinically isolated syndrome and early relapsing-remitting multiple sclerosis. *AJNR American journal of neuroradiology*. 2012; 33: 1573-8.

122. Morgen K, Schneider M, Frolich L, et al. Apolipoprotein E-dependent load of white matter hyperintensities in Alzheimer's disease: a voxel-based lesion mapping study. *Alzheimer's research & therapy*. 2015; 7: 27.
123. Uddin MN, Lebel RM, Seres P, Blevins G and Wilman AH. Spin echo transverse relaxation and atrophy in multiple sclerosis deep gray matter: A two-year longitudinal study. *Multiple sclerosis*. 2015.
124. Modica CM, Bergsland N, Dwyer MG, et al. Cognitive reserve moderates the impact of subcortical gray matter atrophy on neuropsychological status in multiple sclerosis. *Multiple sclerosis*. 2015.
125. Zivadinov R, Havrdova E, Bergsland N, et al. Thalamic atrophy is associated with development of clinically definite multiple sclerosis. *Radiology*. 2013; 268: 831-41.
126. Smith SM, Zhang Y, Jenkinson M, et al. Accurate, robust, and automated longitudinal and cross-sectional brain change analysis. *NeuroImage*. 2002; 17: 479-89.
127. Dwyer MG, Bergsland N and Zivadinov R. Improved longitudinal gray and white matter atrophy assessment via application of a 4-dimensional hidden Markov random field model. *NeuroImage*. 2014; 90: 207-17.
128. Jenkinson M and Smith S. A global optimisation method for robust affine registration of brain images. *Medical image analysis*. 2001; 5: 143-56.
129. Jenkinson M, Bannister P, Brady M and Smith S. Improved optimization for the robust and accurate linear registration and motion correction of brain images. *NeuroImage*. 2002; 17: 825-41.
130. Team RDC. R: A Language and Environment for Statistical Computing. Vienna, Austria: R Foundation for Statistical Computing, 2015.
131. Reuter M and Fischl B. Avoiding asymmetry-induced bias in longitudinal image processing. *NeuroImage*. 2011; 57: 19-21.
132. Reuter M, Schmansky NJ, Rosas HD and Fischl B. Within-subject template estimation for unbiased longitudinal image analysis. *NeuroImage*. 2012; 61: 1402-18.
133. Caramanos Z, Fonov VS, Francis SJ, et al. Gradient distortions in MRI: characterizing and correcting for their effects on SIENA-generated measures of brain volume change. *NeuroImage*. 2010; 49: 1601-11.
134. Langdon DW. Cognition in multiple sclerosis. *Curr Opin Neurol*. 2011; 24: 244-9.
135. Chiaravalloti ND and DeLuca J. Cognitive impairment in multiple sclerosis. *Lancet Neurol*. 2008; 7: 1139-51.
136. Rocca MA, Amato MP, De Stefano N, et al. Clinical and imaging assessment of cognitive dysfunction in multiple sclerosis. *Lancet Neurol*. 2015; 14: 302-17.
137. Batista S, Zivadinov R, Hoogs M, et al. Basal ganglia, thalamus and neocortical atrophy predicting slowed cognitive processing in multiple sclerosis. *Journal of neurology*. 2012; 259: 139-46.
138. Schoonheim MM, Popescu V, Rueda Lopes FC, et al. Subcortical atrophy and cognition: sex effects in multiple sclerosis. *Neurology*. 2012; 79: 1754-61.
139. Houtchens MK, Benedict RH, Killiany R, et al. Thalamic atrophy and cognition in multiple sclerosis. *Neurology*. 2007; 69: 1213-23.
140. Cavallari M, Ceccarelli A, Wang GY, et al. Microstructural changes in the striatum and their impact on motor and neuropsychological performance in patients with multiple sclerosis. *PloS one*. 2014; 9: e101199.

141. Bermel RA, Innus MD, Tjoa CW and Bakshi R. Selective caudate atrophy in multiple sclerosis: a 3D MRI parcellation study. *Neuroreport*. 2003; 14: 335-9.
142. Sbardella E, Petsas N, Tona F, et al. Assessing the correlation between grey and white matter damage with motor and cognitive impairment in multiple sclerosis patients. *PloS one*. 2013; 8: e63250.
143. Jacobsen C, Hagemeier J, Myhr KM, et al. Brain atrophy and disability progression in multiple sclerosis patients: a 10-year follow-up study. *Journal of neurology, neurosurgery, and psychiatry*. 2014; 85: 1109-15.
144. Lublin FD and Reingold SC. Defining the clinical course of multiple sclerosis: results of an international survey. National Multiple Sclerosis Society (USA) Advisory Committee on Clinical Trials of New Agents in Multiple Sclerosis.[see comment]. *Neurology*. 1996; 46: 907-11.
145. Langdon DW, Amato MP, Boringa J, et al. Recommendations for a Brief International Cognitive Assessment for Multiple Sclerosis (BICAMS). *Multiple sclerosis*. 2012; 18: 891-8.
146. Smith A. *Symbol digit modalities test: Manual*. Los Angeles: Western Psychological Services, 1982.
147. Delis DC, Kramer JH, Kaplan E and Ober BA. *Califorina Verbal Learning Test - Second Edition*. San Antonio, TX: The Psychological Corporation, 2000.
148. Benedict RHB. *Brief Visuospatial Memory Test - Revised: Professional Manual*. Odessa, Floriday: Psychological Assessment Resources, Inc., 1997.
149. Parmenter BA, Testa SM, Schretlen DJ, Weinstock-Guttman B and Benedict RH. The utility of regression-based norms in interpreting the minimal assessment of cognitive function in multiple sclerosis (MACFIMS). *Journal of the International Neuropsychological Society : JINS*. 2010; 16: 6-16.
150. Smith SM, Zhang Y, Jenkinson M, et al. Accurate, robust, and automated longitudinal and cross-sectional brain change analysis. *NeuroImage*. 2002; 17: 479-89.
151. Smith SM and Nichols TE. Threshold-free cluster enhancement: addressing problems of smoothing, threshold dependence and localisation in cluster inference. *NeuroImage*. 2009; 44: 83-98.
152. Douaud G, Smith S, Jenkinson M, et al. Anatomically related grey and white matter abnormalities in adolescent-onset schizophrenia. *Brain : a journal of neurology*. 2007; 130: 2375-86.
153. Smith SM. Fast robust automated brain extraction. *Human brain mapping*. 2002; 17: 143-55.
154. Anderson JLR JM, Smith S. Non-linear registration, aka spatial normalisation. 2010.
155. Wright NF, Vann SD, Aggleton JP and Nelson AJ. A critical role for the anterior thalamus in directing attention to task-relevant stimuli. *The Journal of neuroscience : the official journal of the Society for Neuroscience*. 2015; 35: 5480-8.
156. Jankowski MM, Ronnqvist KC, Tsanov M, et al. The anterior thalamus provides a subcortical circuit supporting memory and spatial navigation. *Frontiers in systems neuroscience*. 2013; 7: 45.
157. Bockova M, Chladek J, Jurak P, et al. Complex motor-cognitive factors processed in the anterior nucleus of the thalamus: an intracerebral recording study. *Brain topography*. 2015; 28: 269-78.
158. Child ND and Benarroch EE. Anterior nucleus of the thalamus: functional organization and clinical implications. *Neurology*. 2013; 81: 1869-76.

159. Harrison DM, Oh J, Roy S, et al. Thalamic lesions in multiple sclerosis by 7T MRI: Clinical implications and relationship to cortical pathology. *Multiple sclerosis*. 2015; 21: 1139-50.
160. Vercellino M, Masera S, Lorenzatti M, et al. Demyelination, inflammation, and neurodegeneration in multiple sclerosis deep gray matter. *Journal of neuropathology and experimental neurology*. 2009; 68: 489-502.
161. Visser E, Keuken MC, Douaud G, et al. Automatic segmentation of the striatum and globus pallidus using MIST: Multimodal Image Segmentation Tool. *NeuroImage*. 2015; 125: 479-97.
162. Pereira JB, Ibarretxe-Bilbao N, Marti MJ, et al. Assessment of cortical degeneration in patients with Parkinson's disease by voxel-based morphometry, cortical folding, and cortical thickness. *Human brain mapping*. 2012; 33: 2521-34.
163. Jones EG. The anatomy of sensory relay functions in the thalamus. *Progress in brain research*. 1991; 87: 29-52.
164. Borghi M, Cavallo M, Carletto S, et al. Presence and significant determinants of cognitive impairment in a large sample of patients with multiple sclerosis. *PloS one*. 2013; 8: e69820.
165. Hametner S, Wimmer I, Haider L, Pfeifenbring S, Bruck W and Lassmann H. Iron and neurodegeneration in the multiple sclerosis brain. *Annals of neurology*. 2013; 74: 848-61.
166. Ceccarelli A, Filippi M, Neema M, et al. T2 hypointensity in the deep gray matter of patients with benign multiple sclerosis. *Multiple sclerosis*. 2009; 15: 678-86.
167. Langkammer C, Krebs N, Goessler W, et al. Susceptibility induced gray-white matter MRI contrast in the human brain. *NeuroImage*. 2012; 59: 1413-9.
168. Haider L, Simeonidou C, Steinberger G, et al. Multiple sclerosis deep grey matter: the relation between demyelination, neurodegeneration, inflammation and iron. *Journal of neurology, neurosurgery, and psychiatry*. 2014; 85: 1386-95.
169. Williams R, Buchheit CL, Berman NE and LeVine SM. Pathogenic implications of iron accumulation in multiple sclerosis. *Journal of neurochemistry*. 2012; 120: 7-25.
170. Raz E, Branson B, Jensen JH, et al. Relationship between iron accumulation and white matter injury in multiple sclerosis: a case-control study. *Journal of neurology*. 2015; 262: 402-9.
171. Haacke EM, Mittal S, Wu Z, Neelavalli J and Cheng YC. Susceptibility-weighted imaging: technical aspects and clinical applications, part 1. *AJNR American journal of neuroradiology*. 2009; 30: 19-30.
172. Shmueli K, de Zwart JA, van Gelderen P, Li TQ, Dodd SJ and Duyn JH. Magnetic susceptibility mapping of brain tissue in vivo using MRI phase data. *Magnetic resonance in medicine*. 2009; 62: 1510-22.
173. Bergsland N, Lagana MM, Tavazzi E, et al. Corticospinal tract integrity is related to primary motor cortex thinning in relapsing-remitting multiple sclerosis. *Multiple sclerosis*. 2015.
174. Avants BB, Tustison NJ, Song G, Cook PA, Klein A and Gee JC. A reproducible evaluation of ANTs similarity metric performance in brain image registration. *NeuroImage*. 2011; 54: 2033-44.
175. Schweser F, Dwyer MG, Deistung A, Reichenbach JR and Zivadinov R. Impact of tissue atrophy on high-pass filtered MRI signal phase-based assessment in large-scale group-comparison studies: A simulation study. *Frontiers in Physics*. 2013; 1.

176. Behrens TE, Johansen-Berg H, Woolrich MW, et al. Non-invasive mapping of connections between human thalamus and cortex using diffusion imaging. *Nature neuroscience*. 2003; 6: 750-7.
177. Behrens TE, Berg HJ, Jbabdi S, Rushworth MF and Woolrich MW. Probabilistic diffusion tractography with multiple fibre orientations: What can we gain? *NeuroImage*. 2007; 34: 144-55.
178. Benjamini Y and Hochberg Y. Controlling the False Discovery Rate: A Practical and Powerful Approach to Multiple Testing. *Journal of the Royal Statistical Society Series B (Methodological)*. 1995; 57: 289-300.
179. Klein A, Andersson J, Ardekani BA, et al. Evaluation of 14 nonlinear deformation algorithms applied to human brain MRI registration. *NeuroImage*. 2009; 46: 786-802.
180. Hanspach J, Dwyer M, Bergsland N, et al. Toward a voxel-based analysis (VBA) of quantitative magnetic susceptibility maps (QSM): Strategies for creating brain susceptibility templates. *ISMRM 2016 (Submitted)*.
181. Khalil M, Langkammer C, Pichler A, et al. Dynamics of brain iron levels in multiple sclerosis: A longitudinal 3T MRI study. *Neurology*. 2015; 84: 2396-402.
182. Al-Radaideh AM, Wharton SJ, Lim SY, et al. Increased iron accumulation occurs in the earliest stages of demyelinating disease: an ultra-high field susceptibility mapping study in Clinically Isolated Syndrome. *Multiple sclerosis*. 2013; 19: 896-903.
183. Cobzas D, Sun H, Walsh AJ, Lebel RM, Blevins G and Wilman AH. Subcortical gray matter segmentation and voxel-based analysis using transverse relaxation and quantitative susceptibility mapping with application to multiple sclerosis. *Journal of magnetic resonance imaging : JMRI*. 2015.
184. Walsh AJ, Blevins G, Lebel RM, Seres P, Emery DJ and Wilman AH. Longitudinal MR imaging of iron in multiple sclerosis: an imaging marker of disease. *Radiology*. 2014; 270: 186-96.
185. Schweser F, Hagemeier J, Polak P, et al. Quantitative Susceptibility Mapping (QSM) in patients with clinically isolated syndrome (CIS) and multiple sclerosis (MS) - a large cohort study. *ISMRM 2016 (Submitted)*.
186. Quinn MP, Gati JS, Klassen ML, Lee DH, Kremenchutzky M and Menon RS. Increased deep gray matter iron is present in clinically isolated syndromes. *Multiple sclerosis and related disorders*. 2014; 3: 194-202.
187. Hagemeier J, Yeh EA, Brown MH, et al. Iron content of the pulvinar nucleus of the thalamus is increased in adolescent multiple sclerosis. *Multiple sclerosis*. 2013; 19: 567-76.
188. Xu X, Wang Q, Zhong J and Zhang M. Iron deposition influences the measurement of water diffusion tensor in the human brain: a combined analysis of diffusion and iron-induced phase changes. *Neuroradiology*. 2015; 57: 1169-78.
189. Rulseh AM, Keller J, Tintera J, Kozisek M and Vymazal J. Chasing shadows: what determines DTI metrics in gray matter regions? An in vitro and in vivo study. *Journal of magnetic resonance imaging : JMRI*. 2013; 38: 1103-10.
190. Hagemeier J, Heininen-Brown M, Poloni GU, et al. Iron deposition in multiple sclerosis lesions measured by susceptibility-weighted imaging filtered phase: a case control study. *Journal of magnetic resonance imaging : JMRI*. 2012; 36: 73-83.
191. Wisnieff C, Ramanan S, Olesik J, Gauthier S, Wang Y and Pitt D. Quantitative susceptibility mapping (QSM) of white matter multiple sclerosis lesions: Interpreting positive susceptibility and the presence of iron. *Magnetic resonance in medicine*. 2015; 74: 564-70.

192. Paling D, Tozer D, Wheeler-Kingshott C, Kapoor R, Miller DH and Golay X. Reduced R2' in multiple sclerosis normal appearing white matter and lesions may reflect decreased myelin and iron content. *Journal of neurology, neurosurgery, and psychiatry*. 2012; 83: 785-92.
193. Yablonskiy DA, Luo J, Sukstanskii AL, Iyer A and Cross AH. Biophysical mechanisms of MRI signal frequency contrast in multiple sclerosis. *Proceedings of the National Academy of Sciences of the United States of America*. 2012; 109: 14212-7.
194. Shen X, Nguyen TD, Gauthier SA and Raj A. Robust myelin quantitative imaging from multi-echo T2 MRI using edge preserving spatial priors. *Medical image computing and computer-assisted intervention : MICCAI International Conference on Medical Image Computing and Computer-Assisted Intervention*. 2013; 16: 622-30.
195. Horch RA, Gore JC and Does MD. Origins of the ultrashort-T2 1H NMR signals in myelinated nerve: a direct measure of myelin content? *Magnetic resonance in medicine*. 2011; 66: 24-31.
196. Wilhelm MJ, Ong HH, Wehrli SL, et al. Direct magnetic resonance detection of myelin and prospects for quantitative imaging of myelin density. *Proceedings of the National Academy of Sciences of the United States of America*. 2012; 109: 9605-10.
197. Asaf A, Evan S and Anat A. Injury to white matter tracts in relapsing-remitting multiple sclerosis: A possible therapeutic window within the first 5 years from onset using diffusion-tensor imaging tract-based spatial statistics. *NeuroImage Clinical*. 2015; 8: 261-6.
198. Kezele IB, Arnold DL and Collins DL. Atrophy in white matter fiber tracts in multiple sclerosis is not dependent on tract length or local white matter lesions. *Multiple sclerosis*. 2008; 14: 779-85.
199. De Stefano N, Iannucci G, Sormani MP, et al. MR correlates of cerebral atrophy in patients with multiple sclerosis. *Journal of neurology*. 2002; 249: 1072-7.
200. Schweser F, Bertolino N, Dwyer MG, et al. A longitudinal assessment of brain iron using quantitative susceptibility mapping (QSM) in multiple sclerosis (MS) over 2 years. *ISMRM 2016 (Submitted)*.
201. Kamali A, Kramer LA and Hasan KM. Feasibility of prefronto-caudate pathway tractography using high resolution diffusion tensor tractography data at 3T. *Journal of neuroscience methods*. 2010; 191: 249-54.
202. Rocca MA, Mesaros S, Preziosa P, et al. Wallerian and trans-synaptic degeneration contribute to optic radiation damage in multiple sclerosis: a diffusion tensor MRI study. *Multiple sclerosis*. 2013; 19: 1610-7.
203. Klistorner A, Sriram P, Vootakuru N, et al. Axonal loss of retinal neurons in multiple sclerosis associated with optic radiation lesions. *Neurology*. 2014; 82: 2165-72.
204. Hu B, Ye B, Yang Y, et al. Quantitative diffusion tensor deterministic and probabilistic fiber tractography in relapsing-remitting multiple sclerosis. *European journal of radiology*. 2011; 79: 101-7.
205. Tensaouti F, Lahlou I, Clarisse P, Lotterie JA and Berry I. Quantitative and reproducibility study of four tractography algorithms used in clinical routine. *Journal of magnetic resonance imaging : JMRI*. 2011; 34: 165-72.
206. Rocca MA, Pagani E, Absinta M, et al. Altered functional and structural connectivities in patients with MS: a 3-T study. *Neurology*. 2007; 69: 2136-45.
207. Williams R, Rohr AM, Wang WT, et al. Iron deposition is independent of cellular inflammation in a cerebral model of multiple sclerosis. *BMC neuroscience*. 2011; 12: 59.

208. Cardinale F, Chinnici G, Bramerio M, et al. Validation of FreeSurfer-estimated brain cortical thickness: comparison with histologic measurements. *Neuroinformatics*. 2014; 12: 535-42.
209. Chen N, Dong S, Yan T, Yan N, Ma Y and Yu C. High-frequency stimulation of anterior nucleus thalamus improves impaired cognitive function induced by intra-hippocampal injection of Abeta1-40 in rats. *Chinese medical journal*. 2014; 127: 125-9.
210. Stillova K, Jurak P, Chladek J, et al. The Role of Anterior Nuclei of the Thalamus: A Subcortical Gate in Memory Processing: An Intracerebral Recording Study. *PloS one*. 2015; 10: e0140778.

Appendix A: Abbreviations

AD = axial diffusivity

ANCOVA = analysis of covariance

ANOVA = analysis of variance

ANTs = Advanced Normalization Tools

BBR = Boundary-Based Registration

BET = Brain Extraction Tool

BDI-FS = Beck Depression Inventory – Fast Screen

BVMT-R = Brief Visuospatial Memory Test – Revised

CSF = cerebrospinal fluid

CVLT-2 = California Verbal Learning Test – Second Edition

CST = corticospinal tract

DGM = deep gray matter

DTI = diffusion tensor imaging

EDSS = Expanded Disability Status Scale

EPI = echo planar imaging

ETL = echo train length

FA = fractional anisotropy

FAST = FMRIB's Automated Segmentation Tool

FDR = false discovery rate

FLAIR = fluid-attenuated inversion recovery

FLIP = flip angle

FIRST = FMRIB's Integrated Registration and Segmentation Tool

FLIRT = FMRIB's Linear Image Registration Tool

FNIRT = FMRIB's Nonlinear Image Registration Tool

FOV = field of view

FSL = FMRIB Software Library

FWE = family wise error

GM = gray matter

GMV = gray matter volume

GRE = gradient echo

HARDI = high angular resolution diffusion imaging

HC = healthy control

ICC = intraclass correlation

L. = left

LV = lesion volume

LVV = lateral ventricle volume

MD = mean diffusivity

MNI = Montreal Neurological Institute

MRI = magnetic resonance imaging

MS = multiple sclerosis

NAWM = normal appearing white matter

NP = neuropsychological

PAC = primary auditory cortex

PMC = primary motor cortex

QSM = quantitative susceptibility mapping

R. = right

RD = radial diffusivity

RR = relapsing-remitting

RRMS = relapsing-remitting multiple sclerosis

SD = standard deviation

SE = spin echo

SDMT = Symbol Digit Modalities Test

SIENA(X) = Structural Image Evaluation, using Normalisation, of Atrophy (Cross-sectional)

SP = secondary progressive

SWI = susceptibility-weighted imaging

SWIM = susceptibility-weighted imaging

TBSS = Tract-Based Spatial Statistics

TE = echo time

TI = inversion time

TR = repetition time

VBM = voxel-based morphometry

vol. = volume

WBV = whole brain volume

WM = white matter

WMV = white matter volume

Appendix B: Processing pipelines and software used

Processing pipelines were written using a combination of bash, python and ruby scripts.

Software packages and key components utilized are list.

Software packages

- Advanced Normalization Tools (ANTs) (http://picsl.upenn.edu/software/ants/)
- FMRIB Software Library (FSL) (http://fsl.fmrib.ox.ac.uk/fsl/fslwiki/)
- FreeSurfer (http://freesurfer.net/)
- Java Image Manipulation (JIM) (http://www.xinapse.com/)
- R (https://www.r-project.org/)
- TrackVis (http://trackvis.org/)

Image conversion and viewing

- dcm2nii (http://www.mccauslandcenter.sc.edu/mricro/mricron/dcm2nii.html)
- fslview (part of FSL)
- freeview (part of FreeSurfer)
- JIM
- TrackVis

Lesion segmentation

- Lesion identification and outlining: JIM

Lesion filling pipeline

- Brain extraction: bet (part of FSL)
- Bias field correction: N3 (https://en.wikibooks.org/wiki/MINC/Tools/N3)
- White matter mask generation: FAST (part of FSL)
- Lesion filling: lesion_filling (part of FSL)

Diffusion-weighted imaging processing

- Brain extraction: bet (part of FSL)
- Eddy current correction: eddy_correct (part of FSL)
- Rotation of diffusion vectors to account for rotations induced by eddy current correction: fdt_rotate_bvecs (part of FSL)
- Estimation of diffusion tensor: dtifit (part of FSL)
- Deterministic tractography: TrackVis
- Probabilistic tractography: bedpostx and probtrackx (both part of FSL)
- Linear registration: FLIRT (part of FSL)
- Nonlinear registration: FNIRT (part of FSL) and ANTs
- Tract-Based Spatial Statistics: tbss scripts (part of FSL)

Lesion probability mapping

- Linear registration: FLIRT (part of FSL)
- Nonlinear registration: FNIRT (part of FSL)
- Nonparametric voxelwise testing: randomise (part of FSL)

Morphological reconstruction of the cortex

- Core pipeline: recon-all (part of FreeSurfer)

Subcortical segmentation and vertex-wise analysis

- Core pipeline: run_first_all (part of FSL)
- Tuning of failed registrations: first_flirt (part of FSL)
- Linear registration: FLIRT (part of FSL)
- Calculation of halfway-space: midtrans (part of FSL)

Group-based analysis of SWI high-pass filtered phase data

- T1-weighted template generation: buildtemplateparallel.sh (part of ANTs)
- Linear registration: FLIRT (part of FSL)
- Nonlinear registration: FNIRT (part of FSL)
- Nonparametric voxelwise testing: randomise (part of FSL)